UNIVERSITY OF CALIFORNIA SAN DIEGO

Isocyanide-Based Coordination Networks:

Chemical and Structural Stability in Cu(I) and Ni(0) Frameworks

A dissertation submitted in partial satisfaction of the requirements for

the degree Doctor of Philosophy

in

Chemistry

by

Alejandra Arroyave

Committee in charge:

Professor Joshua S. Figueroa, Chair
Professor Seth M. Cohen
Professor Carolyn M. Kurle
Professor Francesco Paesani
Professor William Trogler

2021

This dissertation of Alejandra Arroyave is approved, and it is acceptable in quality and form for publication on microfilm and electronically:

_____

_____

_____

_____

_____

Chair

University of California San Diego

2021

DEDICATION

To my very supportive sister, Marcela Arroyave

EPIGRAPH

"'Is your glass half empty or half full?' Asked the mole.

'I think I'm grateful to have a glass.' Said the boy"

- Charlie Mackery

TABLE OF CONTENTS

LIST OF FIGURES

LIST OF TABLES

LIST OF SCHEMES

ACKNOWLEDGEMENTS

I have never been much of an extensive planner for my academic career and always thought that I would drift accordingly to my interest to end up in an area that I found satisfying. Now I realize that the real fortune was the people that I came across on my academic journey that not only cultivated my chemistry knowledge but also shaped my perspectives and interest, to you all I am truly grateful.

By far the most influential person in my time in graduate school was my advisor, Joshua Figueroa. I remember rotating in Josh's group with no true intention of joining his lab, just mere curiosity. To my surprise, the style that most students found demanding and intimidating I saw as an opportunity to be challenged. I decided within two weeks of that rotation that this was the advisor and group for me to have an optimal graduate school experience. It was the easiest and best decision I made in graduate school. While, yes demanding, it was always with a purpose, to push you to the limit of your capabilities and then some. I am forever grateful for the way Josh shaped my mind to think and criticize chemistry and pushed me to my limits (and then some). Thank you for giving me the opportunity to be a part of the Figueroa lab.

"Shoot for the moon and land amongst the stars", or something like that. That is what I told myself when I joined the Figueroa lab. The way Brandon Barnett spoke about chemistry during our group meetings made it easy to confuse him for a professor. I could not think of a better suited career choice then a professor for you, congrats! Thank you for all the advice you gave me in our short overlap (e.g., heavy is the crown). Chuck Mokhtarzadeh (definitely had to look that up) is really one of a kind. Chuck's extensive knowledge of reagents to try in a reaction and his ability to fix broken things in lab was impressive, but I think what I admired the most was his generosity

with his time. Chuck helped me with my first of many, two-ish weeklong ligand synth., never complained and did not expect anything in return. Doug Agnew was the most efficient person in lab that I have met. I strived to have that type of discipline in graduate school.

Kyle Mandla exposed me to perhaps the most extreme case of "off-hours" work style. Despite his bizarre schedule, Kyle was an awesome co-worker that I found easily approachable for help/coffee venting sessions. My favorite thing about Kyle was the effort he put in to making sure that everyone felt included. Myles Drance was undeniably a great chemist that could name any chemistry author off the top his head, a skill I wish I had. I am just going to officially say this here, Joanne Chan is my favorite Figueroa member. Her calming presence and aptitude for problem solving served as a role model for me and I am also very lucky to call her my best friend. I was initially very confused by Michael Neville's cheerfulness and natural instinct to get people to talk about themselves, but it makes sense that with these traits he is so well-liked amongst almost any crowd. Needless to say, I have really enjoyed being in the group with you for five years and will probably call you if I have any questions about future gloveboxes that I may use.

Adam and Ritchie, you both have the intelligence and ability to succeed in grad school and I look forward to seeing what you accomplish in graduate school. Krista, you joined the group by yourself and under normal circumstances that would be difficult, but you are well beyond anything normal and I cannot wait to see the results you inevitably roll out. Vincent, I underestimated you the first time I met you when I picked you up from the airport for your interview with our group and you very boldly wore Armani sweatpants and a tee shirt. Now I know that is just what you wear every day. In all seriousness, you are an incredible chemist and the hardest worker. Thank you for all your ideas and helpful conversations.

To all of the amazing faculty that have helped me in graduate school, I am extremely appreciative. Prof. Seth Cohen, thank you a lot for your support as a member of my committee and as my Sloan mentor. You and your students helped me navigate the unknown waters of MOFs and were extremely generous with letting me use your instruments throughout the years. Prof. Paesani, Prof. Trogler and Prof. Kurle, thank you for the insightful conversations and the encouragement during my exams. To the crystallography team, Dr. Curtis Moore, Dr. Milan Gembicky and Dr. Arnold Rheingold, I wish I could have spent more time there collecting more structures but I am glad I even got the chance to experience crystallography-utopia. Dr. Anthony Mrse thank you for your help taking NMR experiments and for all the delightful conversations we had.

To my all-time supporter and fierce protector, Marlow, you always cheered me up after a long day in lab (good and bad) by insisting I give you belly rubs. You grounded me and gave me something else to worry about besides chemistry which I think everyone needs. And in spite of the obvious social ineptitude, you are a good boy. To my human all-time supporter, Austin Parsons, you are truly incredible. You went above understanding my concerns and actively helped me when I needed it the most. Although I cannot understand all of your interest (just Community really), I love you. Thank you for being you. Also, for all the coffee.

To my wonderful family in Miami, thank you for the support throughout the years. For me it was difficult to be away from all of you, but I know you are very proud of me. It was always comforting to know that if I ever fall you all would be there for me. It is perhaps the reason I even risk doing it at all.

Thank you all again for the unwavering support and influence you have had on me. Surely, without it I would not be where I am today.

Chapter 2 is adapted from A. Arroyave, M. Gembicky, A. L. Rheingold, J. S. Figueroa "Aqueous Stability and Ligand Substitution of a Layered Cu(I)/Isocyanide-Based Organometallic Network Material with a Well-Defined Channel Structure," *Inorg. Chem.,* **2020**, 59, 11868-11878. Copyright 2020, American Chemical Society. Permission to include published material in this dissertation has been obtained from all coauthors. The dissertation author is the first author of this paper. Mark Kalaj is thanked for assistance with gas sorption measurements.

In Chapter 3, section 3.3 utilizing liquid assisted anion exchange in a Cu(I) coordination network is in preparation for publication by A. Arroyave, M. Touve, N. Gianneschi, J. S. Figueroa. The dissertation author is the primary author of this manuscript.

Chapter 4 is adapted from a manuscript currently in preparation for publication by A. Arroyave, M. Gembicky, A. L. Rheingold, and J. S. Figueroa. Permission to include published material in this dissertation has been obtained from all coauthors. The dissertation author is the first author of this paper.

VITA

2015 ***Bachelor of Science,*** Chemistry, Florida State University, USA

2017 ***Master of Science,*** Chemistry, University of California San Diego, USA

2021 ***Doctor of Philosophy,*** Chemistry, University of California San Diego, USA

PUBLICATIONS

Dissertation Related

A. Arroyave, M. Gembicky, A. L. Rheingold, J. S. Figueroa "Aqueous Stability and Ligand Substitution of a Layered Cu(I)/Isocyanide-Based Organometallic Network Material with a Well-Defined Channel Structure," *Inorg. Chem.,* **2020**, 59, 11868-11878.

A. Arroyave, M. Gembicky, A. L. Rheingold, J. S. Figeuroa "A Porous, Crystalline Ni(0) Organometallic Network Material with Redox and Structural Flexibility Properties," *In Preparation.*

Others

D. W. Agnew, I. M. Dimucci, **A. Arroyave**, M. Gembicky, C. E. Moore, S. N. MacMillan, A. L. Rheingold, K. M. Lancaster, J. S. Figueroa "Crystalline Coordination Networks of Zero-Valent Metal Centers: Formation of a 3-Dimensional Ni(0) Framework with *m*-Terphenyl Diisocyanides" *J. Am. Chem. Soc.*, **2017**, 48, 17257-17260.

ABSTRACT OF THE DISSERTATION

Isocyanide-Based Coordination Networks:
Chemical and Structural Stability in Cu(I) and Ni(0) Frameworks

by

Alejandra Arroyave

Doctor of Philosophy in Chemistry

University of California San Diego, 2021

Professor Joshua S. Figueroa, Chair

Isocyanide coordination networks (^{ISO}CNs), which feature low-valent metal centers as nodes, are a novel turn for the metal-organic framework (MOF) community. Inspiration was drawn from molecular species to be utilized as motifs for the design of the coordination environment surrounding the low-valent metal node. Specifically, ^{ISO}CNs that are synthesized with a phenylene

spaced *m*-terphenyl isocyanide linker (1,4-$(CNAr^{Mes2})_2C_6H_4$) coordinated to d^{10} Cu(I) and Ni(0) metal centers and the chemical and structural stability in these materials will be the focus of this dissertation. Crystallographic characterization of the framework denoted Cu^{ISO}CN-4 revealed distinct channels in a Cu(I) tris-isocyanide 2D framework. These channels allow for the solvent exchange of the coordinated Cu-THF for Cu-pyridine molecules to occur despite four-fold interpenetration in the framework. Importantly, a spectroscopic/geometric structure relationship with Cu-^{ISO}CNs was found that could aid future analysis of isocyanide-based materials in chemical reactivity. Single-metal Ni(0)-based nodes supported by tetra-isocyanide coordinated linkers, referred to as Ni^{ISO}CN-3, were found to undergo a one-electron redox cycle spectroscopically. Additionally, this 3D diamondiod framework presents features of a flexible MOF structure that regains crystallinity upon solvation.

Chapter 1 Isocyanide as Linkers in Coordination Networks

1.1 Examining Metal-Organic Frameworks vs Coordination Networks

Since the term metal-organic framework, MOF, was first termed in 1995 by Yaghi[1], chemist, biochemist and materials scientist alike have developed an intense interest in this field of research causing rapid increase in the development and progress in these materials. MOFs are formed from the reticular synthesis of organic multitopic linkers and metal ions/clusters as nodes to create crystalline materials that are rigid, porous frameworks in the solid state under solvothermal conditions (Figure 1.1).[2] Taking advantage of the hard soft acid base chemistry principles, these frameworks create strong ionic bonds that produce the robustness inherent in these materials.[3,4] Due to these properties, MOFs have a slew of potential applications, such as, gas storage, chemical/gas separation and heterogenous catalysis, to name a few.[5–9] Furthermore, the lattice rigidity inherent in these frameworks allows for post-synthetic modifications (PSM) to take place on the crystalline material.[10,11] Utilizing PSM has further helped advance the targeting of applications to overcome the synthesis of frameworks that are difficult to obtain *in-situ* by being able to fine tune the metal center (through ion exchange) or adding precision to the ligand to favor selectivity in gas or chemical separations.[12,13] However, those same properties that give it the strength to sustain these processes also limit the capacity and chemical transformations that could propel MOFs to the next level.

Coordination networks were derived from inspiration of Werner complexes, which has helped form and shape the field of coordination chemistry,[14,15] utilizing the same conceptual ideas

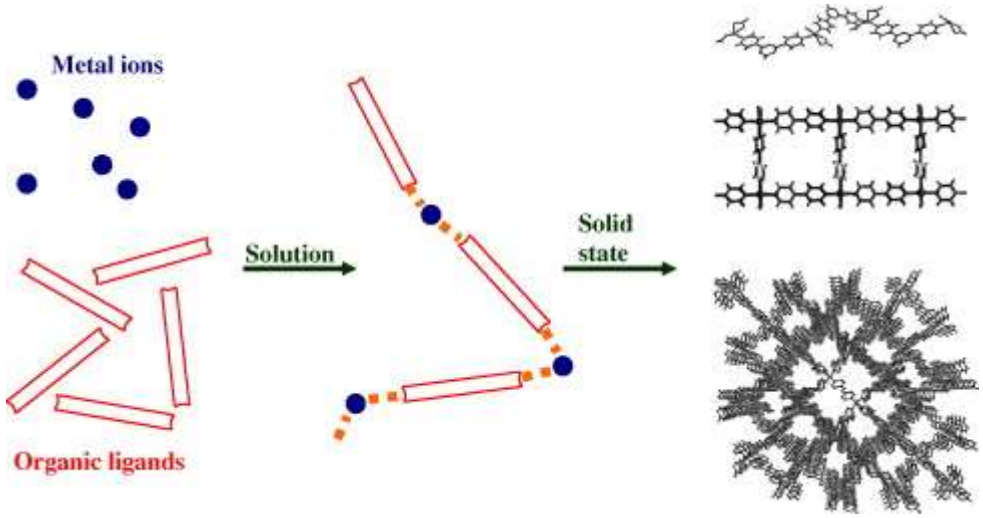

Figure 1.1 Metal ions (or clusters) are combined with organic multitopic ligands that serve as linkers. In solution these substrates coordinate and form amorphous polymers. In the solid state, after solvothermal conditions, these polymers order into 1D, 2D or 3D crystalline frameworks.

pertaining to bonding and geometry in complexes to build extended frameworks.[16] The use of neutral ligands allowed for the investigations of softer metals, such as, Ag(I) and Cu(I), acting as nodal metal centers into discretely formed materials.[17,18] However, these frameworks were found to be thermally and structurally unstable upon removal of the guest/solvent molecules from the pores and lead to the collapse of coordination networks. This lack of stability was attributed to the weak coordination bond between the transition metal and the neutral ligand, where the sole σ-donation from the organic ligand does not contribute significant enough strength in bonding to allow for the same robustness that is commonly found in MOFs. Indeed, this principle of bonding transition metals to organic ditopic linkers extended from coordination networks to metal-organic frameworks.[19] However, the use of hard anionic ligands, such as, carboxylates and imidazolates, paired with medium to high valent metals allows for these frameworks to uphold high temperatures and pressure, even when activated (guest/solvent molecules removed) leaving the porous material available for the use of storage and separation of gases, as well as, allowing substrates to access these pores and therefore allowing reactivity in the pores to take place.[20–22] This important

distinction has perhaps forged the path for MOFs to become ubiquitous in the literature, while less commonly reported coordination networks are now seen.

1.2 Organometallic Neutral Ligand - Isocyanides

The great variety of metal ions and organic linkers available to design a specific framework with certain topologies and chemical traits is one of the most appealing features of coordination networks. Neutral ligands and halides were amongst the first explored ligands for the coordination of metal ions into extended frameworks.[23–26] The use of pyridines and nitriles became commonly seen as the ditopic linker of choice for the extension of soft metals found in molecular complexes. This electrostatic interaction between the Lewis base ligand donating a lone pair of electrons to the positively charged metal cation creates a weak coordination bond between the node and linker. The coordination bond is usually the weakest bond present in the networks (~ 50 kJ/mol),[27] although weaker bonds and interactions such as hydrogen bonding, π-π stacking interactions and van Der Waals interactions can also be present. Accordingly, the desire to pursue stronger nodal connections lead to the use of anionic ligands which form stronger ionic bonds to metal nodal centers. Indeed, the use of imidazolates and carboxylates as organic ligands in combination with metal-oxo/hydroxo clusters have become pervasive in MOF literature because they form strong (~ 180 kJ/mol) and kinetically inert bonds that hold the framework together.[28–31]

Isocyanide ligands are neutral, organometallic ligands that for years had been regarded as an unnatural substance with an unpleasant odor. However, isocyanides function as a toolbox for synthetic chemist to achieve unusual coordination and mimics to compounds that are fleeting in nature. Due to their orthogonal and degenerate π*-orbitals, isocyanides are capable of engaging in π-backdonation with electron rich metal centers. This is complimentary to the σ-donation from the lone pair found on the carbon atom of -CNR. The combination of σ-donation and π-acid features

in isocyanides render the synergistic attributes of this ligand to form strong, kinetically stable bonding interactions with softer metals. In comparison to other organometallic ligands, such as CO, isocyanides feature an -R group that can be modified to accommodate structural properties for particular targets, including, an additional isocyanide group to form multitopic isocyanide ligands.

Isocyanides have a brief history being utilized as multitopic ligands, with few researchers taking advantage of this versatile ligand as a linker. In 1980, marks the first chemical reaction reported with the use of 1,4-diisocyanobenzene and 4,4′-diisocyanobiphenyl by Jaffe.[32] $[Rh(CO)_2Cl]_2$ was utilized as the metal precursor and individually combined with the isocyanide ligands at ambient temperatures to form a polymer that neither dissolved in aqueous or organic media nor melted at temperatures below 300 °C. FTIR analysis revealed strong ν(NC) frequencies indicating the coordination of the isocyanide with the Rh center. In the absence of suitable single crystals, powder X-ray diffraction and models of these coordination polymers were performed. Additionally, diffuse reflectance spectra revealed absorptions that were better understood and assigned utilizing band gap theory instead of molecular orbital theory. With the use of ditopic isocyanide linkers, Jaffe studied the coordination of low-valent metal centers incorporated into materials.[33–37] Coordination polymers, such as, Pd(0), Pt(0) and Rh(I) were synthesized materials that demonstrated viability towards applications as heterogenous catalyst in hydrogenation of alkenes and alkynes.[38–41] However, while these coordination polymers were effective catalyst, they lacked selectivity and further improvement due to postulated metal-metal stacking interactions. In an attempt to circumvent this issue, Tannenbaum judiciously selected d^6 transition metals, e.g., Ru(II), Os(II) and Rh(III), because most of the metal complexes that utilize these metals exhibit octahedral geometries, to template the isocyanide coordination networks that would now be three-

dimensional.[42,43] Despite detailed spectroscopic studies on these materials which allowed for modeling of nodal sites and geometries, no single crystals were obtained from these investigations. Crystallographic information was obtained by Cheung, through the use of isocyanide Fe(II), Pd(II) and Pt(II) complexes that formed networks through hydrogen bonding that held the weak network together instead of a metal-carbon bond.[44] Since this paper in 1998, no work featuring isocyanides as linkers in frameworks has been studied or reported.

1.3 Isocyanide Analogues to Metal Carbonyl Complexes

Metal carbonyl complexes have long captivated the attention of organometallic chemist since the discovery of $Ni(CO)_4$ by L. Mond in 1890.[45] Saturated and unsaturated metal carbonyls like $Ni(CO)_4$ (e.g., $Co(CO)_4$, $Ni(CO)_3$, $Pd(CO)_2$ and $Fe(CO)_4$) (Figure 1.2) have been intensely studied and modeled to understand structural and spectroscopic attributes.[46–54] The intensity of this interest arises from the important role that these species play as active catalyst and intermediates

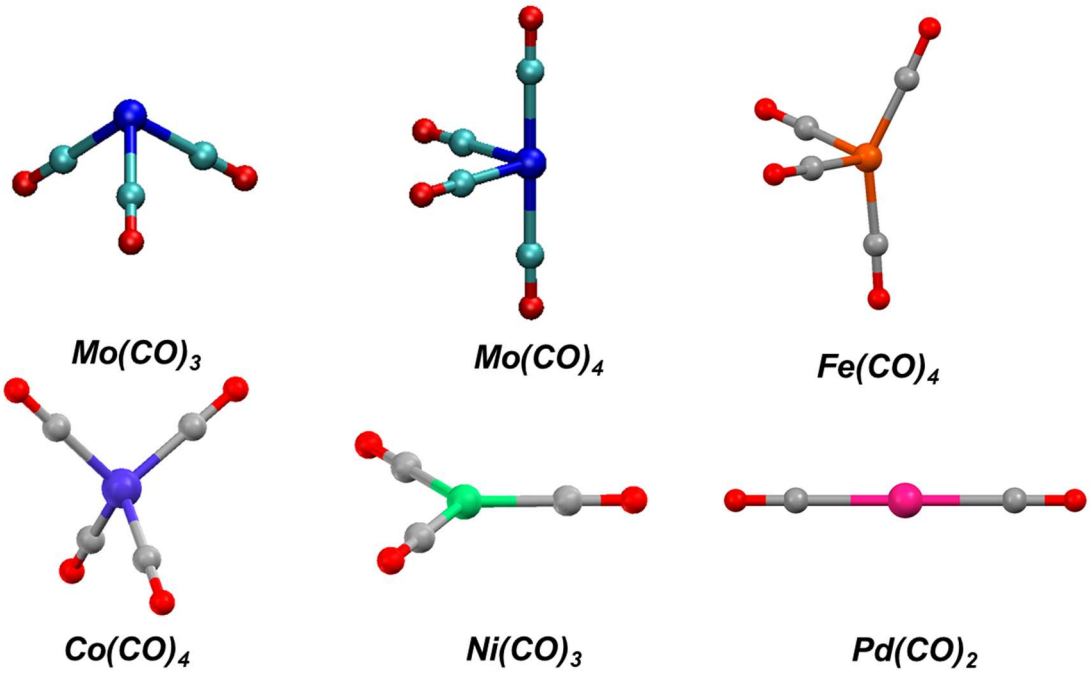

Figure 1.2 Calculated geometries for coordinatively/electronically saturated and unsaturated classic transition metal carbonyl complexes.

in catalytic cycles (e.g., hydroformylation, carbonylation and hydrosilylation).[55,56] Despite these species having only been observed at low temperature cryogenic inert-gas matrices, spectroscopic and theoretical investigations allowed for the understanding of the electronical properties of metal carbonyls.[57–62] Yet, the structural properties in the solid-state and the behavior of these species in solution-state remained elusive due to the difficulty of the isolation of metal carbonyls that is recognized due to the high thermal and kinetic instability of these species.

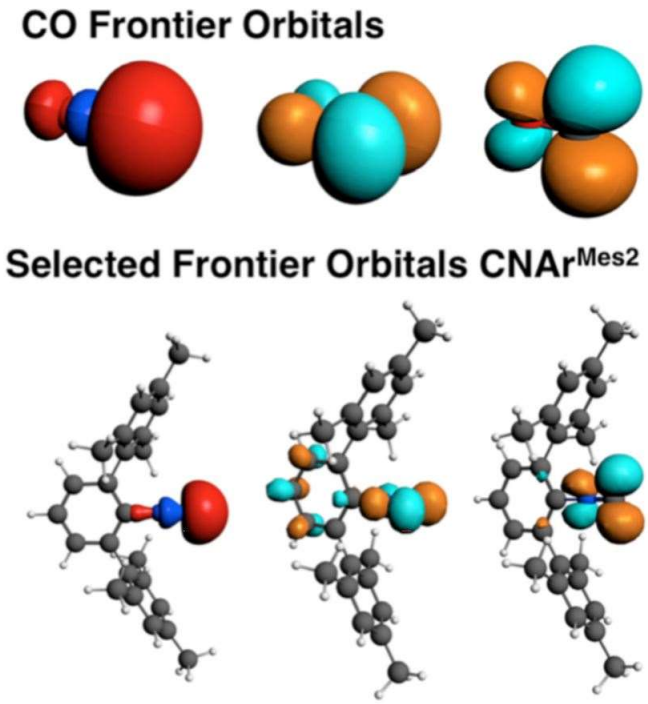

Figure 1.3 Calculated frontier orbitals of carbonyls and isocyanides. Illustrates the availability of sigma orbitals and empty pi* orbitals of both organometallic ligands.

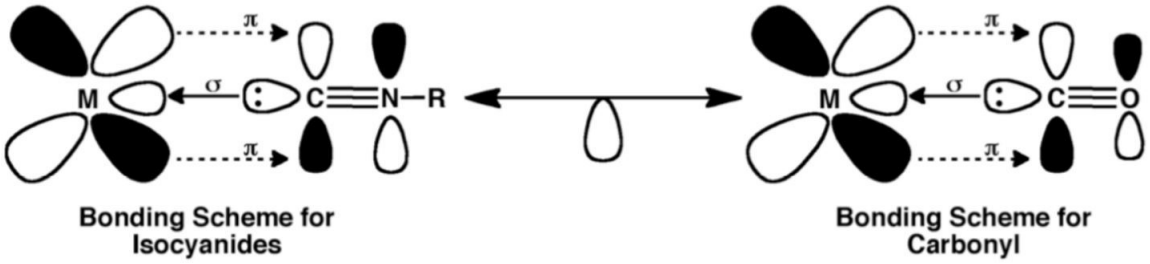

Figure 1.4 Isolobal bonding scheme for isocyanides and carbonyls, showing the sigma donation and pi accepting properties both available for bonding with transition metals.

Inspired by the unknown structural and solution-phase properties of these classic unsaturated binary complexes in the literature, many synthetic chemists chased after analogues of these species utilizing isocyanide ligands. Isocyanides are isolobal analogues to carbonyl ligands, by virtue of having similar frontier orbitals available that can participate in both σ-donation and π-accepting bonding to interact synergistically with transition-metal centers (Figure 1.3). It should be noted, however, that isocyanides are stronger σ-donors and weaker π-accepters than CO. This shift in orbital energies allows for isocyanides to be used as surrogates to isolate neutral and anionic metal carbonyl analogues but should be kept in mind as the limitation to which this analogy can be drawn. Despite this limitation, talented synthetic chemist isolated and characterized air-sensitive negative oxidation states for metal isocyanide analogues to metal carbonyl anions, $[Co(CNXyl)_4]^-$ and $[Fe(CNXyl)_4]^{2-}$,[63,64] effectively demonstrating that isocyanides can stabilize electron rich metal centers through the empty π*-orbital of the carbon-atom on the isocyanide. While these examples provided a direct comparison to the expected structural geometries of saturated metal carbonyl species, the unsaturated metal carbonyl complexes were unattainable with the use of CNXyl (2,6-dimethylphenyl isocyanide).

The incorporation of an *m*-terphenyl substituent group has allowed for a vast variety of unusual coordination complexes where at least one sterically demanding substituent was necessary.[65] Indeed, taking advantage of this synthetic strategy the Figueroa group has succeeded in synthesizing a number of unsaturated metal isocyanide complexes that serve as analogues to unsaturated metal carbonyl species.[66–69] The greater the steric hinderance provided by the *m*-terphenyl isocyanide, the greater steric protection offered to the metal center to prevent a high

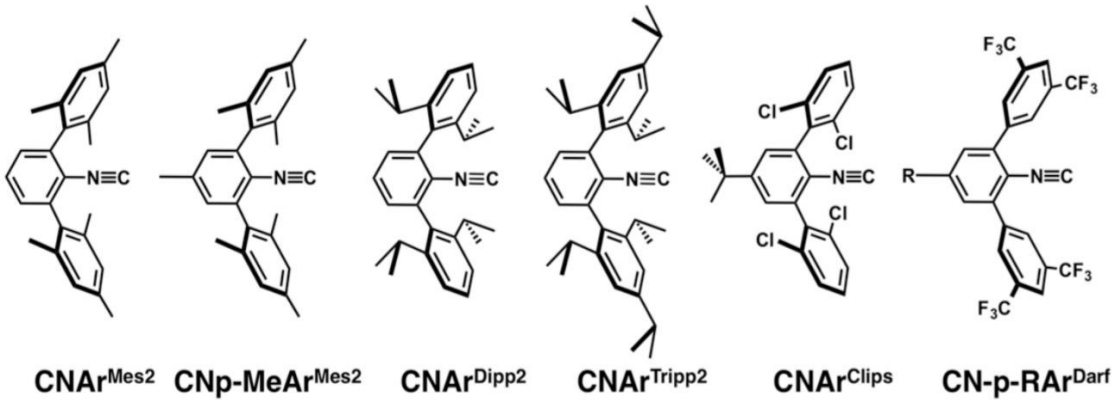

Figure 1.5 Library of *m*-terphenyl isocyanide ligands with fine-tuned steric and electronic profiles.

coordination number. Additionally, these *m*-terphenyl groups provide kinetic stability to the low-valent transition metals to further promote the formation of such species. Accordingly, the Figueroa group has synthesized a library of electronically and sterically modified *m*-terphenyl groups to target specific molecules, some of which may necessitate bulkier properties (Figure 1.5).[70] For example, for the isolation of a Ni-tris isocyanide molecule, analog to $Ni(CO)_3$, utilizing $CNAr^{Mes2}$ (Ar^{Mes2} = 2,6-(2,4,6-$Me_3C_6H_2)_2C_6H_3$) required a clever synthetic strategy. Since low-valent Ni sites can bind Tl^+ in a reversible fashion, it was used as a site protection agent to prevent a fourth Lewis basic isocyanide ligand in order to obtain the coordinatively unsaturated complex. However, utilizing a slightly more sterically encumbered *m*-terphenyl group, $CNAr^{Dipp2}$ (Ar^{Dipp2} = 2,6-(2,6-*i*-$PrC_6H_3)_2C_6H_3$) facilitated the reaction. A stoichiometric amount of $CNAr^{Dipp2}$ could now be combined with $Ni(COD)_2$ to obtain $Ni(CNAr^{Dipp2})_3$ without a protection agent. Other notable examples include the isocyanide stabilized $Cp^*Co(N_2)(CNAr^{Tripp2})$ (Ar^{Tripp2} = 2,6-(2,4,6-(*i*-$Pr)_3C_6H_2)_2C_6H_3$) that served as the scaffold for the side-on-bound nitrous oxide complex,[71] and dianionic metal-based nucleophile, $K_2[Fe(CO)_2(CNAr^{Tripp2})_2$, to stabilize a terminal fluoroborylene complex (Figure 1.6).[72] This speaks to the importance of the *m*-terphenyl group and the reliance not only on the electronic properties of the isocyanide but on the steric profile of these bulky groups to isolate these highly reactive compounds. With the use of these *m*-terphenyl

isocyanide ligands the isolation of low-valent coordinatively unsaturated metal complexes for crystallographic information and spectroscopic analysis was obtained. If these bulky isocyanide ligands could be transformed to accommodate the bridging coordination of two metal centers it could allow the exploration of low-valent metal centers as nodes in materials.

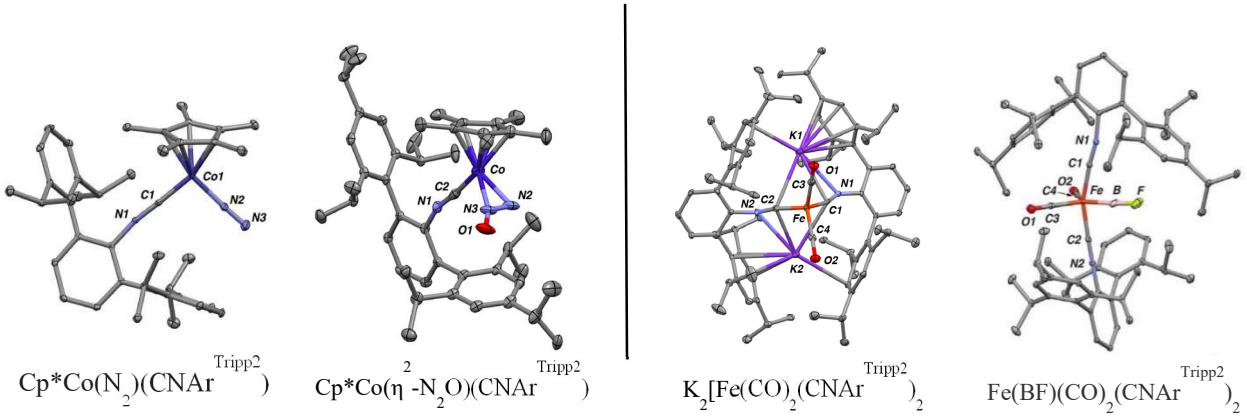

$Cp^*Co(N_2)(CNAr^{Tripp2})$ $Cp^*Co(\eta^2\text{-}N_2O)(CNAr^{Tripp2})$ $K_2[Fe(CO)_2(CNAr^{Tripp2})_2]$ $Fe(BF)(CO)_2(CNAr^{Tripp2})_2$

Figure 1.6 Isocyanide supported late-transition metal complexes. (Left) Coordinatively unsaturated $Cp^*Co(N_2)(CNAr^{Tripp2})$ with labile N_2 to form $Cp^*Co(\eta^2\text{-}N_2O)(CNAr^{Tripp2})$ in the presence of an N_2O atmosphere. (Right) Nucleophilic $K_2[Fe(CO)_2(CNAr^{Tripp2})_2$ for the stabilization of long sought after a terminally bound fluoroborylene complex.

1.4 Ditopic *m*-Terphenyl Isocyanide Linkers to Access Extended Metal-Isocyanide Frameworks

Developing *m*-terphenyl isocyanides as linkers in frameworks is a novel turn for the MOF and coordination network community that permits the study of coordinatively unsaturated soft metal centers as nodes in materials. Utilizing the well characterized and studied molecular species as templates to form extended molecular versions into frameworks, just as Werner complexes had been used as mimics to form coordination networks. It is advantageous to know how to synthesize and handle the molecules to now use as a guide for the formation of the coordination networks. Indeed, the Figueroa group by utilizing these sterically encumbering isocyanides could stabilize low-valent and low coordinate nodal centers as has been reported several times with molecular complexes.

Necessary to create the mimics of these metal-isocyanide complexes into metal-organic materials was to preserve the coordination environment around the metal node. It has been observed in both molecular and material metal-isocyanide systems that the usage of a smaller isocyanide ligand will saturate the coordination number of the metal center. It was also deemed vital by the Figueroa group through previously reported examples, that the inclusion of a sterically encumbering -R substituent affords low-coordinate molecules. Established by the first publication of the Figueroa group with cationic Cu(I)-isocyanide molecular systems using $CNAr^{Mes2}$ it was found that it did not conform to previously reported copper complexes of four-coordinate nature.[73,74] Instead, these Cu(I)-isocyanide complexes are three-coordinate due to the steric repulsion of the *m*-terphenyls, and trigonal pyramidal featuring an apically bound THF molecule to reach electronic saturation. In order to avoid a coordinatively saturated node in a network, the synthesis of a ditopic *m*-terphenyl isocyanide ligand was set after.

With the aim of generating low-coordinate, coordinatively unsaturated isocyanide metal materials we pursued the synthesis of sterically encumbering *m*-terphenyl groups inspired by the work of Powers,[75] Robinson,[76] and others.[77] After multiple steps in a synthesis towards the *m*-terphenyl isocyanide ligand air-stable H_2NAr^{Mes2} is produced. Bromination of the *m*-terphenyl aniline affords an off-white powder of $H_2NAr^{Mes2}Br$, that could now be subjected to Pd-based couplings (e.g., C-B and C-C couplings). Through subsequent Miyauri-Suzuki couplings, the ditopic *m*-terphenyl aniline was obtained. From this synthetic point, the usual formylation and dehydration reactions familiar to Figueroa chemist affords the ditopic *m*-terphenyl isocyanide ligand (Scheme 1.1).[78] Important to note is the ease with which these ligands can be modified to

include an elongated or multitopic ligand through simple modification of the Suzuki coupling step and the judicious selection of the appropriate substrate (Figure 1.7).[79]

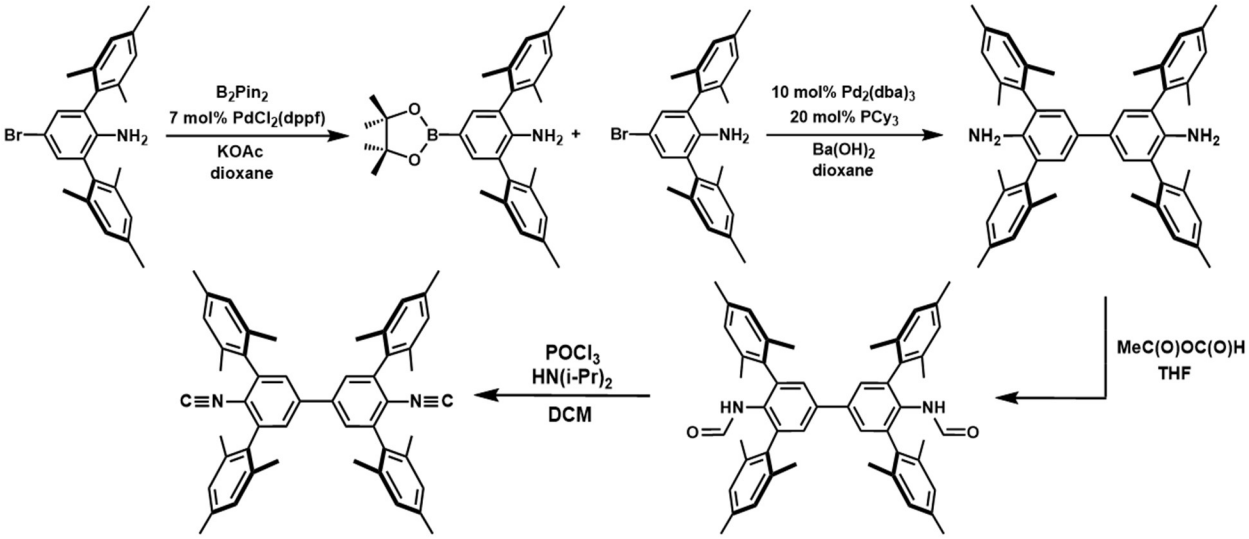

Scheme 1.1 Synthesis of ditopic *m*-terphenyl isocyanide starting at the brominated $H_2NAr^{Mes2}Br$ to Miyauri-Suzuki coupling and create a para-positioned C-C bond, followed by formylation and dehydration.

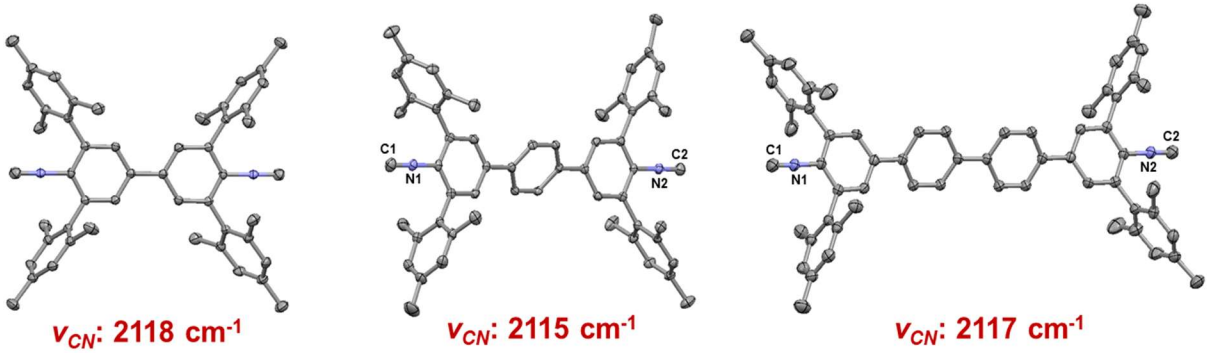

Figure 1.7 Series of ditopic *m*-terphenyl isocyanide ligands that have been modified to systematically lengthen the ligand through phenylene and biphenylene spacers. Left to Right: $[CNAr^{Mes2}]_2$, 1,4-$(CNAr^{Mes2})_2C_6H_4$, and 1,4-$(CNAr^{Mes2})_2C_{12}H_8$.

1.5 Outlook

With the availability of ditopic *m*-terphenyl isocyanide ligands at hand, the development and study of metal-isocyanide frameworks was now accessible. Indeed, the remainder of the chapters in this thesis center around the synthesis and chemical and structural stability of low-valent metal-isocyanide coordination networks. Low-valent metals incorporated into frameworks

in this manner has been an underdeveloped area of research. The value of this research is extensive, as the exploitation of the chemistry available to electron-rich transitions metals in solution state could potentially be enabled in the solid-state and add to the advantageous that heterogenous materials facilitate. Of course, thorough characterization and studies must first be performed to on basic systems to create the path for more chemically reactive isocyanide networks. Accordingly, here-in the studies of Cu(I) and Ni(0) systems modeled around their molecular analogs is discussed.

1.6 References

(1) Yaghi, O. M.; Li, G.; Li, H. *Nature* **1995**, *378* (6558), 703–706.

(2) Robin, A. Y.; Fromm, K. M. *Coord. Chem. Rev*. **2006**, *250*, 2127–2157.

(3) Martin, R. L.; Lin, L.-C.; Jariwala, K.; Smit, B.; Haranczyk, M. *J. Phys. Chem. C* **2013**, *117*, 31.

(4) Nguyen, T. T. M.; Le, H. M.; Kawazoe, Y.; Nguyen, H. L. *Mater. Chem. Front,* **2018**, *2*, 2063.

(5) Zhang, W.; Kauer, M.; Halbherr, O.; Epp, K.; Guo, P.; Gonzalez, M. I.; Xiao, D. J.; Wiktor, C.; LIabrés i Xamena, F. X.; Wöll, C. *Chem. A Eur. J.* **2016**, *22* (40), 14297–14307.

(6) Furukawa, H.; Cordova, K. E.; O'Keeffe, M.; Yaghi, O. M. *Science.* **2013**, *341* (6149).

(7) Li, J.-R.; Kuppler, R. J.; Zhou, H.-C. *Chem. Soc. Rev.* **2009**, *38*, 1477.

(8) Murray, L. J.; Dincă, M.; Long, J. R. *Chem. Soc. Rev.* **2009**, *38*, 1294.

(9) Eddaoudi, M.; Kim, J.; Rosi, N.; Vodak, D.; Wachter, J.; O'Keeffe, M.; Yaghi, O. M. *Science.* **2002**, *295* (5554), 469–472.

(10) Ding, M.; Cai, X.; Jiang, H.-L. *Chem. Sci.* **2019**, *10* (44), 10209–10230.

(11) Yin, Z.; Wan, S.; Yang, J.; Kurmoo, M.; Zeng, M. H. *Coord. Chem. Rev*. **2019**, *378* 500–512.

(12) Evans, J. D.; Sumby, C. J.; Doonan, C. J. *Chem. Soc. Rev.* **2014**, *43*, 5933.

(13) Cohen, S. M. *Chem. Rev.* **2012**, *112*, 970–1000.

(14) Barry, N. P. E.; Sadler, P. J. *Pure Appl. Chem.* **2014**, *86*, 1897–1910.

(15) Bowman-James, K. *Acc. Chem. Res*. **2005**, *38*, 671–678.

(16) Kauffman, G. B.; Girolami, G. S.; Busch, D. H. *Coord. Chem. Rev.* **1993**, *128* (1–2), 1–48.

(17) Roßenbeck, B.; Sheldrick, W. S. *Zeitschrift für Naturforsch.***1999**, *54*, 1510–1516.

(18) Venkataraman, D.; Lee, S.; Moore, J. S.; Zhang, P.; Hirsch, K. A.; Gardner, G. B.; Covey, A. C.; Prentice, C. L. *Chem. Mater.* **1996**, *8* (8), 2030–2040.

(19) Diercks, C. S.; Kalmutzki, M. J.; Diercks, N. J.; Yaghi, O. M. *ACS Cent. Sci.* **2018**, *4* (11), 1457–1464.

(20) Brozek, C. K.; Dincă, M. *Chem. Soc. Rev.* **2014**, *43*, 5456.

(21) McDonald, T. M.; Mason, J. A.; Kong, X.; Bloch, E. D.; Gygi, D.; Dani, A.; Crocellà, V.; Giordanino, F.; Odoh, S. O.; Drisdell, W. S. *Nature* **2015**, *519*, 303.

(22) Cavka, J. H.; Jakobsen, S.; Olsbye, U.; Guillou, N.; Lamberti, C.; Bordiga, S.; Lillerud, K. P. *J. Am. Chem. Soc.* **2008**, *130* (42), 13850–13851.

(23) Liu C. F.; Liu, N. C.; Bailar, J. C. *Inorg. Chem.* **1964**, *3*, 1197 - 1198.

(24) Brown, T. L.; Lee, K. J. *Coord. Chem. Rev.* **1993**, *128* (1–2), 89–116.

(25) Chen, C. T.; Suslick, K. S. *Coord. Chem. Rev.* **1993**, *128* (1–2), 293–322.

(26) Archer, R. D. *Coord. Chem. Rev.* **1993**, *128* (1–2), 49–68.

(27) Aghabozorg, H.; Manteghi, F.; Sheshmani, S. *J. Iran. Chem. Soc.* **2008**, *5* (2), 184–227.

(28) Morris, R. E.; Brammer, L. *Chem. Soc. Rev* **2017**, *5444*, 5444.

(29) Serre, C.; Millange, F.; Thouvenot, C.; Noguès, M.; Marsolier, G.; Louër, D.; Férey, G. *J. Am. Chem. Soc.* **2002**, *124* (45), 13519–13526.

(30) Phan, A.; Doonan, C. J.; Uribe-Romo, F. J.; Knobler, C. B.; Okeeffe, M.; Yaghi, O. M. *Acc. Chem. Res.* **2010**, *43* (1), 58–67.

(31) Chui, S. S. Y.; Lo, S. M. F.; Charmant, J. P. H.; Orpen, A. G.; Williams, I. D. *Science.* **1999**, *283* (5405), 1148–1150.

(32) Efraty, A.; Feinstein, I.; Frolow, F.; Wackerle, L. *J. Am. Chem. Soc*. **1980**, *120*, 6341–6343.

(33) Feinstein-Jaffe, I.; Maisuls, S. E. *J. Organomet. Chem.* **1988**, *350* (1), 57–75.

(34) Feinstein-Jaffe, I.; Biran, I.; Mahalu, D.; Cohen, S.; Lawrence, S. A. *Inorganica Chim. Acta* **1988**, *154* (2), 129–131.

(35) Feinstein-Jaffe, I.; Frolow, F.; Wackerle, L.; Goldman, A.; Efraty, A. *J. Chem. Soc. Dalt. Trans.* **1988**, No. 2, 469–476.

(36) Efraty, A.; Feinstein, I.; Wackerle, L.; Frolow, F. *Angew. Chemie Int. Ed. English* **1980**, *19* (8), 633–634.

(37) Jaffe, I. *Rev. Inorg. Chem.* **1993**, *13* (1), 1–76.

(38) Feinstein-Jaffe, I.; Efraty, A. *J. Mol. Catal.* **1987**, *40* (1), 1–7.

(39) Efraty, A.; Feinstein, I. *Inorg. Chem.* **1982**, *21*, 3115 - 3118.

(40) Feinstein-Jaffe, I.; Efraty, A. *J. Mol. Catal.* **1986**, *35* (3), 285–302.

(41) Jaffe, I.; Segal, M.; Efraty, A. *J. Organomet. Chem.* **1985**, *294* (2), c17–c20.

(42) Tannenbaum, R. *Chem. Mater.* **1994**, *6* (4), 550–555.

(43) Tannenbaum, R. *J. Mol. Catal. A Chem.* **1996**, *107* (1–3), 207–215.

(44) Lau, K. Y.; Mayr, A.; Cheung, K. K. *Inorganica Chim. Acta* **1999**, *285* (2), 223–232.

(45) Mond, L.; Langer, C.; Quincke, F. L. *Journal of the Chemical Society, Transactions*. **1890**, *57*, 749–753.

(46) Hoffmann, R.; Elian, M. *Inorg. Chem.* **1975**, *14* (5), 1058–1076.

(47) Burdett, J. K., *Inorg. Chem.* **1975**, *14*, 375.

(48) Zhou, M.; Andrews, L.; Bauschlicher, C. W. *Chem. Rev*. **2001**, *101*, 1931–1961.

(49) Moggi, L.; Juris, A.; Sandrini, D.; Manfrin, M. F. *Rev. Chem. Intermed.* **1981**, *4* (1–4), 171–223.

(50) Eischens, R. P. *Acc. Chem. Res.* **1972**, *5* (2), 74–80.

(51) Wrighton, M. S.; Ginley, D. S. *J. Am. Chem. Soc.* **1975**, *97* (8), 2065–2072.

(52) Ishikawa, Y. I.; Kawakami, K. *J. Phys. Chem. A* **2007**, *111* (39), 9940–9944.

(53) Andrews, L.; Zhou, M.; Gutsev, G. L. *J. Phys. Chem. A* **2003**, *107* (7), 990–999.

(54) Hynes, R. C.; Preston, K. F.; Springs, J. J.; Williams, A. J. *J. Chem. Soc. Dalt. Trans.* **1990**, *0* (12), 3655–3661.

(55) Bailey, D. C.; Langer, S. H. *Chem. Rev.* **1981**, *81*, 109 - 148.

(56) A. Schroeder, M.; S. Wrighton, M. *J. Organomet. Chem.* **1977**, *128*, 345 – 358.

(57) Rick Fletcher, T.; Rosenfeld, R. N. *J. Am. Chem.* Soc. **1985**, *107*, 2203.

(58) Crichton, O.; Poliakoff, M.; Rest, A. J.; Turner, J. J. *J. Chem. Soc. Dalt. Trans.* **1973**, *12*, 1321–1324.

(59) Perutz, R. N.; Turner, J. J. *J. Am. Chem. Soc.* **1975**, *97* (17), 4791–4800.

(60) Perutz, R. N.; Turner, J. J. *Inorg. Chem.* **1975**, *14* (2), 262–270.

(61) Ganske, J. A.; Rosenfeld, R. N. *J. Phys. Chem.* **1989**, *93* (5), 1959–1963.

(62) Church, S. P.; Poliakoff, M.; Timney, J. A.; Turner, J. J. *J. Am. Chem. Soc.* **1981**, *103* (25), 7515–7520.

(63) Brennessel, W. W.; Ellis, J. E. *Angew. Chemie* **2007**, *119* (4), 604–606.

(64) Warnock, G. F.; Cooper, N. J. *Organometallics* **1989**, *8* (7), 1826–1827.

(65) Clyburne, J. A. C.; McMullen, N. *Coord. Chem. Rev*. **2000**, *210*, 73–99.

(66) Emerich, B. M.; Moore, C. E.; Fox, B. J.; Rheingold, A. L.; Figueroa, J. S. *Organometallics* **2011**, *30* (9), 2598–2608.

(67) Labios, L. A.; Millard, M. D.; Rheingold, A. L.; Figueroa, J. S. *J. Am. Chem. Soc.* **2009**, *131* (32), 11318–11319.

(68) Fox, B. J.; Millard, M. D.; DiPasquale, A. G.; Rheingold, A. L.; Figueroa, J. S. *Angew. Chem. Int. Ed. Engl.* **2009**, *48* (19), 3473–3477.

(69) Drance, M. J.; Figueroa, J. S. *Chem*. **2018**, *4*, 2734–2736.

(70) Carpenter, A. E.; Mokhtarzadeh, C. C.; Ripatti, D. S.; Havrylyuk, I.; Kamezawa, R.; Moore, C. E.; Rheingold, A. L.; Figueroa, J. S. *Inorg. Chem.* **2015**, *54* (6), 2936–2944.

(71) Mokhtarzadeh, C. C.; Chan, C.; Moore, C. E.; Rheingold, A. L.; Figueroa, J. S. *J. Am. Chem. Soc*. **2019**, *141*, 15003–15007.

(72) Drance, M. J.; Sears, J. D.; Mrse, A. M.; Moore, C. E.; Rheingold, A. L.; Neidig, M. L.; Figueroa, J. S. *Science.* **2019**, *363* (6432), 1203–1205.

(73) Bowmaker, G. A.; Hanna, J. V.; Hahn, F. E.; Lipton, A. S.; Oldham, C. E.; Skelton, B. W.; Smith, M. E.; White, A. H. *Dalt. Trans.* **2008**, No. 13, 1710–1720.

(74) Fox, B. J.; Sun, Q. Y.; DiPasquale, A. G.; Fox, A. R.; Rheingold, A. L.; Figueroa, J. S. *Inorg. Chem.* **2008**, *47*, 9010 - 9020.

(75) Rivard, E.; Power, P. P. *Inorg. Chem.* **2007**, *46* (24), 10047–10064.

(76) Wang, Y.; Robinson, G. H. *Organometallics* **2007**, *26*, 2–11.

(77) Smith, R. C.; Gantzel, P.; Rheingold, A. L.; Protasiewicz, J. D. *Organometallics* **2004**, *23*, 5124 - 5126.

(78) Agnew, D. W.; Gembicky, M.; Moore, C. E.; Rheingold, A. L.; Figueroa, J. S. *J. Am. Chem. Soc.* **2016**, *138* (46), 15138–15141.

(79) Arroyave, A.; Gembicky, M.; Rheingold, A. L.; Figueroa, J. S. *Inorg. Chem.* **2020**, *59*, 11868–11878.

Chapter 2 Aqueous Stability and Ligand Substitution of a Layered Cu(I)/Isocyanide-Based Organometallic Network Material with a Well-Defined Channel Structure

2.1 Introduction

Metal-organic frameworks (MOFs) and similar solid-state networks are now well-known as an important and versatile type of materials for applications that as mentioned in Chapter 1 of this thesis include chemical separation, gas storage, electron transfer, and progressively, electro- and thermal catalysis.[1–7] A central idea for the construction of reticular MOF materials, especially those with well-defined empty spaces and permanent porosity, has been the use of strong and kinetically inert metal-ligand bonding interactions.[8] The most common manifestation of this principle, as found in archetypical frameworks MOF-5, UiO-66, and ZIF-8,[9–11] has been taking advantage of the ionic bonding interactions between medium-to-high valent metal centers and anionic linker groups such as carboxylates or azolates.[8,12,13] In contrast, neutral linkers, such as those derived from nitriles and pyridines, have long been known to produce network materials with low thermal stability and the absence of permanent porosity.[8,12] It has been proposed that the inferior bulk-material properties derived from neutral linkers are a result of weaker and more labile metal-ligand bonds, especially when compared to the bonds formed from anionic ligands.[13] Consequently, the study of network materials featuring low-valent metal centers as network structural components (i.e., secondary building unit; SBU) has lagged in development.[14–22] Indeed,

low-valent metal centers are electronically matched to "softer" ligands, which are often neutral in charge and generally associated with molecular organometallic complexes (e.g., CO, PR_3). However, the advancement of strategies leading to robust, well-defined frameworks incorporating low-valent metal structural sites offers a unique opportunity to uncover new species for chemisorption and heterogeneous catalysis, especially if such emergent properties parallel the well-established behavior of low-valent molecular organometallics.[23]

Recently, we reported an approach to overcoming this task by utilizing the rigid and linear ditopic *m*-terphenyl diisocyanide, $[CNAr^{Mes2}]_2$, as a linker group (Ar^{Mes2} = 2,6-(2,4,6-$Me_3C_6H_2$)$_2C_6H_3$; Scheme 2.1).[24,25] Isocyanide ligands have long been known for their ability to behave as both good σ-donors and strong π-acids,[26–33] which are properties that are particularly beneficial for the stabilization of electron-rich metal centers.[34–43,44] Accordingly, regardless of their charge neutrality, the dual bonding interactions provided by isocyanides lead to robust metal-ligand linkages that can be exploited for reticular network formation.[24,25,45] It was demonstrated that $[CNAr^{Mes2}]_2$ could provide a series of robust, single-crystalline frameworks featuring Cu(I)-based single metal structural nodes (i.e., Cu-^{ISO}CNs 1-3; ^{ISO}CN = isocyanide coordination network; Scheme 2.1).[24] In certain instances, these frameworks maintain their thermal integrity up to ca. 500 °C and show marked chemical resistance to both strong Brønsted acids and bases. The insensitivity of these materials to such harsh chemical conditions is significant, originating from both the low hydrolytic susceptibility of the isocyanide metal-carbon bond and the hydrophobic environment provided by the *m*-terphenyl groups. Furthermore, the π-acidity properties of $[CNAr^{Mes2}]_2$ allowed for the formation and stabilization of a three-dimensional, diamondiod framework featuring mono-nuclear, four-coordinate Ni(0) structural nodes (Scheme 2.1).[25] Notably, this latter structure, denoted Ni-^{ISO}CN-2, serves as a rare example of a

crystallographically characterized three-dimensional network material containing a zero-valent metal center as an SBU.

While the results above show that well-defined, crystalline network materials can be generated from charge-neutral metal-isocyanide connections, to date, the short linker length of $[CNAr^{Mes2}]_2$ has impeded the formation of ^{ISO}CNs with significant internal surface area or

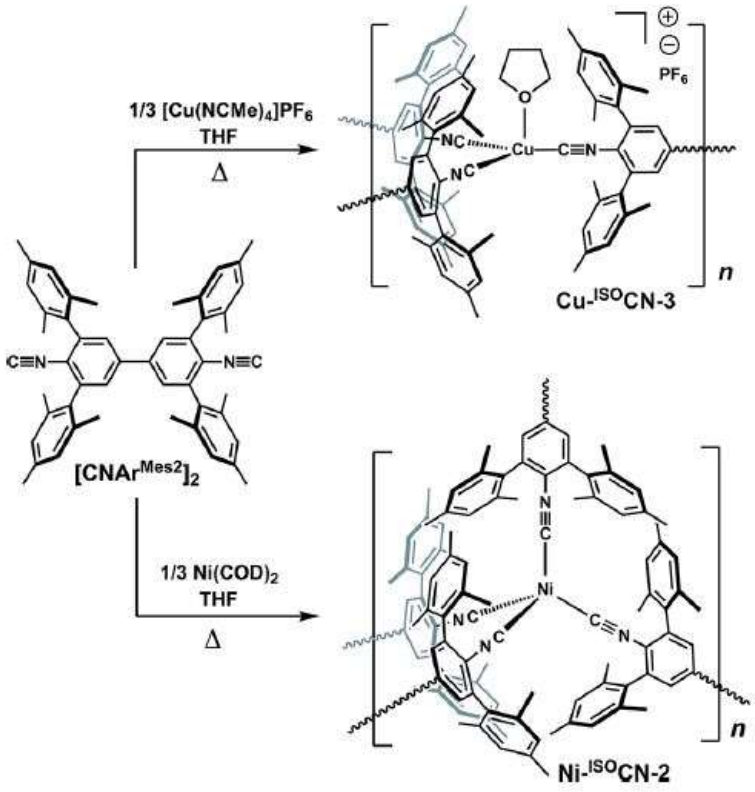

Scheme 2.1 Preparation of ^{ISO}CNs with the Ditopic *m*-Terphenyl Isocyanide $[CNAr^{Mes2}]_2$

porosity.[24,25] As demonstrated by Cu-^{ISO}CN-3, which features a non-interpenetrated hbc (6,3) net morphology,[46–48] close packing of two-dimensional honeycomb sheets and anion inclusion results in a pore-blocked material with low Langmuir surface area (ca. 200 m^2/g). Similarly, Ni-^{ISO}CN-2, which poses as a two-fold interpenetrated diamondiod network, is pore-blocked by entrapped noncoordinated $[CNAr^{Mes2}]_2$ molecules.[25] In Ni-^{ISO}CN-2, the constraints enforced by both interpenetration and the relatively short length of the coordinated diisocyanide linkers preclude the escape and/or displacement of the free $[CNAr^{Mes2}]_2$ units. However, over the past several years,

several strategies have emerged to increase the microporous or mesoporous environments within MOF-type materials. These include vertex modulation,[49] the use of templating agents,[50] systematic defect engineering,[51–53] postsynthetic linker degradation,[54,55] and synthetic expansion of linker lengths.[56,57] Of these approaches, linker expansion continues to be prominent, as it is the foundation of the isoreticular concept and is especially adept at retaining crystallinity properties across amended MOF materials.[8] Accordingly, here we report that simple expansion of the $[CNAr^{Mes2}]_2$ linker scaffold with a central phenylene group produces a thermally and chemically robust single crystalline Cu(I)-^{ISO}CN framework with a well-defined channel structure. Furthermore, we demonstrate that the channels formed within this linker-expanded material allow for chemical exchange of coordinated solvent ligands on the Cu(I) nodes, which can be assessed via single-crystal-to-single-crystal transformations or by direct spectroscopic interrogation.

2.2 Results and Discussion

The route utilized for the synthesis of $[CNAr^{Mes2}]_2$ was readily adaptable for the integration of a phenylene spacer.[24] Suzuki coupling of two equivalents of the *para*-boronic ester substituted aniline, H_2NAr^{Mes2}-*p*-BPin (Pin = pinacol), with 1,4-dibromobenzene provided the ditopic *m*-terphenyl aniline, 1,4-$(H_2NAr^{Mes2})_2C_6H_4$, in 84% yield after work up (Scheme 2.2). Sequential formylation and dehydration of 1,4-$(H_2NAr^{Mes2})_2C_6H_4$ afforded the expanded diisocyanide, 1,4-$(CNAr^{Mes2})_2C_6H_4$, as a colorless, nonvolatile solid in 82% overall yield relative to the ditopic aniline. Crystallographic characterization of 1,4-$(CNAr^{Mes2})_2C_6H_4$ revealed a rigid linear diisocyanide with a coplanar arrangement of the two Ar^{Mes2} groups, which is identical to that found in $[CNAr^{Mes2}]_2$ (Figure 2.1).[24] However, in 1,4-$(CNAr^{Mes2})_2C_6H_4$, the central phenylene, which is canted by ~36° relative to the Ar^{Mes2} groups, provides a ca. 4 Å greater separation between the isocyanide units relative to $[CNAr^{Mes2}]_2$ (16.5(1) Å vs 12.2(1) Å, respectively). The degree of this

expansion is similar to that found for successive phenylene-group additions to IRMOF-74 materials.[57] Diisocyanide 1,4-$(CNAr^{Mes2})_2C_6H_4$ is also characterized by a $^{13}C\{^1H\}$ NMR isocyanide carbon resonance of 167.7 ppm (C_6D_6) and a ν_{CN} stretching band at 2112 cm^{-1} in the solid state. These spectroscopic features are consistent with those of $[CNAr^{Mes2}]_2$ and other monotopic *m*-terphenyl isocyanides.[32,58,59]

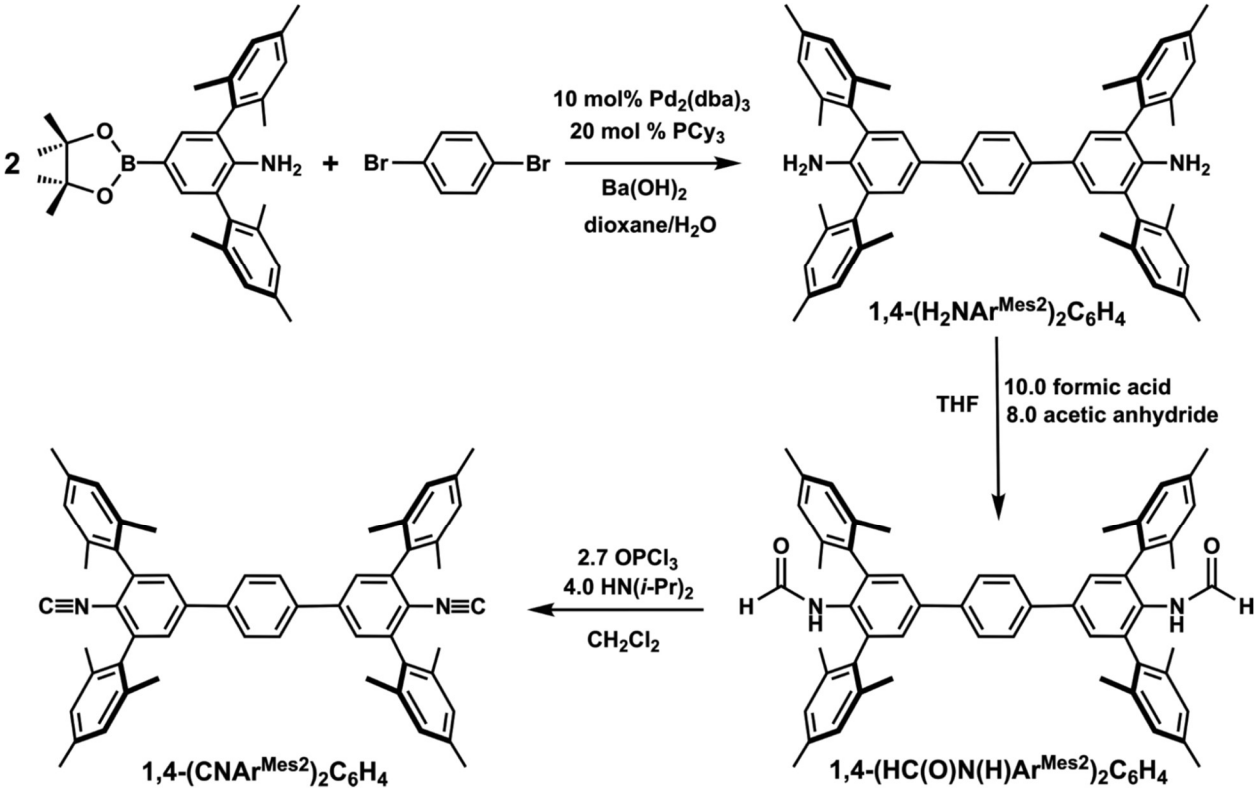

Scheme 2.2 Synthetic Route to the Expanded Ditopic *m*-Terphenyl Isocyanide 1,4-$(CNAr^{Mes2})_2C_6H_4$

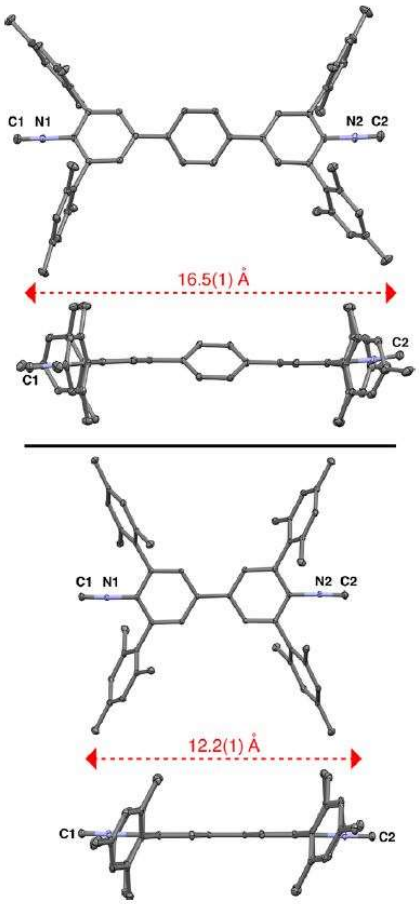

Figure 2.1 Molecular structure of 1,4-$(CNAr^{Mes2})_2C_6H_4$ (top) and topological comparison with $[CNAr^{Mes2}]_2$.

To investigate the utility of 1,4-$(CNAr^{Mes2})_2C_6H_4$ for ^{ISO}CN formation, we targeted the formation of Cu(I)-based frameworks to make direct comparisons with Cu(I)-^{ISO}CNs 1-3.[24] Similar to the synthesis of Cu-^{ISO}CN-3, addition of a THF solution of 1,4-$(CNAr^{Mes2})_2C_6H_4$ to a THF solution of $[Cu(NCMe)_4]PF_6$ at room temperature produced an amorphous pale-yellow polymeric material after stirring for 15 minutes. Heating this material in THF at 120 °C for 24 hours. Followed by slow cooling to 80 °C over the course of 48 hours, yielded large, colorless single crystals. ATR-IR spectroscopic analysis of these crystals revealed a single ν_{CN} band centered at 2142 cm^{-1}, which is similar to that found for the Cu(I)-based network material Cu-^{ISO}CN-3 (ν_{CN} = 2146 cm^{-1}) and indicates the presence of a similar electronic environment for the Cu centers in this

solid. Indeed, crystallographic structure determination revealed the formation of a network material, denoted Cu-^{ISO}CN-4, consisting of mononuclear four-coordinate $[Cu(THF)(CNR)_3]^+$ nodes linked by 1,4-$(CNAr^{Mes2})_2C_6H_4$ units (Scheme 2.3, Figure 2.2). These cationic nodes are well-separated from the $[PF_6]^-$ counterions, which are noncoordinating and located outside of the periphery formed by the three Ar^{Mes2} around the Cu centers. Consistent with the IR spectroscopic data, the $[Cu(THF)(CNR)_3]^+$ nodes in Cu-^{ISO}CN-4 are indistinguishable in composition to those found in Cu-^{ISO}CN-3 as well as the molecular complex $[Cu(THF)(CNAr^{Mes2})_3]OTf$ ($[OTf]^- = [O_3SCF_3]^-$). However, there is an increase in the degree of pyramidalization of the Cu centers in Cu-^{ISO}CN-4 relative to $[Cu(THF)(CNAr^{Mes2})_3]OTf$. This is illustrated by a 14.7° displacement of the Cu centers in Cu-^{ISO}CN-4 relative to the plane of the isocyanide carbon atoms, which is more

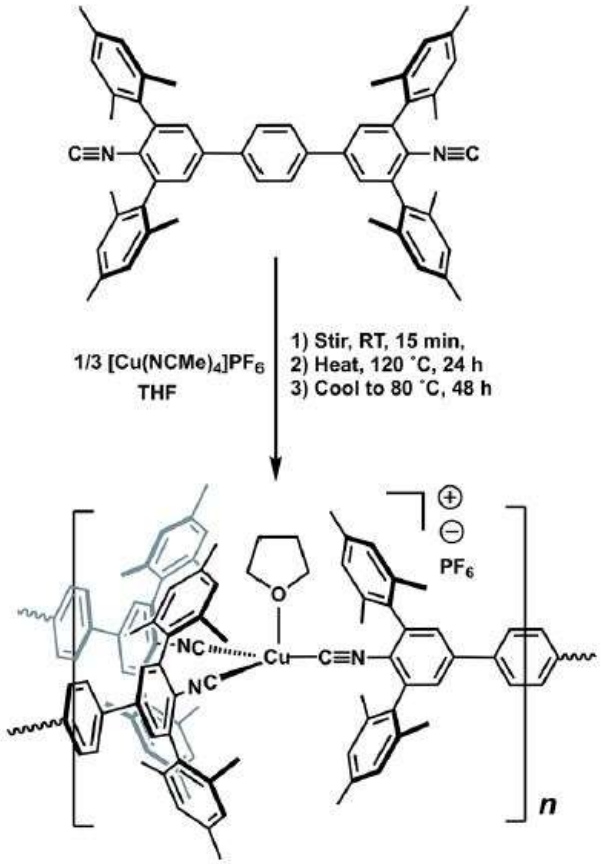

Scheme 2.3 Synthesis of Cu-^{ISO}CN-4 as a THF Adduct

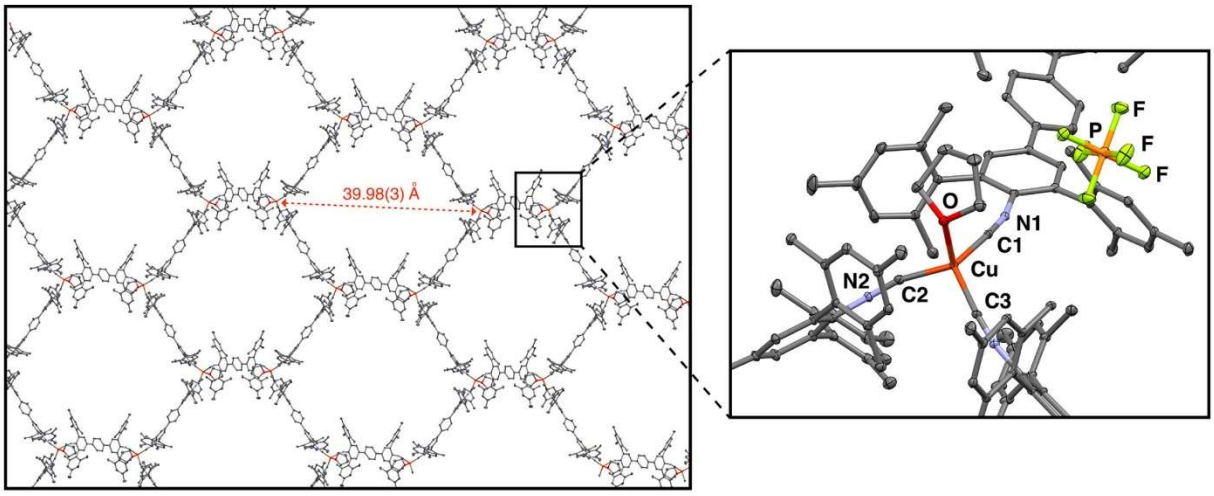

Figure 2.2 (left) Honeycomb structure of the 2D covalent net of Cu-^{ISO}CN-4 from single-crystal X-ray diffraction analysis. The largest distance across the hexagonal pore is indicated. (right) Zoom-in of mononuclear the $[Cu(THF)(CNR)_3]^+$ node that comprises the structural framework of Cu-^{ISO}CN-4 as its THF adduct.

than double that seen in the solid-state structure of $[Cu(THF)(CNAr^{Mes2})_3]OTf$ (6.9°). Given the similar compositional environment of these Cu centers, this structural deformation likely arises from limitations imposed by network formation as a slightly smaller but nonetheless pronounced pyramidalization is also present in Cu-^{ISO}CN-3 (12.7°).

Notably, the ν_{CN} spectroscopic response in these materials can be correlated with the degree of pyramidalization of the $[Cu(THF)(CNR)_3]^+$ core. For example, the molecular complex $[Cu(THF)(CNAr^{Mes2})_3]OTf$ (ν_{CN} = 2160 cm^{-1}) features the least pyramidalized $[Cu(THF)(CNR)_3]^+$ core and correspondingly gives rise to the highest energy ν_{CN} band of the series. Accordingly, as pyramidalization at the copper center increases, a decrease in the energy of the ν_{CN} band is expected to result due to there being less Cu s-orbital character in the Cu/isocyanide σ-bonding interaction. This follows from the well-established observation that metal centers having significant s-orbital character, most notably low-coordinate Cu(I) and Au(I) complexes, are poor π-bases but are

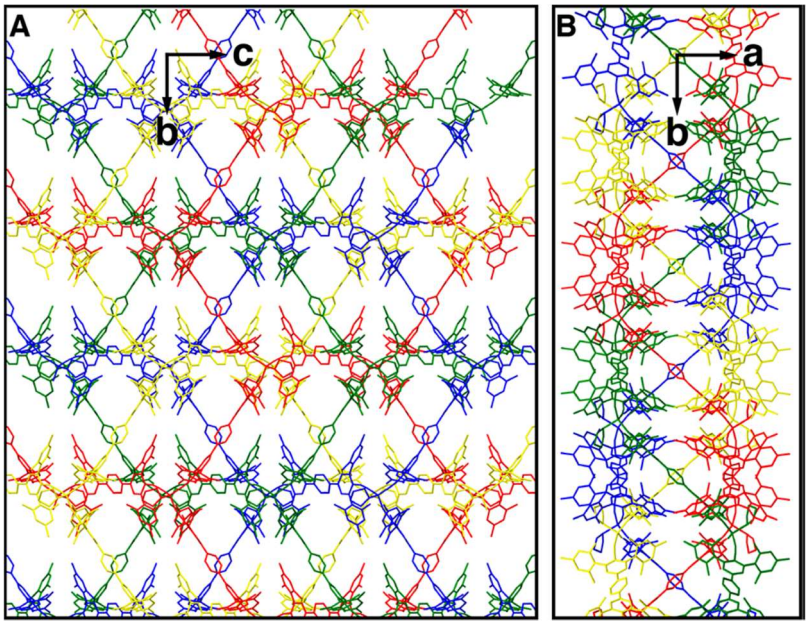

Figure 2.3 Views of the fourfold interpenetrated structure of Cu-^{ISO}CN-4. (left) View of interpenetration in the crystallographic BC plane showing the interweaving of four 2D honeycomb networks to form a dense-packed arrangement. Each independent 2D sheet is color-differentiated. (right) View of one fourfold interpenetrated layer within the crystallographic AB plane. Stacks of these layers form the extended network of Cu-^{ISO}CN-4.

effective at stabilizing the carbon-centered isocyanide lone pair via σ-accepting orbital interaction.[60–62] In the absence of significant π-backdonation, such stabilization of the isocyanide lone pair, which possesses some C-N σ* character, results in a strengthening of the isocyanide CN triple bond and a corresponding increase in energy of the ν_{CN} band. Consistent with this electronic structure description, Cu-^{ISO}CN-4, with the most pyramidalized Cu centers of the series, gives rise to the lowest energy ν_{CN} band. Significantly, as isocyanide linkers allow the metal-based nodes in ^{ISO}CN materials to be directly interrogated by IR spectroscopy, the establishment of such geometric structure/spectroscopic response correlations represents a potentially useful method for identifying and rationalizing nodal structural features, especially for instances where crystallographic information is unavailable.

Similar to Cu-^{ISO}CN-3, the threefold symmetric $[Cu(THF)(CNR)_3]^+$ nodes within Cu-^{ISO}CN-4 covalently organize into a two-dimensional honeycomb network. However, the expanded 1,4-$(CNAr^{Mes2})_2C_6H_4$ linker creates a hexagonal ring structure with a diameter of approximately

4.0 nm at its largest point (Figure 2.2). This is significantly larger than the 2.1 nm-wide ring in Cu-^{ISO}CN-3 formed from the shorter $[CNAr^{Mes2}]_2$ ligand. However, the structural expansion in Cu-^{ISO}CN-4 leads to significant interpenetration through these hexagonal pores, which is a feature not present within the solid-state structure of Cu-^{ISO}CN-3. Inspection of the extended structure of Cu-^{ISO}CN-4 (*Pccn* space group) reveals that it forms a four-fold interpenetrated hcb (6,3) net,[46–48] where four independent two-dimensional sheets interweave to form a covalently linked layer along the crystallographic *BC* plane (Figure 2.3). These interpenetrated layers stack along the *a*-axis to form the extended structure. As shown in Figure 2.3, there are two sets of parallel interpenetration within these discrete layers. Along the *b*-axis, two 2D sheets run parallel to each other in an interwoven manner and intersect at both Cu(I) nodes and the central phenyl unit of the 1,4-$(CNAr^{Mes2})_2C_6H_4$ linker, while the other two parallel-interpenetrated sheets run in the opposite direction with identical intersection points.

Most interestingly, while significant structural interpenetration is usually deleterious for the retention of pore/channel structure in reticular materials,[63,64] the layered morphology of Cu-^{ISO}CN-4 creates a well-defined channel structure that arises as a consequence of interpenetration, As shown in a cross-sectional slice of the *AC* plane (Figure 2.4), Cu-^{ISO}CN-4 features well-defined channels that transverse the crystallographic *b*-axis. Importantly, these channels are formed within the interpenetrated layers/domains of Cu-^{ISO}CN-4 rather than arising from the stacking orientation of the interpenetrated layers themselves. The channels have an aperture size of approximately 28 X 19 Å (Figure 2.4) and are occupied by free THF solvent molecules that presumably incorporated during synthesis. Notably, the $[PF_6]^-$ counterions are not located within the channels traversing the *b*-axis. Instead, these counterions are located in a separate interdomain layer within a matrix formed from the *m*-terphenyl units. Accordingly, while parallel fourfold interpenetration is

responsible for covalently binding an interpenetrated layer, these discrete layers stack through a combination of electrostatic interactions between the $[PF_6]^-$ anions and the cationic $[Cu(THF)(CNR)_3]^+$ nodes as well as through dispersion interactions between ligand aryl groups. Dispersion-type interactions have been previously observed to bind 2D-layered network materials into 3D lattices, especially for network materials that can be mechanically exfoliated into so-called metal-organic nanosheets (MONs).[65–67]

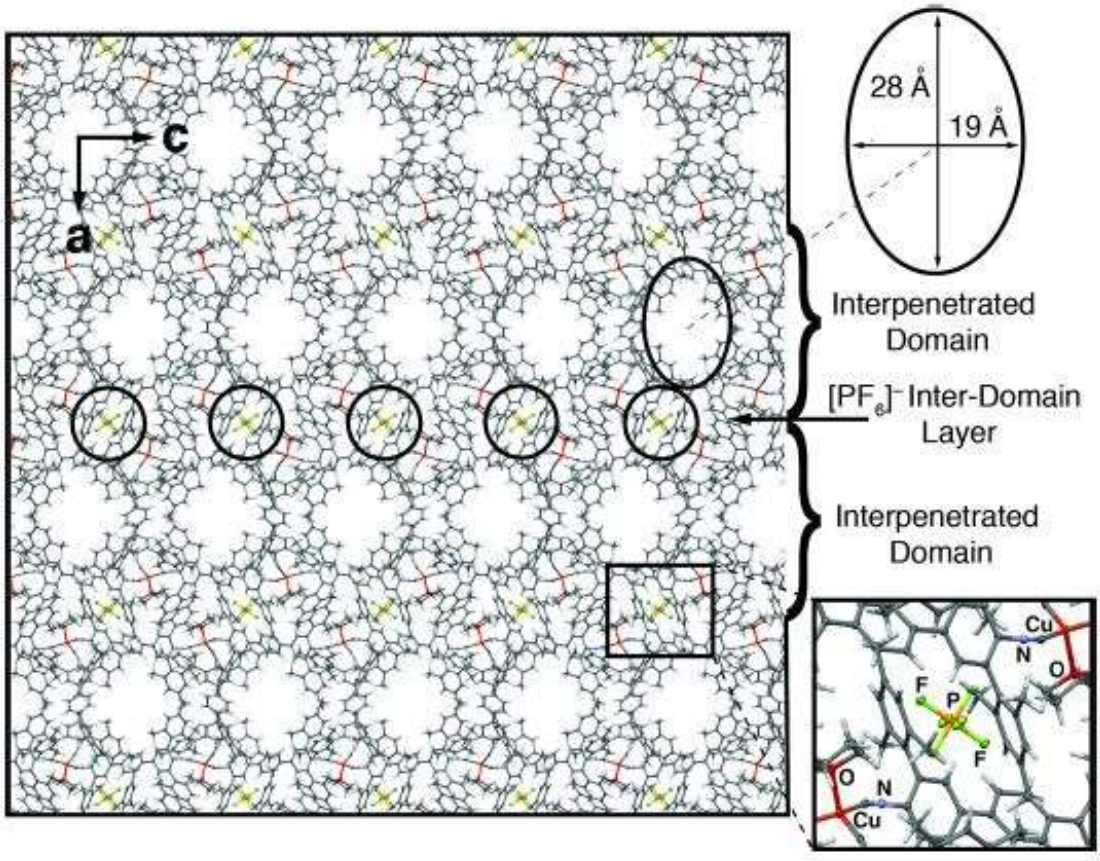

Figure 2.4 Channel structure of Cu-^{ISO}CN-4 viewed down the crystallographic *b* axis. The interpenetrated domain layers are indicated on the right along with the $[PF_6]^-$ anion interdomain layer. Zoom-in on the bottom right depicts an individual $[PF_6]^-$ anion along with relative positioning of two $[Cu(THF)(CNR)_3]^+$ nodes from different interpenetrated domains.

Despite its layered nature, Cu-^{ISO}CN-4 displays good overall thermal stability properties and well-defined thermal behavior of both free and coordinated THF molecules.

Thermogravimetric analysis (TGA) on a single-crystalline sample of Cu-^{ISO}CN-4 harvested from the reaction mixture and subjected to brief drying under vacuum (15 minutes) revealed a downward slope between 75 and 200 °C (Figure 2.22). This feature is attributed to the loss of free THF molecules within the channels of Cu-^{ISO}CN-4 and accounts for a 7.5% mass loss. A second loss of mass, corresponding to 6.0% of the sample, commences at 290 °C and is attributed to thermally induced dissociation of the Cu-coordinated THF molecules. Notably, these sequential mass losses indicate a roughly 1:1 ratio of channel-confined solvent molecules per Cu node in the as-synthesized framework. In addition, dissociation of coordinated THF in Cu-^{ISO}CN-4 occurs at a temperature similar to that of Cu-^{ISO}CN-3 (281 °C),[48] thereby signifying a conserved thermochemical behavior of the $[Cu(THF)(CNR)_3]^+$ nodes despite differing morphological environments. Full decomposition of Cu-^{ISO}CN-4 occurs at 400 °C, which again highlights the overall thermal stability that can be achieved through network formation using organometallic metal-isocyanide linkages.

More remarkably, Cu-^{ISO}CN-4 also displays excellent stability to both air and moisture. For example, crystalline samples of Cu-^{ISO}CN-4 subjected to drying under vacuum overnight are indefinitely stable to ambient atmospheric conditions on the benchtop. As assessed by intermittent (24 hours) ATR-IR analysis, Cu-^{ISO}CN-4 crystals exposed to air over the course of 2 weeks showed no change in the ν_{CN} band and did not indicate the appearance of the free 1,4-$(CNAr^{Mes2})_2C_6H_4$ linker. Similarly, addition of Cu-^{ISO}CN-4 crystals to deionized water, in which they are insoluble, resulted in no chemical degradation over the course of 5 days when sample was filtered, dried under vacuum, and analyzed by ATR-IR spectroscopy. However, while the Cu-^{ISO}CN-4 is chemically resistant to liquid water, PXRD analysis after 1 and 5 days of exposure revealed that the crystallinity of the material slowly degrades, which we believe is likely due to disruption of

the $[PF_6]^-$ interlayer domain (Figure 2.20). Notably, in these experiments, Cu-^{ISO}CN-4 was buoyant in liquid water. We believe this macroscopic property is derived from a combination of its relatively low calculated density from crystallographic studies (ρ_{calc} = 1.01 g/cm^3) and surface tension effects arising from the hydrophobic nature of the *m*-terphenyl group environment.[68] Consistent with the former notion, the theoretical mass contribution of heavy elements (i.e., Cu + P) in the unsolvated form of Cu-^{ISO}CN-4 is only 7.3% of the total mass. This property indicates that Cu-^{ISO}CN-4 can be considered an intrinsically low-density solid-state organometallic material despite a heavy degree of interpenetration and compact channel structure. Furthermore, contact angle hydrophobicity determination resulted in a measured value of 120°, which rivals that of fluorinated polyolefin materials and supports the notion that Cu-^{ISO}CN-4 presents a distinctly hydrophobic surface environment.[69–71] However, the overall stability of Cu-^{ISO}CN-4 to liquid water at room temperature is likely also aided by the hydrolytic insensitivity of the metal-isocyanide M-C bond to oxygen-based nucleophiles at neutral pH.[72]

Whereas placement of Cu-^{ISO}CN-4 in water does not lead to chemical degradation, inspection of the internal channel structure reveals that it is lined with $[Cu(THF)(CNR)_3]^+$ nodal sites (Figure 2.5), which are presumably accessible to solvent and/or substrate molecules that penetrate the channels. Porosimetry measurements with either N_2 (77 K) or CO_2 (298 K) on samples of Cu-^{ISO}CN-4 activated at 200 °C for 24 hours revealed negligible observed surface area (Figure 2.23 and Figure 2.24), which, as determined by PXRD measurements, is a consequence of collapse of the crystalline layer structure upon thermal activation (Figure 2.21).[73–75] However, it is important to emphasize that in the ATR-IR spectrum of H_2O-treated Cu-^{ISO}CN-4, there is no change in the position of the ν_{CN} band (Figure 2.14). This observation suggests that the Cu-bound THF molecules are retained on the nodal sites and that H_2O likely does not penetrate the channels

within inactivated (i.e., as prepared) Cu-^{ISO}CN-4 in concentrations high enough to displace coordinated THF. While this presumed lack of H_2O penetration can be rationalized in terms of the hydrophobic environment within the channels of Cu-^{ISO}CN-4, it also suggests that nonpolar but more Lewis basic substrates may readily access the channels and displace the Cu-coordinated THF ligands. Consistent with this hypothesis, placement of single crystals of Cu-^{ISO}CN-4 in a THF solution containing pyridine (py; 5.0 equivalents/Cu center) for 12 hours followed by redetermination of the X-ray crystal structure resulted in displacement of the coordinated THF ligand by pyridine (Scheme 2.4, Figure 2.6). As this represents a single-crystal-to-single-crystal transformation, the morphological properties of THF- and py-coordinated Cu-^{ISO}CN-4 are identical, and the coordinated py-ligand is present at 100% occupancy. Notably, the copper centers in py-coordinated Cu-^{ISO}CN-4 display a higher degree of pyramidalization (17.4°) than that of the THF-coordinated framework. This increased pyramidalization is consistent with the stronger σ-donor strength of pyridine relative to THF, which has been noted previously to affect the metal-core structural properties in Cu(I) *m*-terphenyl isocyanide complexes.[58] Furthermore, consistent with greater Cu-core pyramidalization, ATR-IR analysis of py-coordinated Cu-^{ISO}CN-4 gives rise to a ν_{CN} band centered at 2126 cm^{-1}, which further supports the notion that IR spectroscopic properties of these ^{ISO}CN materials can directly report on the structural aspects of the framework nodes. However, in this latter case, it is important to emphasize that a direct correlation between the ν_{CN} band of Cu-^{ISO}CN-4 and the σ-donor strength of pyridine can also be used to spectroscopically assess a substrate binding event from a fluid mixture.

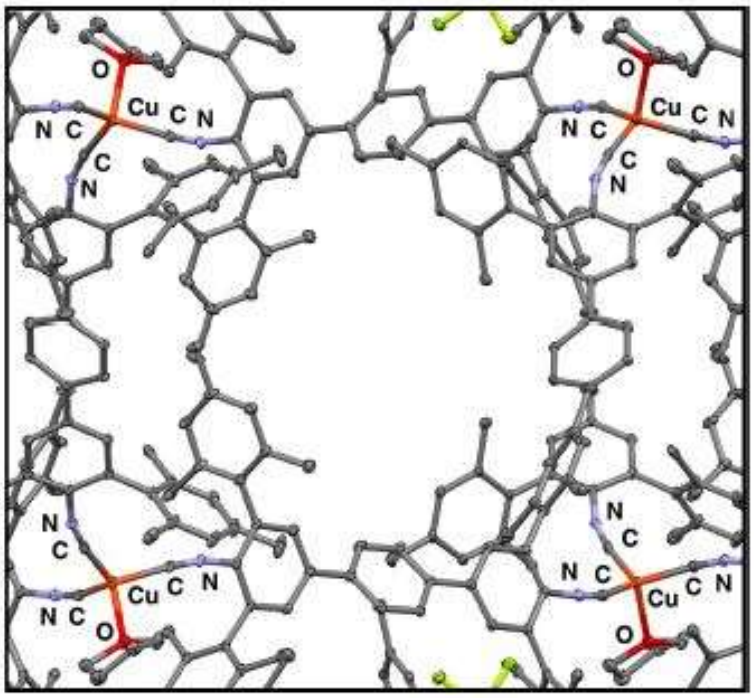

Figure 2.5 View of an individual channel of THF-coordinated Cu-^{ISO}CN-4 showing position of $[Cu(THF)(CNR)_3]^+$ nodes.

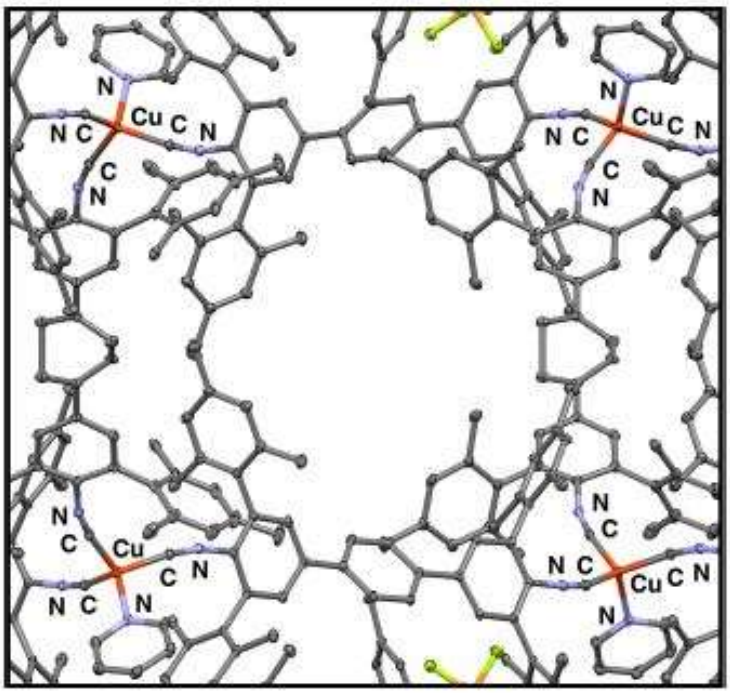

Figure 2.6 View of an individual channel of pyridine-coordinated Cu-^{ISO}CN-4 showing full pyridine for THF exchange on the Cu(I) nodes.

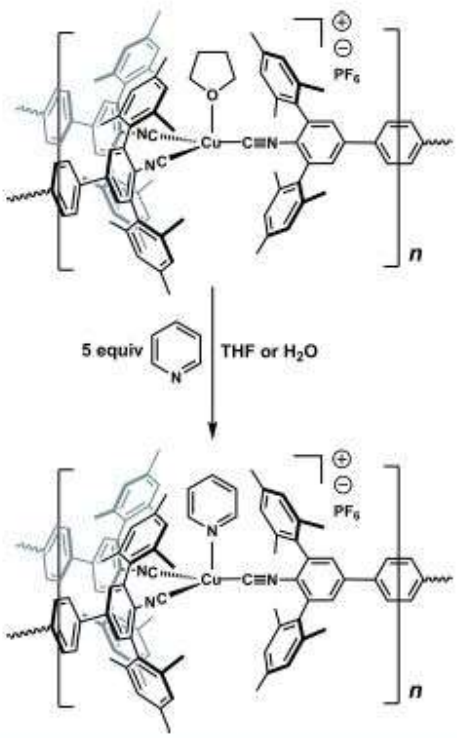

Scheme 2.4 Pyridine-for-THF Ligand Exchange in Cu-^{ISO}CN-4

Given the findings that Cu-^{ISO}CN-4 seemingly repels H_2O from its internal structure but covalently binds pyridine, we postulated that this network could potentially extract pyridine from aqueous solution. Pyridine is a known industrial wastewater contaminant and is highly soluble in aqueous media over a broad pH range (either as free base or pyridinium ion),[76–78] thereby rendering separation difficult. To assess this potential, as-synthesized Cu-^{ISO}CN-4 was placed in 10 mL of deionized water containing 5.0 equivalents of pyridine (per Cu center). ATR-IR spectroscopic analysis of dried crystals that had been soaked in this mixture for 24 hours, where negligible decreases in crystallinity are observed, showed the formation of a ν_{CN} band indicative of py-coordinated Cu-^{ISO}CN-4 (Figure 2.16). After 24 hours, the IR data suggest that this THF/py exchange reaction in H_2O proceeded with approximately 85% efficiency. However, this result suggests that the hydrophobic interior of Cu-^{ISO}CN-4 may adequately partition some nonpolar

organic compounds from aqueous solution, while the substitutionally labile Cu center provides a well-defined chemisorption site for substrates having Lewis basicity properties greater than the THF ligand arising from solvothermal synthesis. Accordingly, additional investigations into the scope, energetics, and general applicability of such separations are in progress.

2.3 Conclusions

In conclusion, the isocyanide coordination network Cu-^{ISO}CN-4, possessing a phenylene-expanded ditopic *m*-terphenyl isocyanide linker, serves as an additional example of a robust hybrid metal-organic framework material constructed from metal-carbon bonds. Similar to the previously reported material Cu-^{ISO}CN-3, the presence of *m*-terphenyl groups within Cu-^{ISO}CN-4 encourages the formation of a cationic $[Cu(THF)(CNR)_3]^+$ core that is well-defined and functions as a single-metal structural node. While the topological expansion of 1,4-$(CNAr^{Mes2})_2C_6H_4$ linker resulted in a highly interpenetrated internal structure, confinement of this interpenetration into layers fortuitously resulted in formation of solvent accessible channels along a unique axis within Cu-^{ISO}CN-4. While these channels enable facile exchange of the Cu-coordinated THF ligand with pyridine, the distinctly hydrophobic environment created by the ditopic *m*-terphenyl backbone excludes water from the interior of Cu-^{ISO}CN-4. This property is also responsible for a marked stability of Cu-^{ISO}CN-4 toward both liquid water and air. Accordingly, we believe this combination of metal-based reactivity and degradative resistance toward ambient environmental conditions renders Cu-^{ISO}CN-4 and related ^{ISO}CN materials as potentially promising candidates for applications in chemical separations and catalysis. As a final note, this study has also demonstrated that geometric structure/spectroscopic response correlations can be developed for a series of ^{ISO}CN materials. This is a unique and beneficial property offered by isocyanide linker groups, as they enable direct and facile spectroscopic interrogation of network material structural nodes. We

anticipate that such correlations will be invaluable to aiding the determination of structural and chemical outcome applications where ^{ISO}CN materials are employed.

2.4 Experimental Section

General Considerations. Unless otherwise stated, all manipulations were performed under an atmosphere of dry dinitrogen using standard Schlenk and glovebox techniques. Solvents were dried and degassed according to standard procedures.[79] Unless otherwise stated, reagent grade starting materials were purchased from commercial sources and purified where necessary according to standard procedures.[80] The boronic ester H_2NAr^{Mes2}-*p*-BPin was prepared as previously reported. Solution ^{1}H and ^{13}C{^{1} H} NMR spectra were recorded on a Bruker 300 spectrometer, a Varian 400 spectrometer, a Varian X-Sens 500 spectrometer, or a JEOL ECA-500 spectrometer. ^{1}H and ^{13}C{^{1} H} NMR chemical shifts are reported in ppm relative to $SiMe_4$ (^{1}H and ^{13}C{^{1} H} δ = 0.0 ppm) with reference to residual proton resonances of δ = 7.16 ppm (^{1} H, C_6D_6) and δ = 7.26 ppm (^{1}H $CDCl_3$).[81] Solid-state IR spectra were collected at 2 cm^{-1} resolution as either a KBr pellet or using a Bruker Platinum Alpha ATR-IR equipped with a diamond crystal. The following abbreviations are used to describe the intensity and characteristics of important IR absorption bands: vs = very strong, s = strong, m = medium, w = weak, vw = very weak, b = broad, vb = very broad, sh = shoulder. Samples for powder X-ray diffraction were mounted on nylon loops with minimal Paratone oil and were analyzed at 300 K under a dinitrogen stream using Cu Kα radiation (l = 1.54178 Å) on a Bruker Kappa diffractometer equipped with a VÅNTEC-500 area detector and an Oxford Cryostream 700. HR-MS spectra were recorded at the UCSD Molecular Mass Spectrometry Facility using an Agilent 6230 Accurate-Mass TOFMS.

Synthesis of 1,4-(H_2NAr^{Mes2})$_2C_6H_4$. A resealable ampule was charged with H_2NAr^{Mes2}-*p*-BPin (1.00 g, 2.45 mmol, 2.0 equiv), 1,4- dibromobenzene (0.288 g, 1.22 mmol, 1.0 equiv), Pd_2dba_3

(0.112 g, 0.122 mmol, 10 mol %; dba = dibenzylideneacetone), PCy_3 (0.068 g, 0.244 mmol, 20 mol %), and $Ba(OH)_2$ (0.730 g, 4.27 mmol, 3.5 equiv) and dioxane (20 mL). To this was added degassed, deionized H_2O (5.5 mL), and the mixture was vigorously stirred at 80 °C for 24 hours under an atmosphere of N_2. The mixture was cooled, filtered through a medium porosity fritted funnel packed with Celite, and the filter cake was extracted with CH_2Cl_2 (3 × 15 mL). The filtrate was stripped of volatiles under reduced pressure, providing a yellow solid. The solid was dissolved in 100 mL CH_2Cl_2 and washed with aqueous HCl (100 mL, pH ≈ 6), neutral H_2O (100 mL) and brine (150 mL). The aqueous washes were then combined and extracted with CH_2Cl_2 (3 × 100 mL). The organic extracts were combined, dried over $MgSO_4$, filtered, and volatiles were removed by rotary evaporation. The resultant solid was purified by column chromatography (silica gel) using a gradient of 0 to 3% EtOAc/hexanes, collecting the middle fractions. The fractions were combined and concentrated under reduced pressure to provide [$(H_2NAr^{Mes2})_2C_6H_4$] as a light yellow solid. Yield: 0.750 g, 1.02 mmol, 84%. ^{1}H NMR (300 MHz, $CDCl_3$, 20 °C): δ = 7.57 (s, 4H, *p*-Ph), 7.26 (s, 4H, *m*-Ar), 6.99 (s, 8H, *m*-Mes), 3.24 (bs, 4H, N*H*$_2$), 2.34 (s, 12H, *p*-Mes−C*H*$_3$), 2.10 (s, 24H, *o*-Mes−C*H*$_3$) ppm. ^{13}C{^{1}H} NMR (125.7 MHz, $CDCl_3$, 20 °C) 140.2, 138.7, 137.1, 137.0, 135.3, 130.3, 128.4, 126.8, 126.2, 126.1, 21.1 (*p*-Mes-*C*H$_3$), 20.2 (*o*-Mes-*C*H$_3$) ppm. FTIR-ATR (diamond surface, 20 °C) 3463 (w), 3365 (w), 3389 (w), 3339 (w), 3219 (w), 3009 (w), 2935 (w), 2968 (w), 2883 (w), 1607 (m), 1450 (s), 1240 (w), 1024 (m), 849 (s) cm^{-1}. HR-MS (ESI-TOFMS): Predicted *m/z* for $[C_{54}H_{57}N_2]^+$: 733.4516. Found *m/z* = 733.4518 ($[M + H]^+$).

Synthesis of 1,4-(HC(O)N(H)Ar^{Mes2})$_2$C$_6$H$_4$. Formic acid (0.471 g, 10.2 mmol, 10.0 equiv) was added dropwise via syringe to a stirring THF solution of 1,4-$(H_2NAr^{Mes2})_2C_6H_4$ (0.750 g, 1.02 mmol, 1.0 equiv). While the mixture was vigorously stirring, acetic anhydride (0.833 g, 8.16

mmol, 8 equiv) was added dropwise via syringe. The mixture was stirred for 16 h at room temperature, after which all volatiles were removed by rotary evaporation. Excess formic acid and acetic acid was removed upon heating the mixture to 80 °C for 2 h under dynamic vacuum. This resulted in the isolation of the bisformamide 1,4-(HC(O)N(H)Ar^{Mes2})$_2C_6H_4$ as light yellow solid, which was used without further purification. Yield: 0.764 g, 0.968 mmol, 95%. ^{1}H NMR (300 MHz, $CDCl_3$, 20 °C): δ = 7.69 (s, 2H, NHC(O)*H*), 7.65 (s, 4H, *p*-Ph), 7.44 (s, 4H, *m*-Ar), 6.98 (s, 8H, *m*-Mes), 6.77 (s, 2H, N*H*C(O)H), 2.33 (s, 12H, *p*-Mes−C*H*$_3$), 2.07 (s, 24H, *o*-Mes−C*H*$_3$). $^{13}C\{^1H\}$ NMR (125.7 MHz, $CDCl_3$, 20 °C) 162.4 (H*C*(O)N), 138.7, 138.1, 137.1, 135.8, 134.3, 133.6, 128.9, 128.5 128.3, 127.2, 21.1 (*p*-Mes-*C*H$_3$), 20.5 (*o*-Mes-*C*H$_3$) ppm. FTIR ATR (diamond surface, 20 °C): ν_{CO} = 1696 cm^{-1} (s), ν_{NH} = 3372 cm^{-1}(w), also 2946 (w), 2915 (w), 2852 (w), 1610 (w), 1456 (m), 1376 (w), 1257 (m) cm^{-1}. HR-MS (ESI-TOFMS): Predicted *m/z* for $[C_{56}H_{57}N_2O_2]^+$: 789.4415. Found *m/z* = 789.4412 ($[M + H]^+$).

Synthesis of 1,4-($CNAr^{Mes2}$)$_2C_6H_4$. To a stirring CH_2Cl_2 solution of 1,4-(HC(O)N(H)Ar^{Mes2})$_2C_6H_4$ (0.764 g, 0.968 mmol, 1 equiv) was added diisopropylamine (0.392 g, 3.88 mmol, 4 equiv) via syringe. After stirring for 5 min, $OPCl_3$ (0.402 g, 2.62 mmol, 2.7 equiv) was added dropwise via syringe and the solution was stirred for 24 h. Aqueous Na_2CO_3 (1.5 M, 75 mL) was added and the resulting mixture was stirred for 2 h. The organic and aqueous layers were then separated, and the organic layer was washed with 50 mL H_2O. The aqueous layers were combined and extracted with CH_2Cl_2 (3 × 50 mL). The organic extracts were combined and dried over $MgSO_4$, filtered, and volatiles were removed by rotary evaporation. The resultant solid was washed with cold acetonitrile, collected by filtration, and dried under reduced pressure. Yield: 0.635 g, 0.841 mmol, 87%. ^{1}H NMR (300 MHz, $CDCl_3$, 20 °C): δ = 7.68 (s, 4H, *p*-Ph), 7.51 (s, 4H, *m*-Ar), 7.00 (s, 8H, *m*-Mes), 2.34 (s, 12 H, *p*-Mes−C*H*$_3$), 2.09 (s, 24H, *o*-Mes−C*H*$_3$). $^{13}C\{^1H\}$

NMR (125.7 MHz, $CDCl_3$, 20 °C) 167.5 (C≡N), 141.1, 139.9, 138.9, 137.9, 135.7, 133.9, 128.5, 127.7, 127.5, 124.9, 21.2 (*p*-Mes-*C*H_3), 20.3 (*o*-Mes- *C*H_3) ppm. FTIR-ATR (diamond surface, 20 °C) ν_{CN} = 2112 cm^{-1} (s), also 2956 (s), 2927 (s), 2867 (s), 1607 (m), 1570 (w), 1458 (m), 1368 (s), 1103 (m), 878 (s) cm^{-1}. HR-MS (ESI-TOFMS): Predicted *m/z* for $[C_{54}H_{53}N_2]^+$: 753.4203. Found *m/z* = 753.4197 ($[M + H]^+$).

Synthesis of Cu-^{ISO}CN-4. To a stirring THF solution of $[Cu(MeCN)_4]PF_6$ (0.004 g, 0.011 mmol, 2 mL) in a thick-walled pressure tube was added a THF solution of 1,4-$(CNAr^{Mes2})_2C_6H_4$: (0.020g, 0.026 mmol, 2 mL; 2.4 equiv) over 30 sec. Upon addition of approximately half the solution of 1,4-$(CNAr^{Mes2})_2C_6H_4$, a white suspension evolved and remained throughout the rest of the addition. The mixture was allowed to stir for 15 min and an amorphous polymer was deposited on the tube wall. The supernatant was removed, and the solid was gently washed with THF (3 × 10 mL). Fresh THF (2 mL) was added to the solid, and the tube was then sealed with a Teflon screw cap equipped with a Viton O-ring. The tube was placed in an oven with a temperature program set to heat at 120 °C for 24 h and cool to 80 °C over the course of 48 h. In place of the amorphous polymer was a colorless crystalline solid, which single crystals could be selected for X-ray crystallographic analysis. Bulk collection of the material is performed via the addition of 5 mL THF, followed by 10 min sonication in a room temperature bath. The suspended solid was subjected to centrifugation. The supernatant removed via pipet and the remaining solid was then in vacuo to afford microcrystalline material. Yield: 0.014 g, 0.010 mmol (based on the Cu-based repeat unit), 38% (based on linker). FTIR-ATR (diamond surface, 20 °C) 2142 cm^{-1}.

Synthesis of Pyridine-Coordinated Cu-^{ISO}CN-4. To large single crystals of Cu-^{ISO}CN-4 (0.008 g, 0.003 mmol, 1.0 equiv) was added a THF solution containing pyridine (0.001 mg, 0.0143 mmol,

5.0 equiv; 5 mL). This mixture was left to sit 12 h, whereupon single the crystals were removed and analyzed by X-ray diffraction. Single crystal structure analysis on two independent samples revealed the formation of py-coordinated Cu-^{ISO}CN-4. FTIR-ATR analysis on bulk crystals (diamond surface, 20 °C): 2126 cm^{-1}.

2.5 Spectroscopic Data

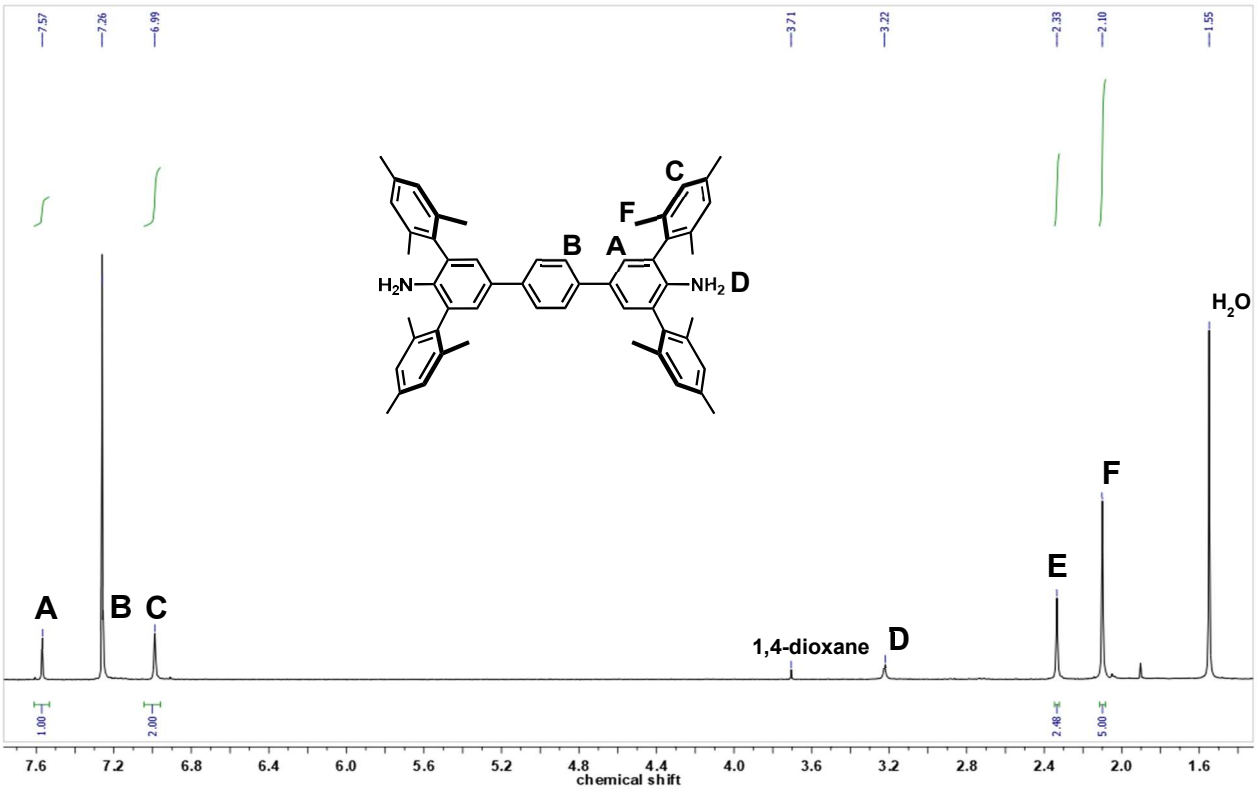

Figure 2.7 [1] H NMR spectrum ($CDCl_3$, 300 MHz, 20 ˚C) of 1,4-$(NH_2Ar^{Mes2})_2C_6H_4$.

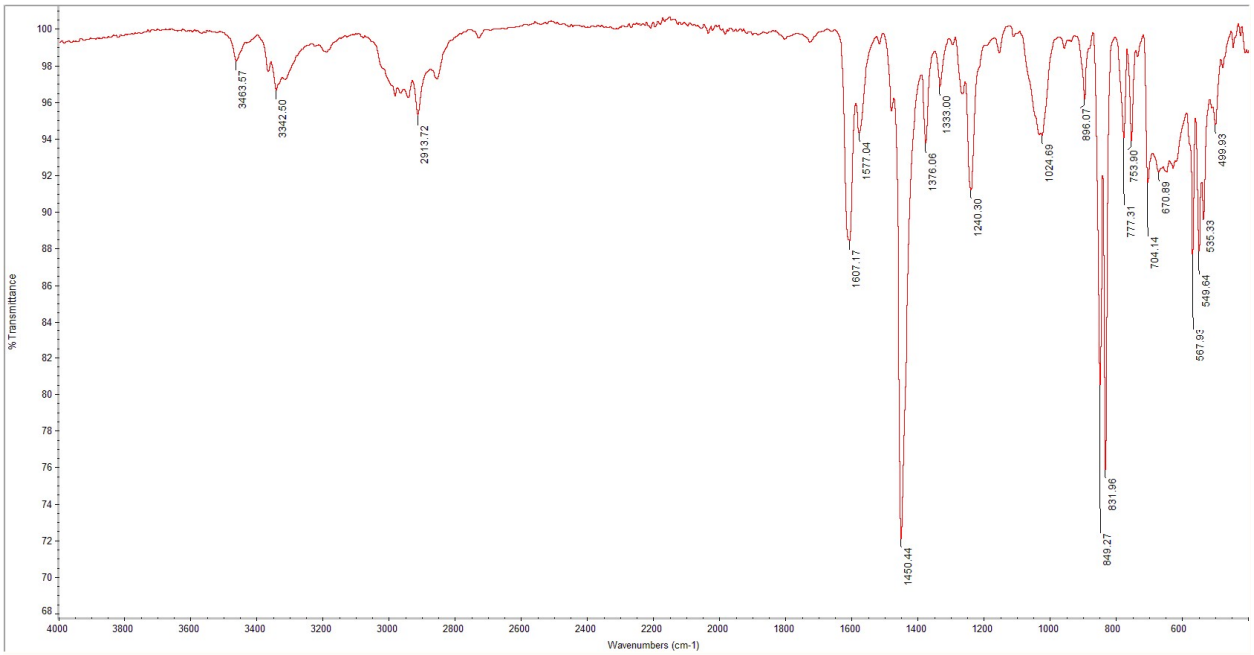

Figure 2.8 ATR-IR spectrum (20 ˚C) of 1,4-$(NH_2Ar^{Mes2})_2C_6H_4$.

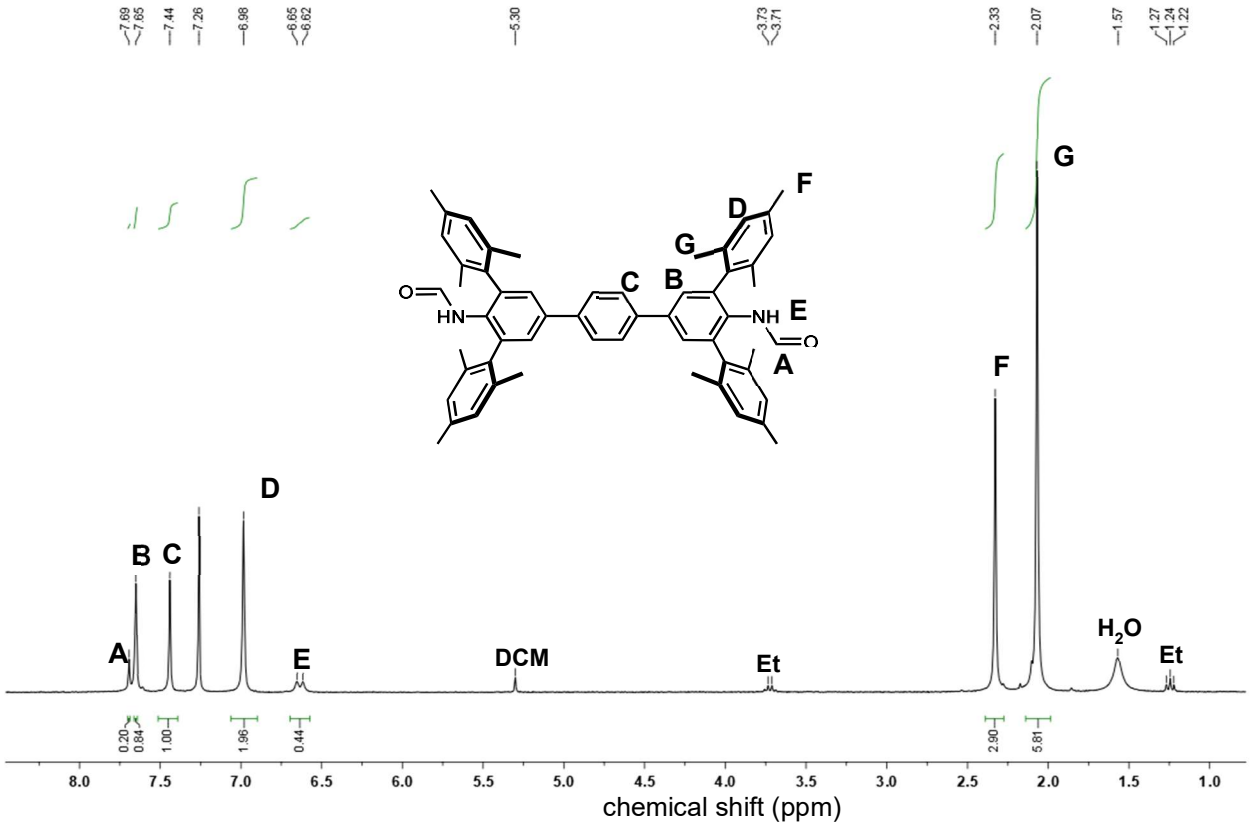

Figure 2.9 ^{1}H NMR spectrum ($CDCl_3$, 300 MHz, 20 ˚C) of 1,4-(HC(O)NHAr^{Mes2})$_2$C$_6$H$_4$.

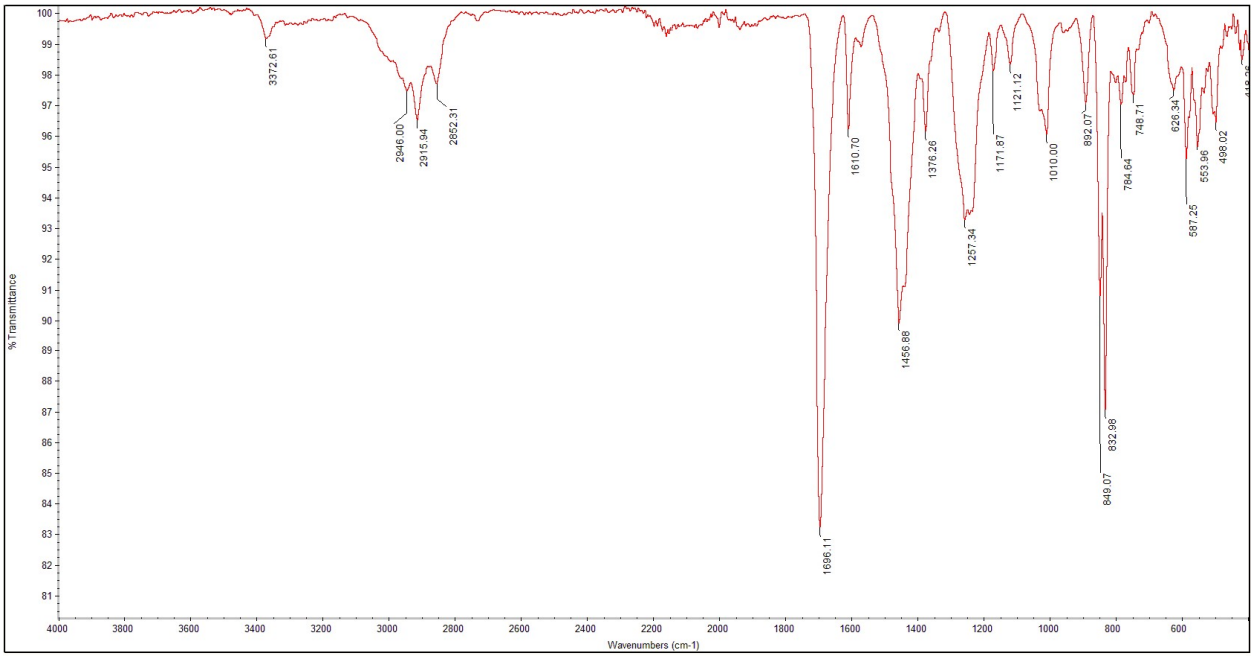

Figure 2.10 ATR-IR spectrum (20 ˚C) of 1,4-(HC(O)NHAr^{Mes2})$_2$C$_6$H$_4$.

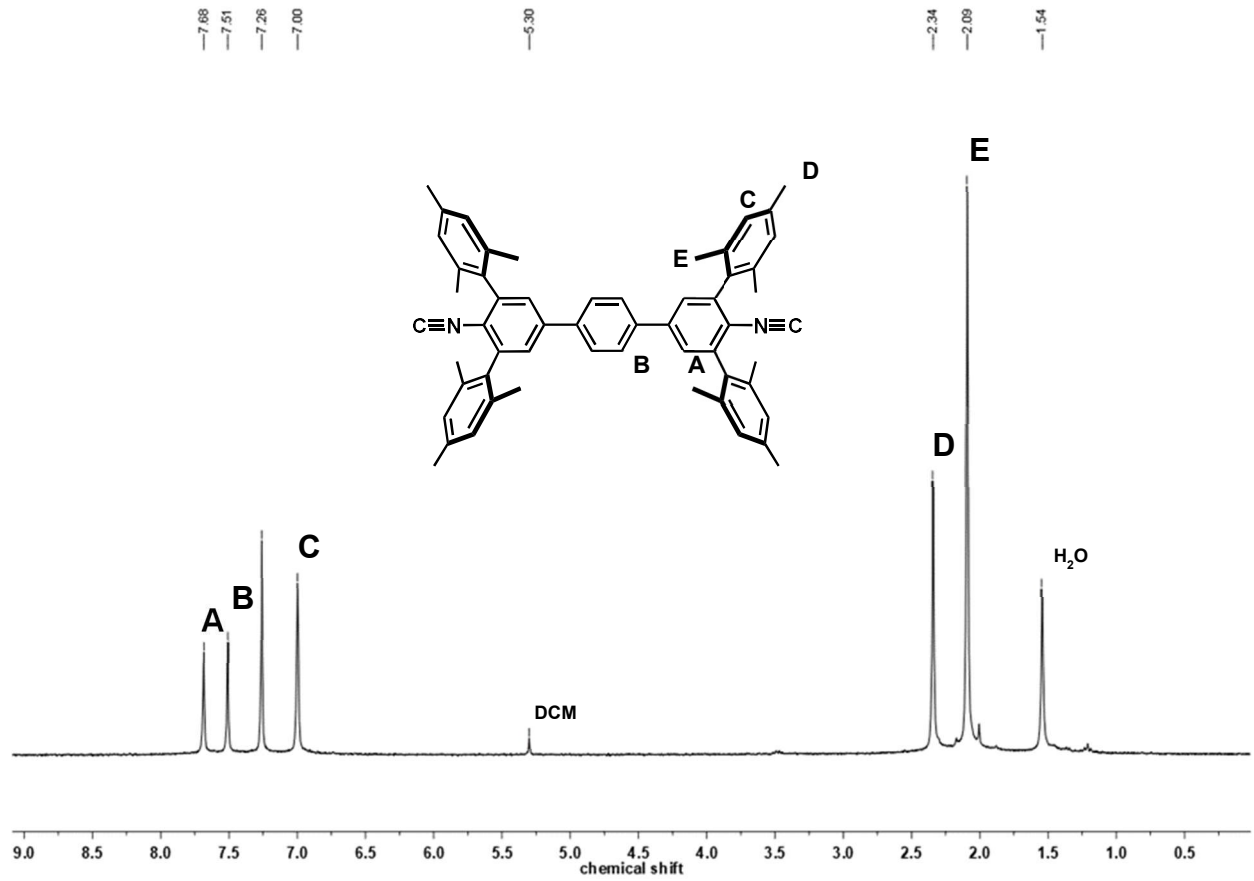

Figure 2.11 [1] H NMR spectrum ($CDCl_3$, 300 MHz, 20 ˚C) of 1,4-$(CNAr^{Mes2})_2C_6H_4$.

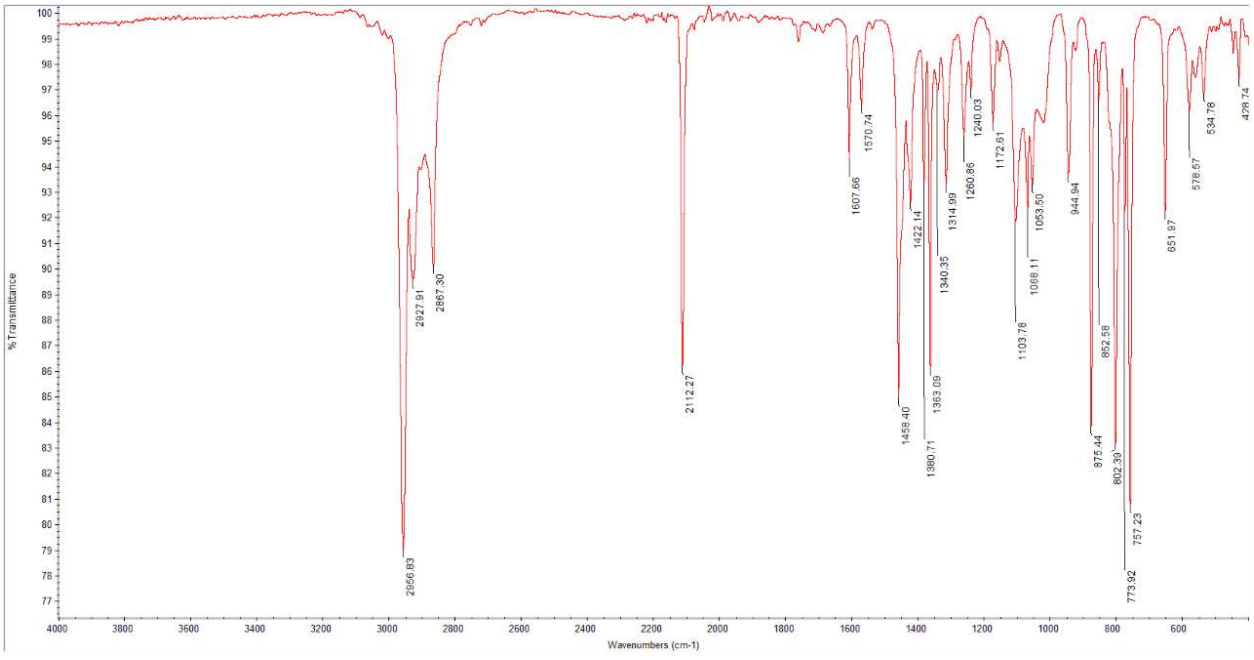

Figure 2.12 ATR-IR spectrum (20 ˚C) of 1,4-$(CNAr^{Mes2})_2C_6H_4$.

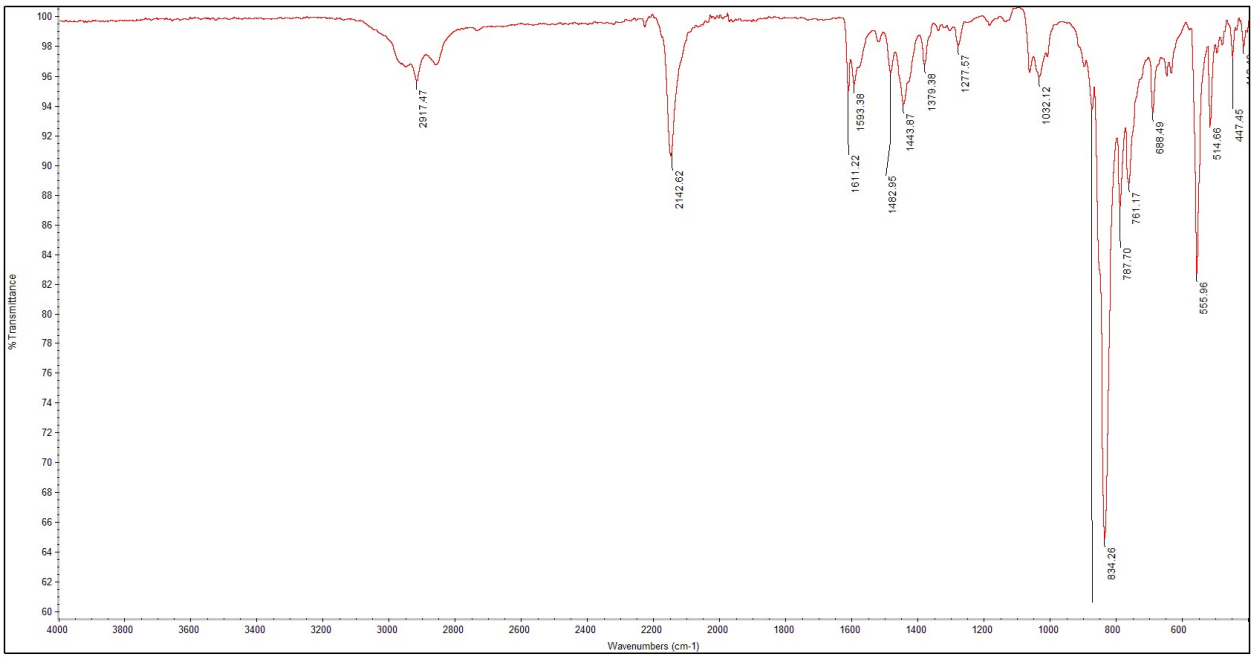

Figure 2.13 ATR-IR spectrum (20 ˚C) of "as-prepared" THF-coordinated $Cu^{ISO}CN$-4.

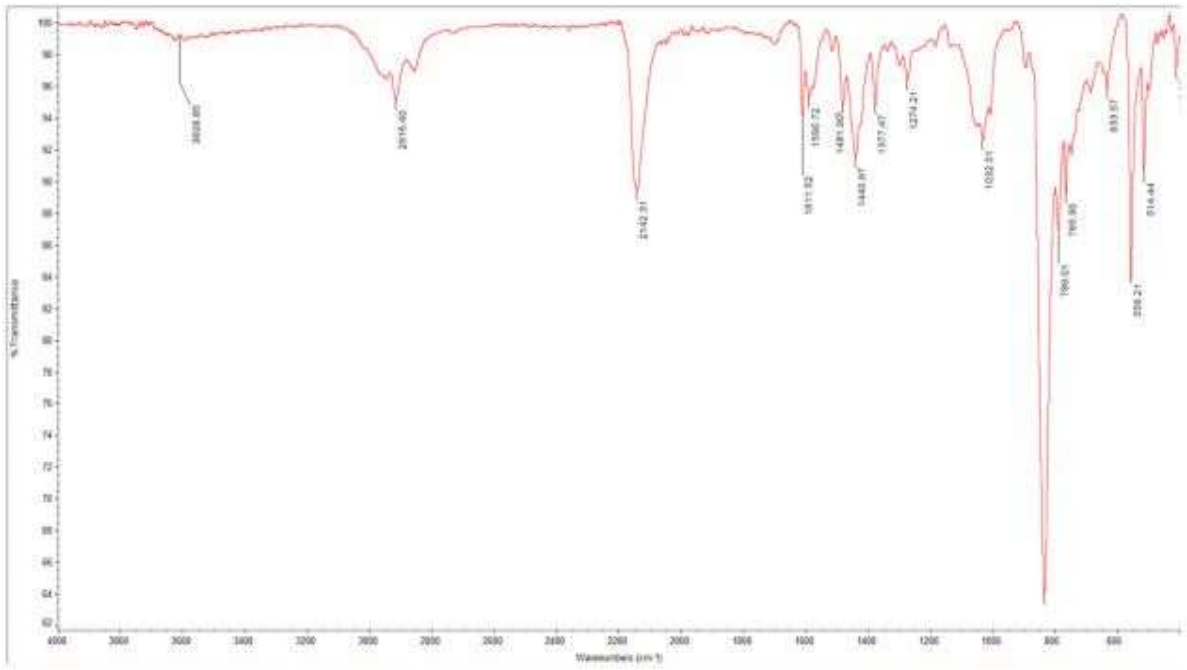

Figure 2.14 ATR-IR spectrum (20 ˚C) of THF-coordinated Cu-^{ISO}CN-4 after exposure to deionized H_2O for 5 d (120 h). Note: the low-intensity ν_{OH} band centered at 3609 cm^{-1} is likely derived from residual surface H_2O.

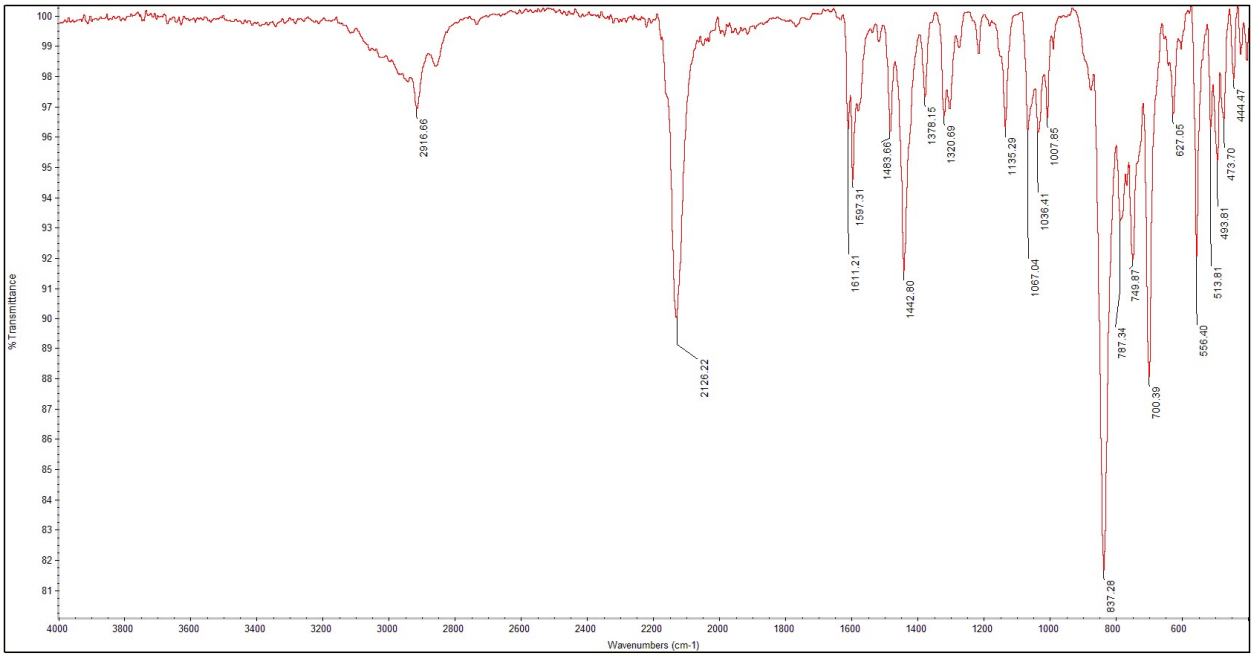

Figure 2.15 ATR-IR spectrum (20 ˚C) of pyridine-coordinated Cu-^{ISO}CN-4, obtained from treatment of THF-coordinated Cu-^{ISO}CN-4 with 5.0 equiv pyridine in THF (12 h).

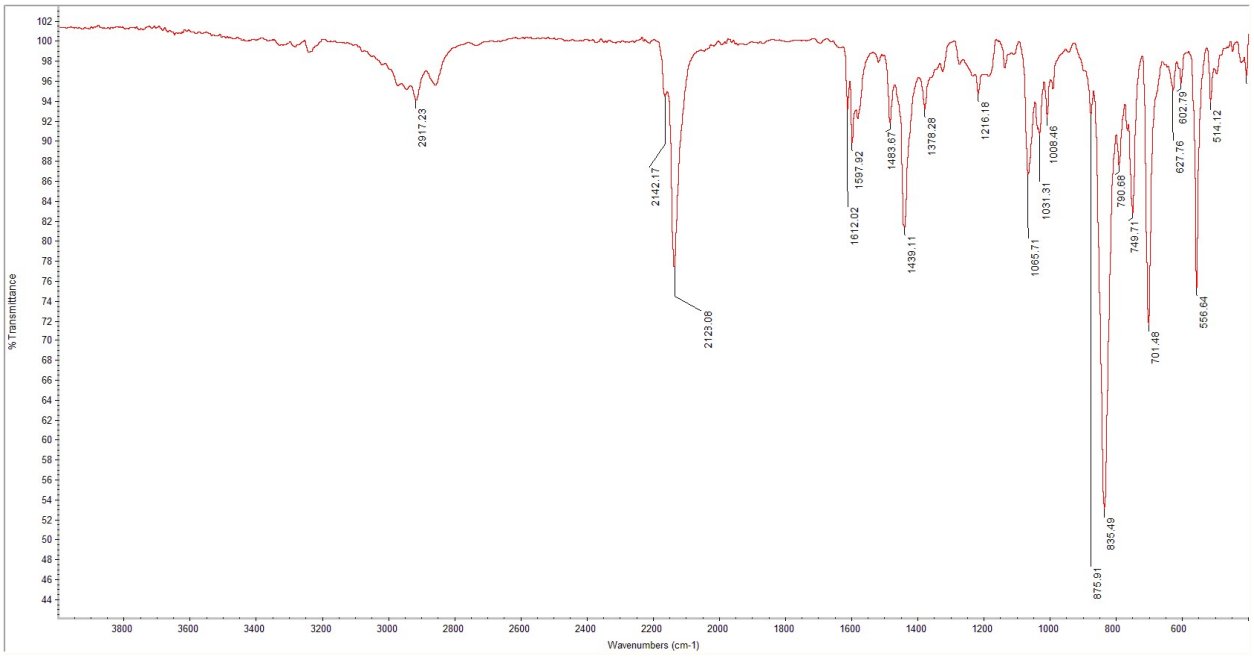

Figure 2.16 ATR-IR spectrum (20 ˚C) of pyridine-coordinated Cu-^{ISO}CN-4, obtained from treatment of THF-coordinated Cu-^{ISO}CN-4 with 5.0 equiv pyridine in H_2O (24 h). Based on the relative intensity of the 2142 cm^{-1} band, an 85% substitution efficiency is estimated.

2.6 Details of X-ray Single-Crystal and Powder Diffraction Studies

General. Single X-ray structure determinations were performed at 100 K on Bruker Platform Diffractometers equipped with Mo-K_α or Cu-K_α radiation source and an APEX-II CCD area detector. All structures were solved via direct methods with SHELXS[82] and refined by full-matrix least-squares procedures using SHELXL within the Olex2 software package.[83] Crystallographic data collection and refinement information are listed in Table 2.1. For both THF- and pyridine coordinated Cu-^{ISO}CN-4, disordered and non-stoichiometric THF solvent molecules of co-crystallization are present within the solvent-accessible channels. The Platon routine SQUEEZE[84] was used to account for the electron density of this disordered solvent as a diffuse contribution to the overall scattering without specific atom positions.

Powder X-ray diffraction studies on Cu-^{ISO}CN-4 were performed at room temperature on a Bruker D8 Advanced LynxEye CCD diffractometer, equipped with Cu-K_α radiation (λ = 1.54178 Å) and K_β filter. Diffraction measurements were set to 40V and 40 mA.

Specifics of Structure Solutions.

Cu-^{ISO}CN-4. The $[PF_6]^-$ counteranion is positionally disordered and was modeled and refined anisotropically. Two carbon atoms present on the para-phenyl linker are positionally disordered and were modeled by parts and refined anisotropically. One carbon atom on the coordinated THF is positionally disordered and was modeled by parts and refined anisotropically. Significant disorder was observed for 6.5 THF solvent molecules of co-crystallization for the asymmetric unit cell. These were treated with SQUEEZE and their electron density removed prior to refinement.

Cu-^{ISO}CN-py. Para-phenyl linker present on one isocyanide ligand is positionally disordered and was modeled by parts and refined anisotropically. Significant disorder was observed for 5.5 THF

solvent molecules of co-crystallization for the asymmetric unit cell. These were treated with SQUEEZE and their electron density removed prior to refinement.

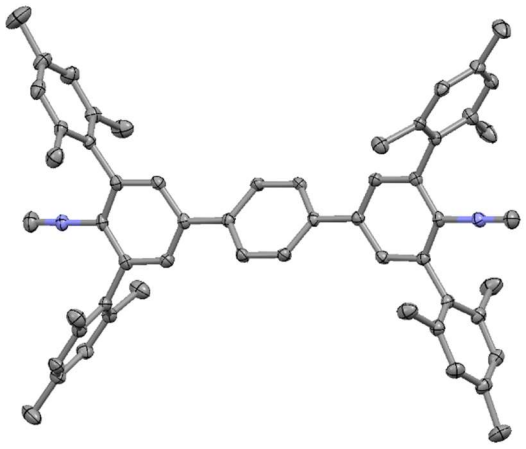

Figure 2.17 Molecular structure of 1,4-$(CNAr^{Mes2})_2C_6H_4$.

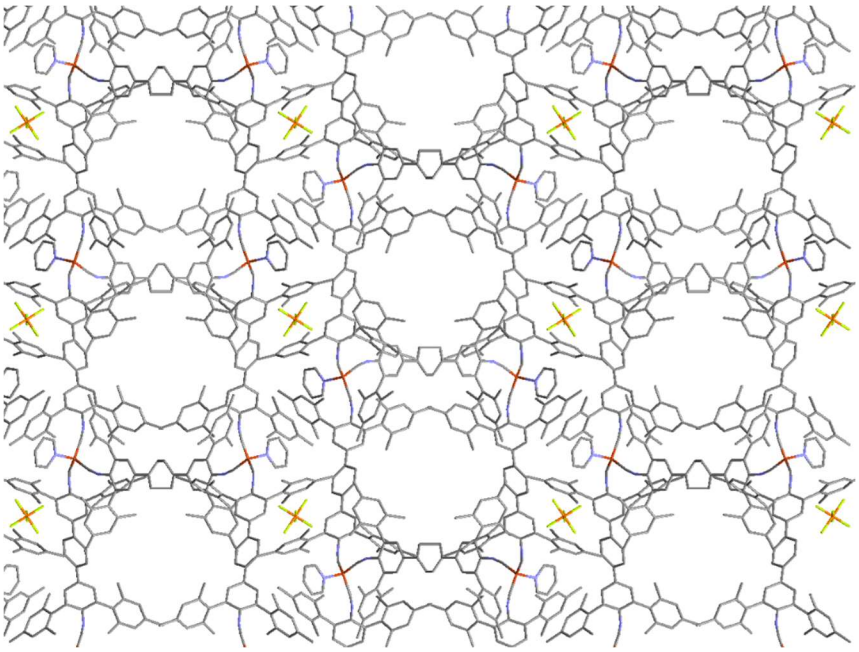

Figure 2.18 Single-crystal X-ray structure of Cu-^{ISO}CN-py with view of the channel structure down the crystallographic *b*-axis.

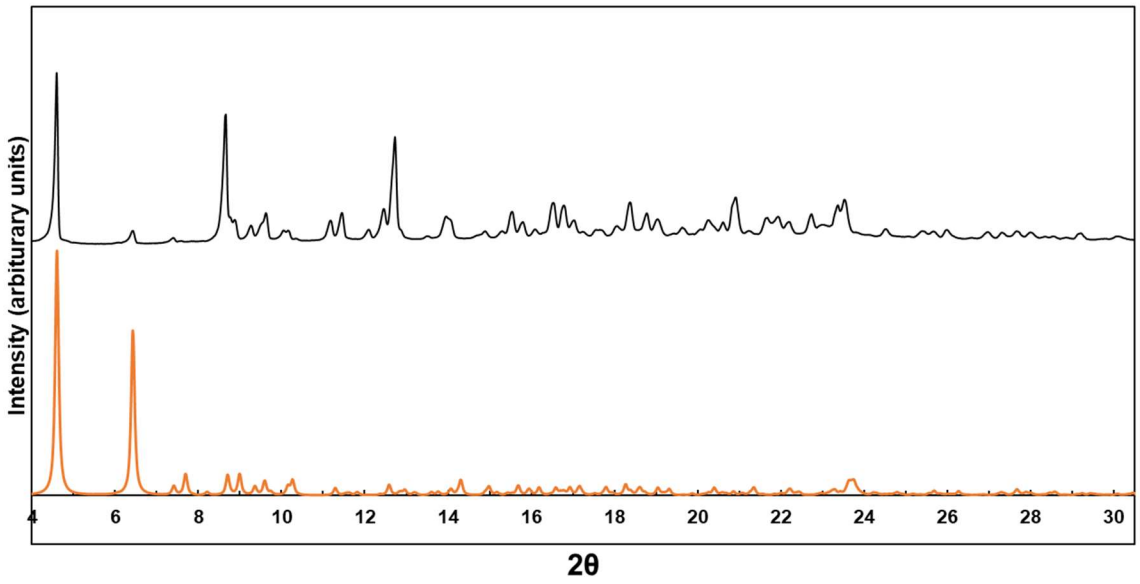

Figure 2.19 PXRD pattern of Cu-^{ISO}CN-4, experimental (black) and simulated from single crystal diffraction (orange).

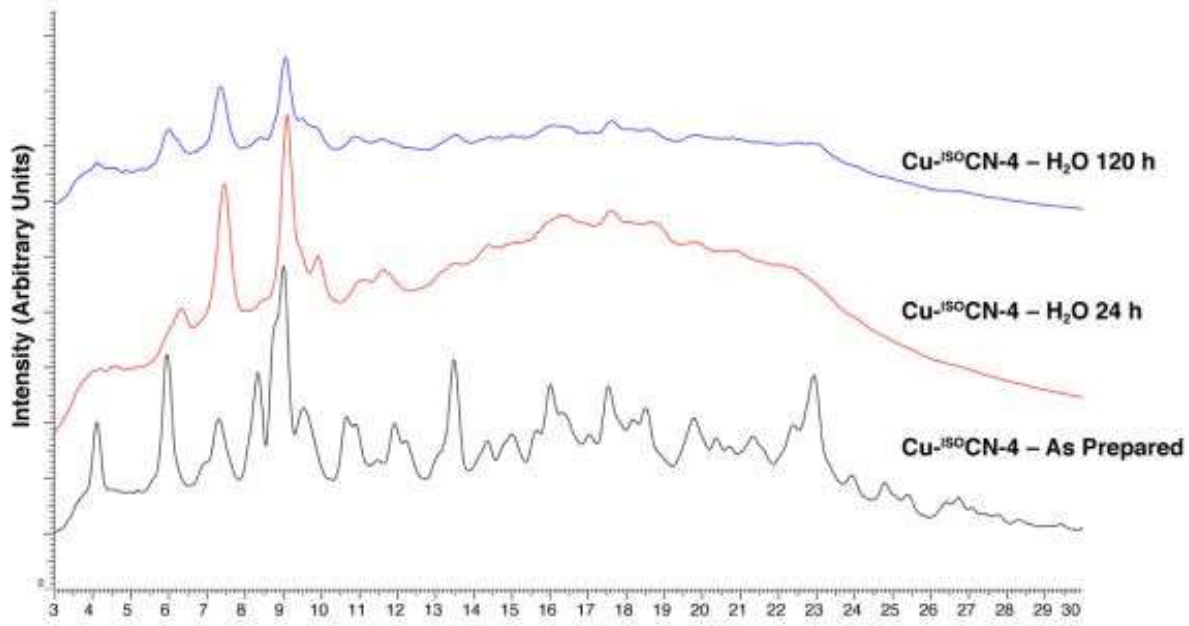

Figure 2.20 PXRD patterns of "as-prepared" Cu-^{ISO}CN-4 (bottom) and after exposure to deionized water for 24 h (middle) and 120 h (top), respectively. A loss in crystallinity is observed as a function of exposure time.

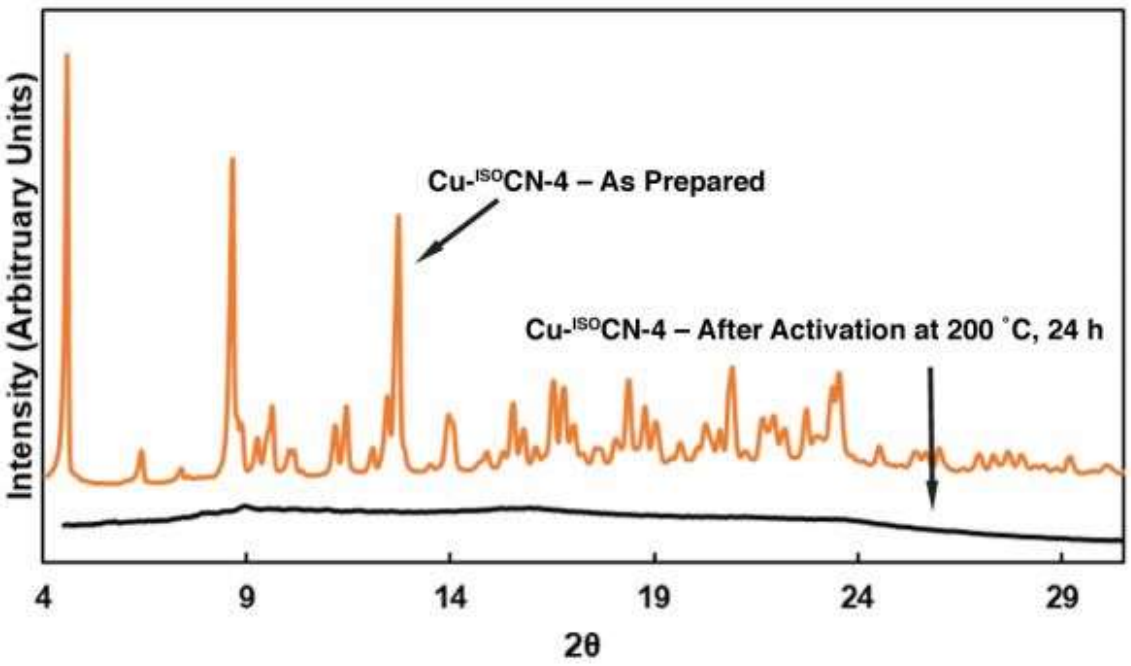

Figure 2.21 PXRD pattern of "as-prepared" Cu-^{ISO}CN-4 (orange) and after activation at 200 ˚C for 24 h (black). After activation, complete framework collapse and loss of crystallinity is indicated.

Table 2.1 Crystallographic Data Collection and Refinement Information

Name	$Cu^{ISO}CN$-4	$Cu^{ISO}CN$-py	1,4-$(CNAr^{Mes2})_2C_6H_4$
Formula	$C_{176}H_{172}Cu_2F_6N_6O_2P$	$C_{178}H_{166}Cu_2F_6N_8P$	$C_{56}H_{54}N_2$
Crystal System	Orthorhombic	Orthorhombic	Monoclinic
Space Group	Pccn	Pccn	$P2_1/n$
a, Å	43.0814(5)	43.5731(7)	15.7545(15)
b, Å	12.8155(2)	12.7500(2)	19.9193(13)
c, Å	31.7705(4)	31.8860(6)	16.1735(11)
α, deg	90	90	90
β, deg	90	90	115.950(3)
γ, deg	90	90	90
V, $Å^3$	17540.8(4)	17714.5(5)	4563.8(6)
Z	4	4	4
Radiation (λ, Å)	Cu-Kα, 1.54178	Cu-Kα, 1.54178	Mo-Kα, 0.71073
ρ (calcd.), g/cm^3	1.013	1.008	1.099
μ (Mo Ka), mm^{-1}	0.807	0.797	0.063
Temp, K	100	100	100
θ max, deg	68.280	50.602	25.694
data/parameters	16031/899	9344/904	8660/535
R_1	0.0645	0.0587	0.0478
wR_2	0.1689	0.1587	0.1244
GOF	1.028	1.016	1.021

2.7 Contact Angle Measurements, TGA/DSC and Gas Sorption Analyses

Thermal Analysis. Thermogravimetric analysis was performed on ~5–15 mg of material that had been dried under dynamic vacuum. Analysis was conducted under a stream of dry dinitrogen gas (80 mL/min) using a Mettler Toledo TGA/DSC 1 STARe System running from 30 ˚C to 800 ˚C with a ramping rate of 5 ˚C/min.

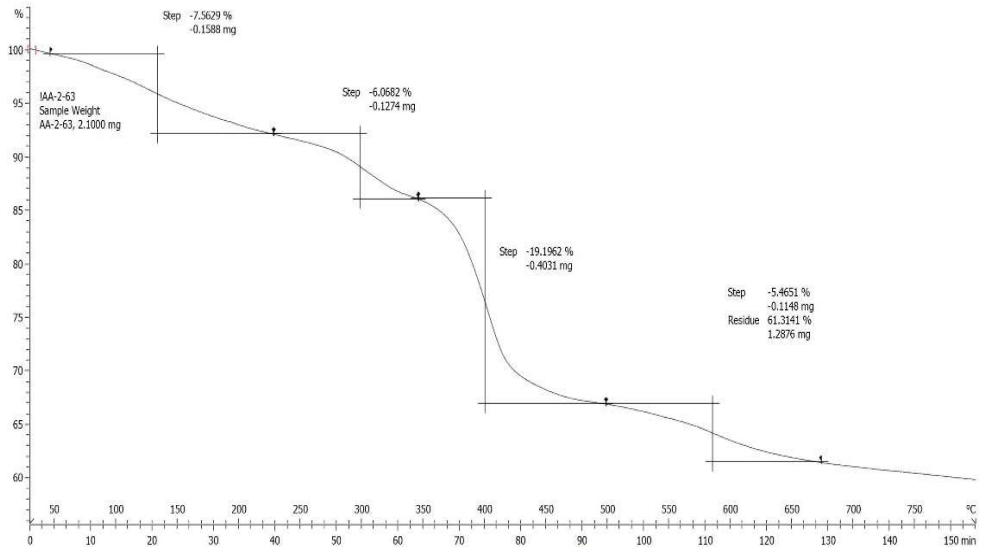

Figure 2.22 Thermogravimetric analysis of Cu-^{ISO}CN-4.

Surface Area Analysis. Samples were prepared on and measured using a Micrometrics ASAP 2020 Adsorption Analyzer. Approximately 33 mg of material was transferred to a pre-weighed sample tube and degassed at 200 ˚C for at least 24 hours or until the outgas rate was below 5 mmHg. The sample tube was reweighed to obtain a mass for the sample. Measurements were collected on three independent samples at 77 K employing N_2 of 99.999% purity using the volumetric technique. Analyses performed on Cu^{ISO}CN-4 degassed at 105 ˚C revealed insignificant surface areas.

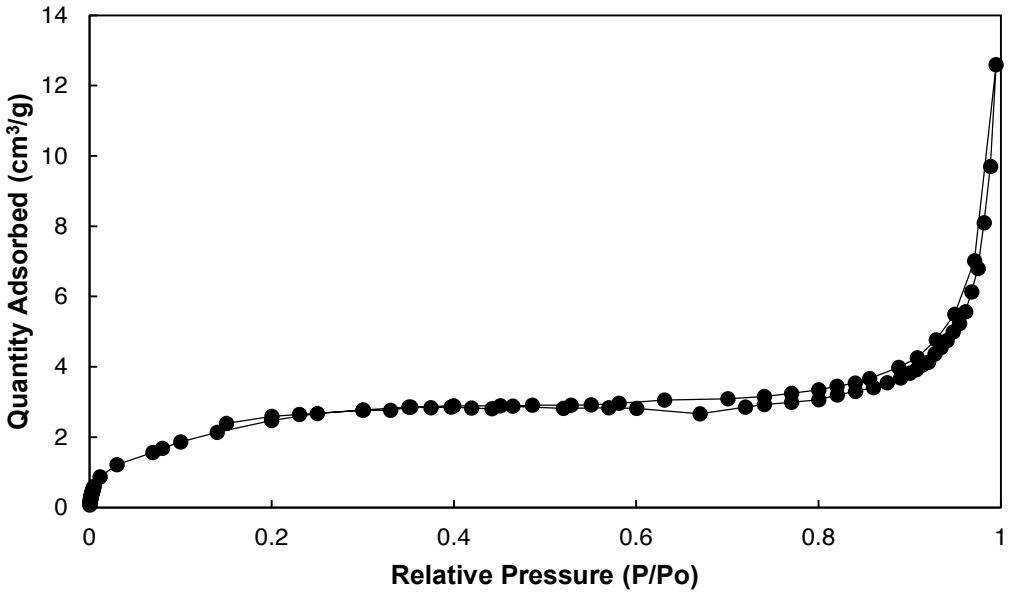

Figure 2.23 N_2 sorption isotherm analysis of $Cu^{ISO}CN$-4 after activation at 200 °C.

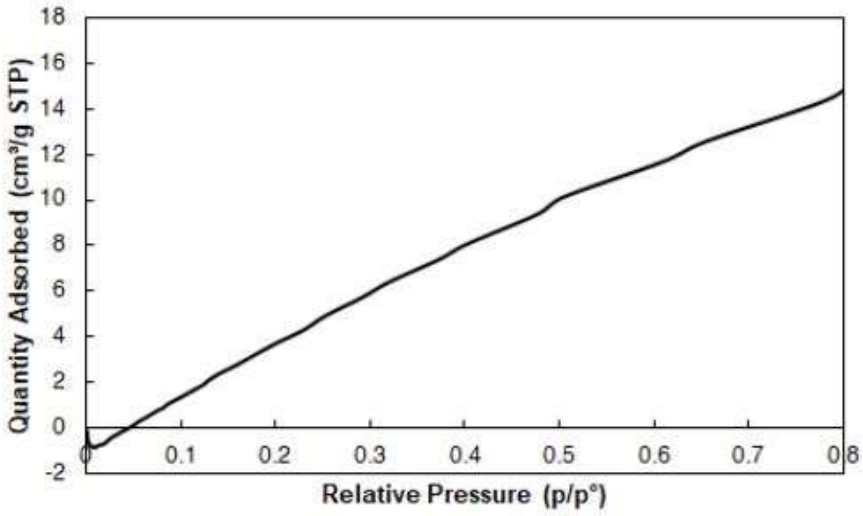

Figure 2.24 CO_2 sorption isotherm analysis at room temperature of Cu-^{ISO}CN-4 after activation at 200 ˚C.

Contact Angle Measurements on Cu-^{ISO}CN-4. Contact angle measurements were recorded using a Tantec CAM-micro Contact Angle Meter. Samples of Cu-^{ISO}CN-4 were prepared as described previously and dried under dynamic vacuum prior to analysis. Samples were then pressed onto a glass slide using a spatula. A drop of water (tested to 18.2 MW) was slowly dropped from a microsyringe and the contact angle measured.

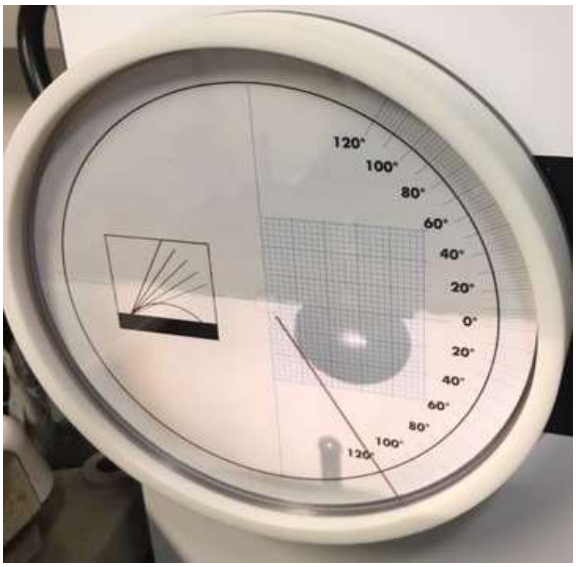

Figure 2.25 A representative image of the contact angle meter upon addition of a drop of H_2O to Cu^{ISO}CN-4.

2.8 Acknowledgements

Chapter 2 is adapted from A. Arroyave, M. Gembicky, A. L. Rheingold, J. S. Figueroa "Aqueous Stability and Ligand Substitution of a Layered Cu(I)/Isocyanide-Based Organometallic Network Material with a Well-Defined Channel Structure," *Inorg. Chem.,* **2020**, 59, 11868-11878. Copyright 2020, American Chemical Society. Permission to include published material in this dissertation has been obtained from all coauthors. The dissertation author is the first author of this paper. Mark Kalaj is thanked for assistance with gas sorption measurements.

2.9 References

(1) Long, J. R.; Yaghi, O. M. *Chem. Soc. Rev.* **2009**, *38*, 1213–1214.

(2) Murray, L. J.; Dincă, M.; Long, J. R. *Chem. Soc. Rev.* **2009**, *38*, 1294.

(3) Getman, R. B.; Bae, Y. S.; Wilmer, C. E.; Snurr, R. Q. *Chem. Rev*. **2012**, *112*, 703–723.

(4) Li, J. R.; Sculley, J.; Zhou, H. C. *Chem. Rev*. **2012**, *112*, 869–932.

(5) Pascanu, V.; González Miera, G.; Inge, A. K.; Martín-Matute, B. *J. Am. Chem. Soc*. **2019**, *141*, 7223–7234.

(6) Aiyappa, H. B.; Masa, J.; Andronescu, C.; Muhler, M.; Fischer, R. A.; Schuhmann, W. *Small Methods* **2019**, *3* (8), 1800415.

(7) Xie, L. S.; Skorupskii, G.; Dincă, M. *Chem. Rev*. **2020**, *120*, 8536-8580.

(8) Yaghi, O. M.; O'Keeffe, M.; Ockwig, N. W.; Chae, H. K.; Eddaoudi, M.; Kim, J. *Nature* **2003**, *423*, 705–714.

(9) Li, H.; Eddaoudi, M.; O'Keeffe, M.; Yaghi, O. M. *Nature* **1999**, *402*, 276–279.

(10) Park, K. S.; Ni, Z.; Côté, A. P.; Choi, J. Y.; Huang, R.; Uribe-Romo, F. J.; Chae, H. K.; O'Keeffe, M.; Yaghi, O. M. *Proc. Natl. Acad. Sci.* **2006**, *103*, 10186 – 10191.

(11) Cavka, J. H.; Jakobsen, S.; Olsbye, U.; Guillou, N.; Lamberti, C.; Bordiga, S.; Lillerud, K. P. *J. Am. Chem. Soc.* **2008**, *130*, 13850–13851.

(12) Susumu, K.; Ryo, K.; Shin-ichiro, N. *Angew. Chemie Int. Ed.* **2004**, *43*, 2334–2375.

(13) Diercks, C. S.; Kalmutzki, M. J.; Diercks, N. J.; Yaghi, O. M. *ACS Cent. Sci.* **2018**, *4*, 1457-1464.

(14) Nuñez, A. J.; Shear, L. N.; Dahal, N.; Ibarra, I. A.; Yoon, J.; Hwang, Y. K.; Chang, J. S.; Humphrey, S. M. *Chem. Commun.* **2011**, *47*, 11855–11857.

(15) Bohnsack, A. M.; Ibarra, I. A.; Bakhmutov, V. I.; Lynch, V. M.; Humphrey, S. M. *J. Am. Chem. Soc.* **2013**, *135*, 16038–16041.

(16) Václavík, J.; Servalli, M.; Lothschütz, C.; Szlachetko, J.; Ranocchiari, M.; van Bokhoven, J. A. *Chem. Cat. Chem.* **2013**, *5*, 692–696.

(17) Falkowski, J. M.; Sawano, T.; Zhang, T.; Tsun, G.; Chen, Y.; Lockard, J. V.; Lin, W. *J. Am. Chem. Soc.* **2014**, *136*, 5213–5216.

(18) He, J.; Waggoner, N. W.; Dunning, S. G.; Steiner, A.; Lynch, V. M.; Humphrey, S. M. *Angew. Chemie Int. Ed.* **2016**, *55*, 12351–12355.

(19) Bezrukov, A. A.; Dietzel, P. D. C. *Inorg. Chem.* **2017**, *56*, 12830–12838.

(20) Sawano, T.; Lin, Z.; Boures, D.; An, B.; Wang, C.; Lin, W. *J. Am. Chem. Soc.* **2016**, *138*, 9783–9786.

(21) He, S.; Allemond, L. L.; Dunning, S. G.; Reynolds, J. E.; Lynch, V. M.; Humphrey, S. M. *Chem. Commun.* **2020**, *56*, 1286–1289.

(22) Eric Sikma, R.; Kunal, P.; Dunning, S. G.; Reynolds, J. E.; Lee, J. S.; Chang, J. S.; Humphrey, S. M. *J. Am. Chem. Soc.* **2018**, *140*, 9806–9809.

(23) Dincă, M.; Gabbaï, F. P.; Long, J. R. *Organometallics* **2019**, *38*, 3389–3391.

(24) Agnew, D. W.; Gembicky, M.; Moore, C. E.; Rheingold, A. L.; Figueroa, J. S. *J. Am. Chem. Soc.* **2016**, *138*, 15138–15141.

(25) Agnew, D. W.; DiMucci, I. M.; Arroyave, A.; Gembicky, M.; Moore, C. E.; MacMillan, S. N.; Rheingold, A. L.; Lancaster, K. M.; Figueroa, J. S. *J. Am. Chem. Soc.* **2017**, *139*, 17257–17260.

(26) Cotton, F. A.; Zingales, F. *J. Am. Chem. Soc.* **1961**, *83*, 351–355.

(27) Sarapu, A. C.; Fenske, R. F. *Inorg. Chem.* **1972**, *11*, 3021–3025.

(28) Sarapu, A. C.; Fenske, R. F. *Inorg. Chem.* **1975**, *14*, 247–253.

(29) Treichel, P. M.; Mueh, H. J.; Bursten, B. E. *J. Organomet. Chem.* **1976**, *110*, C49–C52.

(30) Essenmacher, G. J.; Treichel, P. M. *Inorg. Chem.* **1977**, *16*, 800–806.

(31) Treichel, P. M.; Mueh, H. J. *Inorg. Chem.* **1977**, *16*, 1167–1169.

(32) Carpenter, A. E.; Mokhtarzadeh, C. C.; Ripatti, D. S.; Havrylyuk, I.; Kamezawa, R.; Moore, C. E.; Rheingold, A. L.; Figueroa, J. S. *Inorg. Chem.* **2015**, *54*, 2936–2944.

(33) Applegate, J. C.; Okeowo, M. K.; Erickson, N. R.; Neal, B. M.; Berrie, C. L.; Gerasimchuk, N. N.; Barybin, M. V. *Chem. Sci.* **2016**, *7*, 1422–1429.

(34) Weber, L. *Angew. Chem., Int. Ed*. **1998**, *37*, 1515–1517.

(35) Ellis, J. E. *Inorg. Chem*. **2006**, *45*, 3167–3186.

(36) Yamamoto, Y. *Coord. Chem. Rev.* **1980**, *32*, 193–233.

(37) Labios, L. A.; Millard, M. D.; Rheingold, A. L.; Figueroa, J. S. *J. Am. Chem. Soc.* **2009**, *131*, 11318–11319.

(38) Margulieux, G. W.; Weidemann, N.; Lacy, D. C.; Moore, C. E.; Rheingold, A. L.; Figueroa, J. S. *J. Am. Chem. Soc.* **2010**, *132*, 5033–5035.

(39) Carpenter, A. E.; Margulieux, G. W.; Millard, M. D.; Moore, C. E.; Weidemann, N.; Rheingold, A. L.; Figueroa, J. S. *Angew. Chem., Int. Ed.* **2012**, *51*, 9412–9416.

(40) Mokhtarzadeh, C. C.; Margulieux, G. W.; Carpenter, A. E.; Weidemann, N.; Moore, C. E.; Rheingold, A. L.; Figueroa, J. S. *Inorg. Chem.* **2015**, *54*, 5579–5587.

(41) Barnett, B. R.; Figueroa, J. S. *Chem. Commun.* **2016**, *52*, 13829–13839.

(42) Carpenter, A. E.; Chan, C.; Rheingold, A. L.; Figueroa, J. S. *Organometallics* **2016**, *35*, 2319–2326.

(43) Mokhtarzadeh, C. C.; Moore, C. E.; Rheingold, A. L.; Figueroa, J. S. *Angew. Chem., Int. Ed.* **2017**, *56*, 10894–10899.

(44) Mokhtarzadeh, C. C.; Moore, C. E.; Rheingold, A. L.; Figueroa, J. S. *J. Am. Chem. Soc.* **2018**, *140*, 8100–8104.

(45) Dong, Y.; Jv, J. J.; Wu, X. W.; Kan, J. L.; Lin, T.; Dong, Y. Bin. *Chem. Commun.* **2019**, *55*, 14414–14417.

(46) R., B. S.; Richard, R. *Angew. Chemie Int. Ed.* **1998**, *37*, 1460–1494.

(47) Tranchemontagne, D. J.; Mendoza-Cortes, J. L.; O'Keeffe, M.; Yaghi, O. M. *Chem. Soc. Rev.* **2009**, *38*, 1257.

(48) O'Keeffe, M.; Yaghi, O. M. *Chem. Rev*. **2012**, *112*, 675–702.

(49) An, J.; Farha, O. K.; Hupp, J. T.; Pohl, E.; Yeh, J. I.; Rosi, N. L. *Nat. Commun.* **2012**, *3*, 1–6.

(50) Bradshaw, D.; El-Hankari, S.; Lupica-Spagnolo, L. *Chem. Soc. Rev.* **2014**, *43*, 5431.

(51) Fang, Z.; Dürholt, J. P.; Kauer, M.; Zhang, W.; Lochenie, C.; Jee, B.; Albada, B.; Metzler-Nolte, N.; Pöppl, A.; Weber, B. *J. Am. Chem. Soc.* **2014**, *136*, 9627–9636.

(52) Zhang, W.; Kauer, M.; Guo, P.; Kunze, S.; Cwik, S.; Muhler, M.; Wang, Y.; Epp, K.; Kieslich, G.; Fischer, R. A. *Eur. J. Inorg. Chem.* **2017**, *2017*, 925–931.

(53) Dissegna, S.; Vervoorts, P.; Hobday, C. L.; Düren, T.; Daisenberger, D.; Smith, A. J.; Fischer, R. A.; Kieslich, G. *J. Am. Chem. Soc.* **2018**, *140*, 11581–11584.

(54) Liu, C.; Zeng, C.; Luo, T.-Y.; Merg, A. D.; Jin, R.; Rosi, N. L. *J. Am. Chem. Soc.* **2016**, *138*, 12045–12048.

(55) Guillerm, V.; Xu, H.; Albalad, J.; Imaz, I.; Maspoch, D. *J. Am. Chem. Soc.* **2018**, *140*, 15022–15030.

(56) Eddaoudi, M.; Kim, J.; Rosi, N.; Vodak, D.; Wachter, J.; O'Keeffe, M.; Yaghi, O. M. *Science.* **2002**, *295*, 469 – 472.

(57) Deng, H.; Grunder, S.; Cordova, K. E.; Valente, C.; Furukawa, H.; Hmadeh, M.; Gándara, F.; Whalley, A. C.; Liu, Z.; Asahina, S.; *Science.* **2012**, *336*, 1018 – 1023.

(58) Fox, B. J.; Sun, Q. Y.; DiPasquale, A. G.; Fox, A. R.; Rheingold, A. L.; Figueroa, J. S. *Inorg. Chem.* **2008**, *47*, 9010–9020.

(59) Ditri, T. B.; Fox, B. J.; Moore, C. E.; Rheingold, A. L.; Figueroa, J. S. *Inorg. Chem.* **2009**, *48*, 8362–8375.

(60) Robertson, M. J.; Angelici, R. J. *Langmuir* **1994**, *10*, 1488–1492.

(61) Shih, K.-C.; Angelici, R. J. *Langmuir* **1995**, *11*, 2539–2546.

(62) Henderson, J. I.; Feng, S.; Bein, T.; Kubiak, C. P. *Langmuir* **2000**, *16*, 6183–6187.

(63) Gong, Y.-N.; Zhong, D.-C.; Lu, T.-B. *Cryst. Eng. Comm.* **2016**, *18*, 2596.

(64) Haldar, R.; Sikdar, N.; Maji, T. K. *Mater. Today* **2015**, *18*, 97–116.

(65) Ashworth, D. J.; Roseveare, T. M.; Schneemann, A.; Flint, M.; Bernáldes, I. D.; Vervoorts, P.; Fischer, R. A.; Brammer, L.; Foster, J. A. *Inorg. Chem.* **2019**, *58*, 10837–10845.

(66) Tan, J. C.; Saines, P. J.; Bithell, E. G.; Cheetham, A. K. *ACS Nano* **2012**, *6*, 615–621.

(67) Zhao, M.; Lu, Q.; Ma, Q.; Zhang, H. *Small Methods* **2017**, *1*, 1600030.

(68) Liptrot, D. J.; Power, P. P. *Nat. Rev. Chem*. **2017**, *1*, 1–12.

(69) Fox, H. W.; Zisman, W. A. *J. Colloid Sci.* **1950**, *5*, 514–531.

(70) Lau, K. K. S.; Bico, J.; Teo, K. B. K.; Chhowalla, M.; Amaratunga, G. A. J.; Milne, W. I.; McKinley, G. H.; Gleason, K. K. *Nano Lett.* **2003**, *3*, 1701–1705.

(71) Song, H. J.; Zhang, Z. Z.; Men, X. H. *Appl. Phys. A Mater. Sci. Process.* **2008**, *91*, 73–76.

(72) Boyarskiy, V. P.; Bokach, N. A.; Luzyanin, K. V.; Kukushkin, V. Y. *Chem. Rev*. **2015**, *115*, 2698–2779.

(73) Bae, Y. S.; Dubbeldam, D.; Nelson, A.; Walton, K. S.; Hupp, J. T.; Snurr, R. Q. *Chem. Mater.* **2009**. *21*, 4768-4777.

(74) Mondloch, J. E.; Karagiaridi, O.; Farha, O. K.; Hupp, J. T. *Cryst. Eng. Comm.* **2013**, *15*, 9258.

(75) Dodson, R. A.; Wong-Foy, A. G.; Matzger, A. J. *Chem. Mater.* **2018**, *30*, 6559–6565.

(76) Zhao, H.; Liang, L.; wen Liu, H. *J. Environ. Sci.* **2011**, *23*, S156–S158.

(77) Zalat, O. A.; Elsayed, M. A. *J. Environ. Chem. Eng.* **2013**, *1*, 137–143.

(78) Toxicological Profile for Pyridine. U.S. Public Health Service, Agency for Toxic Substances and Disease Registry, Sept. 1992; https://www.atsdr.cdc.gov/toxprofiles/tp52.pdf (accessed Sep 30, 2020).

(79) Pangborn, A. B.; Giardello, M. A.; Grubbs, R. H.; Rosen, R. K.; Timmers, F. J. *Organometallics* **1996**, *15*, 1518–1520.

(80) Armarego, W. L. F.; Li, C.; Chai, L.; York, N.; *Purification of Laboratory Chemical,* 7th ed.; Elsevier 2013.

(81) Fulmer, G. R.; Miller, A. J. M.; Sherden, N. H.; Gottlieb, H. E.; Nudelman, A.; Stoltz, B. M.; Bercaw, J. E.; Goldberg, K. I. *Organometallics* **2010**, *29*, 2176-2179.

(82) Sheldrick, G. M. *Acta Crystallogr., Sect. A: Found. Crystallogr*. **2008**, *64*, 112–122.

(83) Dolomanov, O. V.; Bourhis, L. J.; Gildea, R. J.; Howard, J. A. K.; Puschmann, H. *J. Appl. Crystallogr.* **2009**, *42*, 339–341.

(84) Van Der Sluis, P.; Spek, A. L. *Acta Crystallogr. Sect. A* **1990**, *46*, 194–201.

Chapter 3 Exploration of Ligand and Anion Exchange in a Cu(I)/Isocyanide Based Coordination Network

3.1 Introduction

The development of novel coordination network and metal-organic framework (MOF) structures that have been reported over the last twenty years has seen an exponential growth reported in the Cambridge Crystallographic Data Center (CCDC).[1–3] With the addition of a substantial amount of structures, it opens the opportunity for chemical reactivity and structural transformation studies for the discovery of new properties that novel frameworks can bring about. Cu-^{ISO}CN-4 is a first of a kind framework that is uniquely assembled utilizing ditopic *m*-terphenyl diisocyanide linkers that are coordinated to a single Cu(I) node featuring an apically bound THF molecule.[4] While the thorough characterization of the novel Cu-^{ISO}CN-4 was previously described in Chapter 2 of this thesis, additional exploration into the chemical and structural features of this novel material is vital to understanding the benefits that can emerge from utilizing isocyanide ligands in coordination networks and accordingly will be discussed in this chapter.

A continuation of post-synthetic ligand substitution in Cu-^{ISO}CN-4 was investigated specifically utilizing varying electronic and steric profiles of phosphine ligands. Taking a page from the metal-organic framework community, we decided to exploit the two-dimensionality present in the sheets of the Cu-^{ISO}CN-4 and explored liquid-assisted anion exchange. Furthermore, preliminary imagery studies have been performed with electron and atomic force microscopy on

the Cu(I) network to relate single crystal to bulk structural properties. Lastly, a non-interpenetrated polymorph of Cu-^{ISO}CN-4 was found.

3.2 Exploring Phosphine Ligand Substitution

Many metal-carbonyl analogues that have been reported have used phosphine molecules as the coordinating ligand although it was found that the charge transfer from the metal to the molecule was more important for stabilizing the low-valent metal complexes.[5–7] In addition, phosphine ligands are stronger σ-donors but weaker π-acids than carbonyls and isocyanides so the molecular orbital and therefore the electronics of these systems do not provide a good match for proper comparison to metal carbonyl complexes.[8] Nevertheless, the σ-donation properties of phosphine's enable the ligand to act as a nucleophile. Previously, it was reported that a ligand substitution for a coordinated THF molecule for a stronger donor pyridine nucleophile molecule in a Cu(I)/isocyanide-based network occurred over 12 hours.[9] Similarly, we explored other nucleophiles to probe the limits of this ligand exchange in the Cu-^{ISO}CN-4 system, specifically phosphine ligands since they are an organometallic ligand that could result in a unique combination of synergistic bonding within the framework.[10,11] With the target of synthetically accessing an isocyanide/phosphine low-valent framework that would be challenging to achieve utilizing *in-situ* solvothermal conditions due to the lack of directionality from a single metal ion, we set out to investigate this route through post-synthetic modification of the Cu(I) network.

To gain a complete understanding of the process and constraints with this phosphine ligand exchange we investigated this transformation utilizing different steric effects and electronics of phosphines. Single-crystal to single-crystal transformation technique was used to perform these studies.[12–14] Approximately 5 mg of single crystals of Cu-^{ISO}CN-4 was added to 1 mL of THF. To this mixture was added the phosphine ligands. Up to 5 equivalents of triphenyl phosphine (PPh_3)

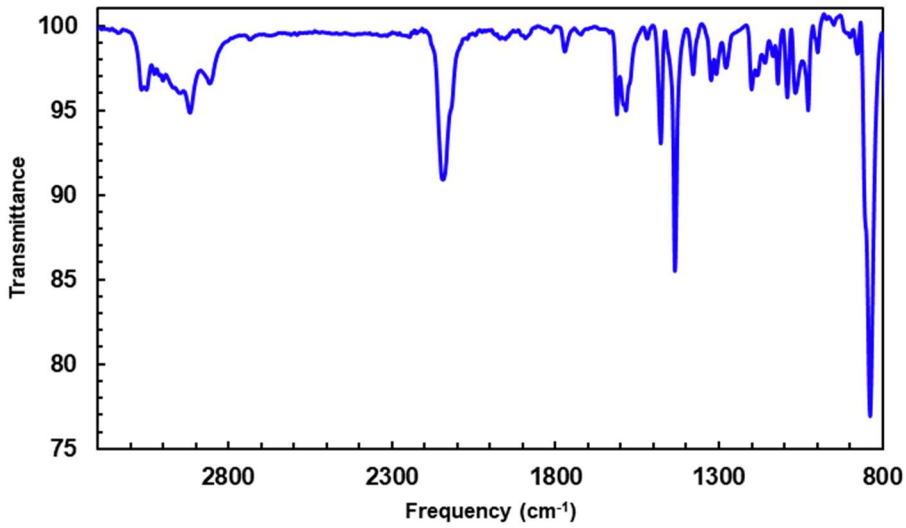

Figure 3.1 FTIR of Cu-^{ISO}CN-4 mixed with PPh_3, the lack of shift in the IR suggest no reaction occurred presumably due to the steric bulkiness of the phenyl groups present in the reagent PPh_3.

was added. Following this reaction using FTIR spectroscopy, there was no significant shift of the ν_{CN} band from the original 2142 cm^{-1} pertaining to Cu-^{ISO}CN-4 indicating that no reaction had occurred (Figure 3.1). We attribute this lack of reactivity not only to the relatively weaker σ-donor properties of PPh_3 but also due to the steric hinderance of the phenyl groups that may not be able to assess the channels in the Cu-^{ISO}CN-4 to displace the coordinated THF molecule. It has been previously reported that when a substrate cannot properly diffuse into the pores of framework it attenuates the reactivity expected.[15–18] Accordingly, we moved to attempt less sterically encumbered phosphine ligands systematically. Diphenyl phosphine (PPh_2H) parallel to PPh_3 showed no reactivity when 5 equivalents were added to Cu-^{ISO}CN-4. Again, suggesting that the presence of the two phenyl groups still inhibits proper access to the channels where the phosphine could interact with the Cu(I) nodes. Dimethyl-phenyl-phosphine ($PPhMe_2$) featuring only one aromatic phenyl group was attempted with a 5-equivalent addition to Cu-^{ISO}CN-4. While no diffraction of these crystals were obtained, presumably due to a sufficient distortion of the lattice,[19–21] FTIR spectroscopy showed a small red shift in the ν_{CN} band to 2130 cm^{-1} and the presence of free ligand (2114 cm^{-1}) (Figure 3.2). The presence of free ligand is in accord with the

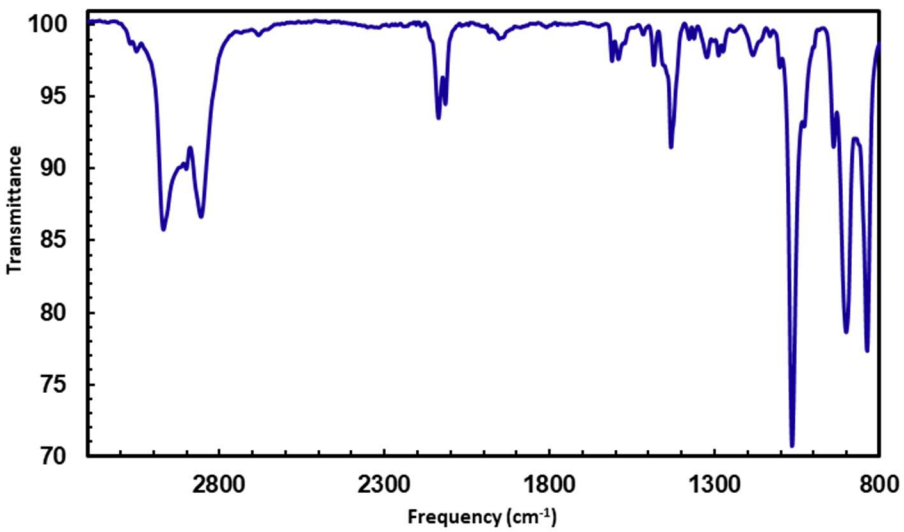

Figure 3.2 FTIR of Cu-^{ISO}CN-4 reacted with $PPhMe_2$. Two ν_{CN} peaks at 2130 and 2114 cm^{-1} indicating a reaction with the phosphine ligand and the presence of free ligand.

lack of diffraction present in these crystals, indicating that while some of the phosphine ligands may have effectively diffused into the channels and exchanged with the THF to become bound to the Cu(I) centers in the materials, the phosphine ligands were also displacing the isocyanide ligand leading to the destruction of the Cu-^{ISO}CN-4. While $PPhMe_2$ may now have been sufficient in size to properly diffuse, the electronics of this system indicate that the σ-donation from this phosphine ligand can rival that of isocyanides especially in weak π-base metal centers such as Cu(I).

In order to fully access the impacts of the electronic features of the phosphine ligands, a solution of trimethyl phosphine (2.0 M PMe_3 in toluene) was utilized. Due to the observations from the $PPhMe_2$ where an excess of the phosphine present in the sample lead to the displacement of the isocyanides, we utilized a substoichiometric amount (0.5 eq) addition to Cu-^{ISO}CN-4 to disfavor that process from occurring. Moreover, we rationalized that if a $PPhMe_2$ molecule could access the channels of this material to enact change in the FTIR then PMe_3 should also be able to diffuse through the channels and would not necessitate the extra push that extra equivalents would add. An hour after the addition of PMe_3 to Cu-^{ISO}CN-4, the single crystals had completely dissolved indicating that the σ-donation of PMe_3 far out competes isocyanides and destroys the

material by the displacement of the linker ligands. FTIR showed the complete disappearance of the original ν_{CN} 2142 cm^{-1} band and the appearance of a new band at 2127 cm^{-1} with the addition of free ligand also present. Furthermore, after another hour the solution that had been sitting under an inert atmosphere at room temperature were now large, single crystals. Diffraction of these single crystals, $[CuL_{ph0.5}(PMe_3)_3]PF_6$ (Figure 3.3), revealed a dinuclear structure where two Cu(I) centers were linked by one ditopic *m*-terphenyl isocyanide ligand. Each of the Cu(I) metals were also coordinated to three PMe_3 ligands to maintain a tetrahedral like geometry in the triclinic, *P*1 space group. This multinuclear to dinuclear transformation has been observed before with post-synthetic modifications attempting to perform a single-crystal to single-crystal transformation, however, the initial dissolution implies that it lost its crystallinity during the conversion to the dinuclear species and as such is not qualified as a solid-state structural transformation. Nevertheless, this dinuclear Cu(I) species adds to our library of exploring supramolecular multinuclear complexes with facile synthesis of ligand exchange and an electronically and sterically unique ligand set.

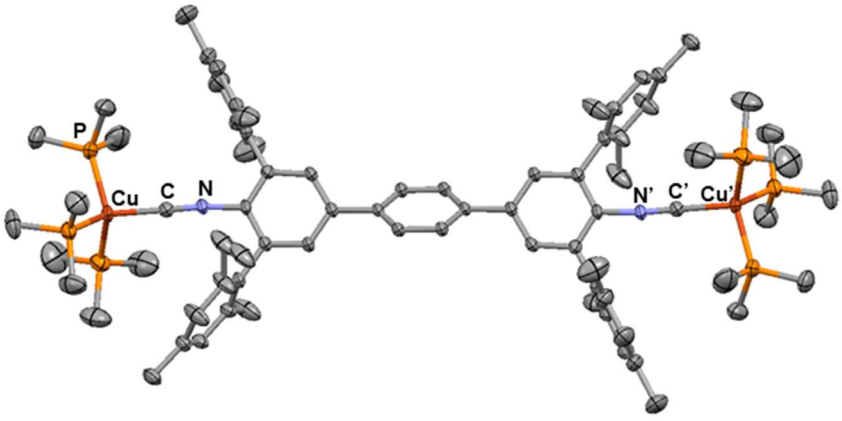

Figure 3.3 Crystal structure of dinuclear species $[CuL_{ph0.5}(PMe_3)_3]PF_6$ synthesized from the dissolution of a coordination network and the addition of 0.5 eq of PMe_3. The PF_6 counteranion has been omitted for clarity.

3.3 Liquid Assisted Anion Exchange

Micromechanical cleavage (Scotch tape method) of graphite to form graphene nanosheets was the start of investigation towards methods of dispersion and exfoliation to control the thinness of a material to improve upon the intrinsic properties available.[22] Another one of those methods commonly employed to remove nanosheets off of each other is sonication.[23–25] While sonication has seen a lot of success in forming thinner sheets of materials it is considered an aggressive method for delicate systems due to the shear stress imparted by the sonication waves that can result in weariness and defects in the nanosheets. Surfactant molecules or inorganic ions have previously been utilized to obtain two-dimensional (2D) nanomaterials specifically with thickness of just one or limited atomic layers with *in-situ* practices by creating a lower surface tension between the solid and the liquid.[26,27]

Combining the attributes of surfactants as exfoliates with a postsynthetic anion exchange transformation that is ubiquitous in literature seemed like a proper approach to achieving thinner 2D sheets in Cu-^{ISO}CN-4.[28–31] A frequently encountered challenge in postsynthetic exchange reactions for metal-organic materials is the proper diffusion of the substrate into the pores/channels of the material for access to the entire framework to prevent solely having reactivity occur at the surface of the material. However, Cu-^{ISO}CN-4 features $[PF_6]^-$ counterions that are located in the interdomain layer of the four-fold interpenetrated sheets. Therefore, with the introduction of an ionic solution it was hypothesized that the ionic surfactant could break the weak electrostatic and dispersion interactions formed between the $[PF_6]^-$ with Cu(I) and ligand aryl groups, respectively, and displace the anion. Sodium dodecyl sulfate (SDS) is an anionic surfactant that contains a sulfate group attached to a 12-carbon tail. Since SDS demonstrates great solubility in water, a solution of SDS in deionized water (DI) below the critical micelle formation concentration was

prepared (Figure 3.4).[32] The SDS solution was added to a mixture of Cu-^{ISO}CN-4 (~ 5 mg) in DI water.

Despite the hydrophobic nature of this framework (contact angle 120°) upon addition of SDS the material quickly has a physical transformation by loss of its buoyancy properties to form a colloidal like suspension in DI water. After 8 hours the suspension settles at the bottom of the vial as seen in Figure 3.4. Importantly, decanting off the solution of water and SDS, followed by 5 washes with water to remove excess SDS and pumping off remaining water results in a colorless powder material. FTIR analysis reveals an ν_{CN} band at 2142 cm^{-1}, unchanged from the starting Cu-^{ISO}CN-4 framework. This lack of shift by FTIR, indicating no chemical change to the isocyanide electronics and therefore no alteration to the environmental coordination of the Cu(I) node, coupled with a physical change by loss of hydrophobicity suggest a secondary sphere anion exchange between the $[PF_6]^-$ counterions and the SDS molecules.

Figure 3.4 (Far right) Solution of SDS in DI water. (Right) Cu-^{ISO}CN-4 floating on top of DI water, demonstrating its hydrophobicity properties and lack of mixture into the water. (Far left) Cu-^{ISO}CN-4 after the addition of SDS solution forming a colloidal like suspension and exhibiting a lack of hydrophobicity. (Left) Cu-^{ISO}CN-4 solid with SDS solution settled at the bottom of the vial after 8 hours of sitting.

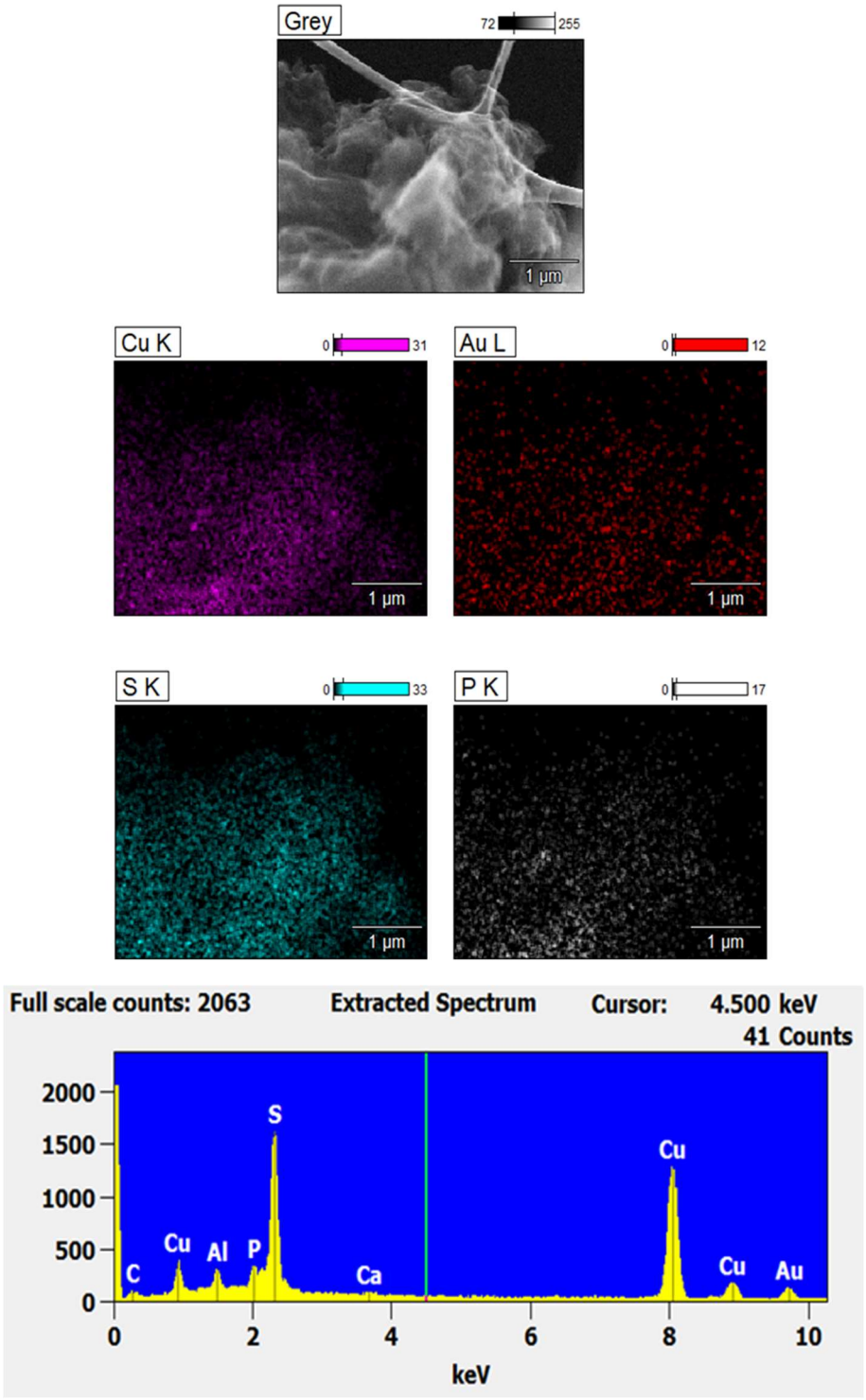

Figure 3.5 (Top) TEM image of post-synthetically exposed Cu-^{ISO}CN-4 to an SDS solution reveals an amorphous material that has lost its crystallinity. EDS K-shell energy for Cu, P and S elements have been mapped out indicating that the sample remains well-disbursed. Sulfur signal is now detected due to the presence of SDS and anion exchange. (Bottom) Quantified EDS results expose a higher level of detection for sulfur signal vs phosphorus signal from the $[PF_6]^-$ relative to the Cu signal.

Long carbon chain surfactants utilized for exfoliation of 2D layered materials are known to disrupt crystal lattice formation because of the large accommodation needed for the incorporation of the anion.[33] The transmission electron microscopy (TEM) of Cu-^{ISO}CN-4 after exposure to SDS, seen in Figure 3.5 (top), presents this loss of crystallinity to the material as well. The once microcrystalline framework now appears as an amorphous solid. In lieu of crystallographic information, to further investigate this anion exchange electron-dispersive X-ray spectroscopy (EDS) was performed for a solid-state elemental analysis.[34,35] Figure 3.5 (bottom) shows the analysis for the K-shell energy of the elements Cu, P and S atoms present in the sample. Copper metal analysis confirms the presence of the material well-disbursed onto the TEM grid, it also serves as a proper one to one comparison of the location and ratio of the anionic elements to be traced. Sulfur elements would be present only from the dodecyl sulfate anion from the exchange process and is detected on the mapped-out EDS analysis and within well agreement of the location with respect to the Cu atoms. In addition, the extracted spectrum quantifies the relative abundance of sulfur as a similar amount to the copper atoms present. This feature is important as it indicates that the sulfur present in a one to one ratio to copper serves as an electronically balancing anion to a cation. It also indicates that the sulfur detected is not from excess SDS that would have been presumed to be removed with multiple DI water washes of the sample. Phosphorous element is also detected with a significantly weaker signal present in the mapping images relative to the sulfur and copper maps. The extracted spectrum quantifies this value of phosphorous detection as much lower than the sulfur present. This suggest that while dodecyl sulfate anions may have exchanged with some $[PF_6]^-$ counterions, that the exchange may not be complete and some scattered $[PF_6]^-$ still remain in the sample. Further investigations into this anion exchange to determine if the 2D Cu-^{ISO}CN-4 sheets are exfoliated and the exact structural composition of the framework (e.g.,

determining the exact location of the dodecyl sulfate anions and the direction they extend in) still remain to be done.

3.4 A Non-Interpenetrated Polymorph Cu(I) Coordination Network

Polymorphs are solid materials with the ability to exist in two or more crystalline forms with different arrangements or conformations in the crystal lattice and are quite abundant in metal-organic frameworks.[36–38] Commonly seen among extended frameworks is the capability of one polymorph of a material to behave differently than the other, particularly for applications in gas storage and separation, which therefore causes them to possess varying properties between the networks.[39–43] However, it is less common to come across a polymorph of a metal-organic material that share different degrees of interpenetration as the connected linkers and nodes should be identical between the two. Interpenetration occurs due to the material avoiding empty space in the pore to minimize the systematic energy and void filling presumably for stabilization of the crystal lattice formation of the framework occurs. However, it also narrows the pores/channels that are now occupied with an additional network. As such, interpenetration is considered detrimental to the crystalline network as most of the applications for MOFs depend on pore accessibility for passage or gas/chemical storage in the cavities.[44,45] As a consequence, many techniques have been developed to impede or control interpenetration. Judicious selection of the organic ligand linkers utilized has been found to be of upmost importance. Employing mixed carboxylic acid linkers, flexible bis(triazole) ligands and the removal and addition of solvent molecules coordinating as ligands are methods reported to hinder the interpenetration of the coordination network.[46–49] In addition, the utilization of templating agents such as oxalic acid and differing solvent conditions can also be useful for the avoidance of interpenetration.[50] Polymorphs that feature varying degrees

of interpenetration is a technique that is more difficult to control since polymorphism usually arises from small incontrollable variables during the synthesis.

In chapter 2, Cu-^{ISO}CN-4 was described as a 2D four-fold interpenetrated framework as a result of the large apertures (~41 Å) that the addition of a phenylene spacer in the *m*-terphenyl diisocyanide linker produced.[4] To avert a large void and form energetically stabilized large single crystals, the material accommodated three interwoven networks that ran in a parallel fashion into the pores of another coordination network. Heavy interpenetration in a framework usually precludes any reactivity from taking place since the pores are essentially obstructed by other networks, fortunately, large channels developed as a result of the interpenetrated domains that allowed for passage of small molecules such as pyridine. Despite this fortunate luck, developing a non-interpenetrated isocyanide coordination network with significantly sized pores was of interest.

A polymorph of Cu-^{ISO}CN-4 was observed utilizing the same procedures and oven program previously described to synthesis Cu-^{ISO}CN-4. Crystallographic analysis of this polymorph, designated Cu-^{ISO}CN-5, revealed a 2D coordination network (P-1 space group) with a **hcb** net (6,3) identical to Cu-^{ISO}CN-4. However, Cu-^{ISO}CN-5 deviates in the pyramidalization (C-Cu-centroid =7.44°), which forms less puckered nodes than the ones found in Cu-^{ISO}CN-4. Indeed, comparison of the 2D sheet materials along the *a*-axis quickly makes this feature apparent (Figure 3.6), the Cu-^{ISO}CN-4 presenting wavier sheets in comparison to Cu-^{ISO}CN-5 with flatter sheets. Most

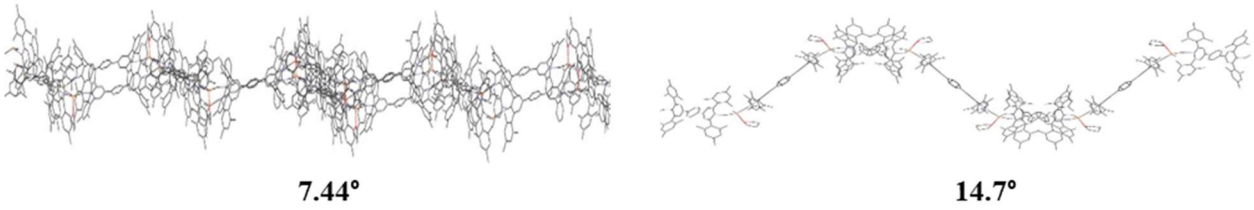

Figure 3.6 View along the *a*-axis of 2D Cu-^{ISO}CN-5 (left) with a pyramidalization of 7.44° indicating flatter sheets than Cu-^{ISO}CN-4 (right) with pyramidalization of 14.7° featuring wavy like sheets.

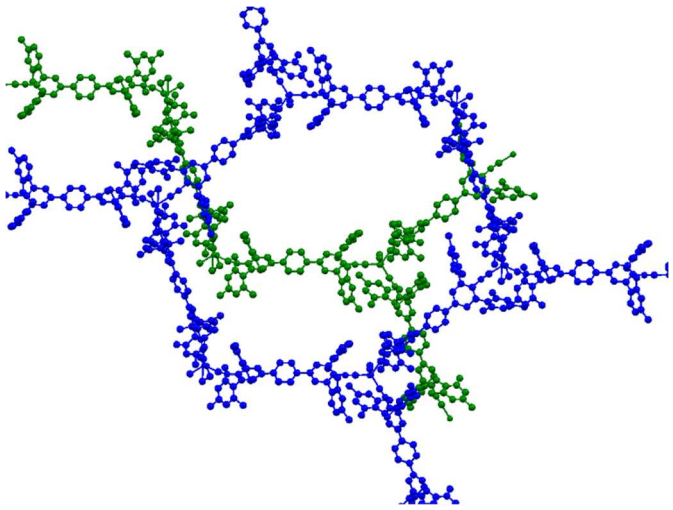

Figure 3.7 Cu-^{ISO}CN-5 with an example of two independent color-coded sheets for simplification stacked on each other in a staggered-like manner. The tightly packed sheets accommodate the flanking *m*-terphenyl groups in the pores of another framework.

importantly, however, Cu-^{ISO}CN-5 is a non-interpenetrated material whose sheets stack in a staggered-like conformation relative to each other as can be seen in Figure 3.7 presumably to create tightly packed sheets that accommodate the sterically hindering mesityl groups on the backbone of the ditopic isocyanide linker. Despite similar aperture size to Cu-^{ISO}CN-4 (~41 Å) present in the structure, the lack of interpenetration is surprising since this behavior usually arises to stabilize the huge void fractions that occur in large unit cells.[51–53] Clever efforts towards the prevention of interpenetration of the pores have been made by careful selection of short axis and net topologies for the reticular synthesis of metal-organic materials.[54,55] Yet, no changes to the organic linker or nodes were made, therefore, we postulate that this polymorphic crystal structure may have been stabilized by weaker interactions (van der Waals forces) that arise from the closely packed, staggered layers in the absence of interpenetration.[56,57] This tight packing/stacking of sheets is not observed in more pyramidal sheets like Cu-^{ISO}CN-4. It is important to note that while crystallographic characterization of Cu-^{ISO}CN-5 was obtained, the synthesis for selectively forming this coordination network is not a reliable or reproducible result. Cu-^{ISO}CN-5 could have formed large single crystals due to a difference in concentration (slight over dilution of starting

reagents[58]) and/or uncontrollable variables, such as, inconspicuous impurities that may have served as unintentional modulators. Still, on-going research aiming to selectively form Cu-^{ISO}CN-5 is currently underway to gain a better understanding of the crystal stability of these coordination networks.

3.5 Supplemental Information

Table 3.1 Crystallographic Data Collection and Refinement Information

Name	$[CuL_{ph0.5}(PMe_3)_3]PF_6$	$Cu^{ISO}CN\text{-}5$
Formula	$C_{41}H_{62.5}CuF_6NOP_4$	$C_{176}H_{172}Cu_2F_6N_6O_2P$
Crystal System	Triclinic	Triclinic
Space Group	P-1	P-1
a, Å	11.5755(16)	13.4915(5)
b, Å	13.475(3)	26.0080(11)
c, Å	16.088(2)	28.0688(11)
α, deg	71.214(8)	78.372(2)
β, deg	75.956(6)	78.721(2)
γ, deg	80.129(12)	77.816(2)
V, Å^3	2292.9(7)	9308.3(6)
Z	2	4
Radiation (λ, Å)	Cu-Kα, 1.54178	Cu-Kα, 1.54178
ρ (calcd.), g/cm^3	1.285	0.816

μ (Mo Ka), mm^{-1}	2.458	0.595
Temp, K	100	100
θ max, deg	134.352	105.38
data/parameters	7974/517	20850/1599
R_1	0.0702	0.1065
wR_2	0.1943	0.3090
GOF	1.063	1.046

3.6 Acknowledgments

In Chapter 3, section 3.3 utilizing liquid assisted anion exchange in a Cu(I) coordination network is in preparation for publication by A. Arroyave, M. Touve, N. Gianneschi, J. S. Figueroa. The dissertation author is the primary author of this manuscript.

3.7 References

(1) Gándara, F.; Bennett, T. D. *IUCrJ* **2014**, *1*, 563–570.

(2) Moghadam, P. Z.; Li, A.; Liu, X. W.; Bueno-Perez, R.; Wang, S. D.; Wiggin, S. B.; Wood, P. A.; Fairen-Jimenez, D. *Chem. Sci.* **2020**, *11*, 8373–8387.

(3) Øien-ØDegaard, S.; Shearer, G. C.; Wragg, D. S.; Lillerud, K. P. *Chem. Soc. Rev*. **2017**, 4867–4876.

(4) Arroyave, A.; Gembicky, M.; Rheingold, A. L.; Figueroa, J. S. *Inorg. Chem.* **2020**, *59*, 11868–11878.

(5) Eller, P. G.; Bradley, D. C.; Hursthouse, M. B.; Meek, D. W. *Coord. Chem. Rev.* **1977**, *24*, 1–95.

(6) Aresta, M.; Nobile, C. F.; Sacco, A. *Inorganica Chim. Acta* **1975**, *12*, 167–178.

(7) Ugo, R. *Coord. Chem. Rev.* **1968**, *3*, 319–344.

(8) Dick, D. G.; Stephan, D. W.; Campana, C. F. *Can. J. Chem.* **1990**, *68*, 628–632.

(9) Arroyave, A.; Gembicky, M.; Rheingold, A. L.; Figueroa, J. S. *Inorg. Chem.* **2020**, *59*, 11868–11878.

(10) Bordignon, E.; Croatto, U.; Mazzi, U.; Orio, A. A. *Inorg. Chem.* **1974**, 13, 935-940.

(11) Mathieson, T.; Schier, A.; Schmidbaur, H. *J. Chem. Soc. Dalt. Trans.* **2001**, *0*, 1196–1200.

(12) Chaudhary, A.; Mohammad, A.; Mobin, S. M. *Cryst. Growth Des*. **2017**, 17, 2893–2910.

(13) Lee, E. Y.; Suh, M. P. *Angew. Chemie* **2004**, *116*, 2858–2861.

(14) Li, J.; Huang, P.; Wu, X. R.; Tao, J.; Huang, R. Bin; Zheng, L. S. *Chem. Sci.* **2013**, *4*, 3232–3238.

(15) Gao, W.; Cardenal, A. D.; Wang, C.; Powers, D. C. *Chem. – A Eur. J.* **2019**, *25*, 3465–3476.

(16) Haldoupis, E.; Nair, S.; Sholl, D. S. *J. Am. Chem. Soc.* **2010**, *132*, 7528–7539.

(17) Osborn Popp, T. M.; Plantz, A. Z.; Yaghi, O. M.; Reimer, J. A. *Chem. Phys. Chem.* **2020**, *21*, 32–35.

(18) Heinke, L.; Gu, Z.; Wöll, C. *Nat. Commun.* **2014**, *5*, 4562.

(19) O'Keeffe, M.; Yaghi, O. M. *Chem. Rev*. **2012**, *112*, 675–702.

(20) Liu, L.; Zhang, D.; Zhu, Y.; Han, Y. *Commun. Chem.* **2020**, *3*, 1–14.

(21) Zhou, Y.; Zhou, Y.; Xu, X.; Xu, X.; Carlsson, A.; Lazar, S.; Pan, Z.; Ma, Y.; Terasaki, O.; Deng, H.; *Chem. Mater.* **2020**, *32*, 4966–4972.

(22) Ravula, S.; Baker, S. N.; Kamath, G.; Baker, G. A. *Nanoscale*. **2015**, *7*, 4338–4353.

(23) Turner, P.; Hodnett, M.; Dorey, R.; Carey, J. D. *Sci. Rep.* **2019**, *9*, 1–8.

(24) Durge, R.; Kshirsagar, R. V.; Tambe, P. *Procedia Eng.* **2014**, *97*, 1457–1465.

(25) Yi, M.; Shen, Z. *J. Mater. Chem. A*. **2015**, *3*, 11700–11715.

(26) Wang, S.; Yi, M.; Shen, Z. *RSC Adv.* **2016**, *6*, 56705–56710.

(27) Wang, F.; Seo, J. H.; Luo, G.; Starr, M. B.; Li, Z.; Geng, D.; Yin, X.; Wang, S.; Fraser, D. G.; Morgan, D.; *Nat. Commun.* **2016**, *7*, 1–7.

(28) Noori, Y.; Akhbari, K. *RSC Adv*. **2017**, 1782–1808.

(29) Zhao, X.; Bu, X.; Wu, T.; Zheng, S. T.; Wang, L.; Feng, P. *Nat. Commun.* **2013**, *4*, 1–9.

(30) Fei, H.; Rogow, D. L.; Oliver, S. R. J. *J. Am. Chem. Soc.* **2010**, *132*, 7202–7209.

(31) López-Cabrelles, J.; Espallargas, G. M.; Coronado, E. *Polymers* **2016**, *8*, 171.

(32) Hao, X.; Lei, J. L.; Li, N. B.; Luo, H. Q. *Anal. Chim. Acta.* **2014**, *852*, 63–68.

(33) Zhao, Z.; Shi, S.; Cao, H.; Li, Y. *J. Memb. Sci.* **2017**, *530*, 220–231.

(34) Schmidt, R.; Fitzek, H.; Nachtnebel, M.; Mayrhofer, C.; Schroettner, H.; Zankel, A. *Macromol. Symp.* **2019**, *384*, 1800237.

(35) Chen, Z.; Taplin, D. J.; Weyland, M.; Allen, L. J.; Findlay, S. D. *Ultramicroscopy* **2017**, *176*, 52–62.

(36) Bernstein, J. *Polymorphism in Molecular Crystals.* Oxford University Press, **2010**.

(37) Cruz-Cabeza, A. J.; Bernstein, J. Conformational Polymorphism. *Chem. Rev*. **2014**, *114*, 2170–2191.

(38) Desiraju, G. R. *Science* **1997**, *278*, 404 – 405.

(39) Bon, V.; Senkovska, I.; Baburin, I. A.; Kaskel, S. *Cryst. Growth Des.* **2013**, *13*, 1231–1237.

(40) Lee, S. J.; Mancuso, J. L.; Le, K. N.; Malliakas, C. D.; Bae, Y. S.; Hendon, C. H.; Islamoglu, T.; Farha, O. K. *ACS Mater. Lett.* **2020**, *2*, 499–504.

(41) Karadeniz, B.; Žilić, D.; Huskić, I.; Germann, L. S.; Fidelli, A. M.; Muratović, S.; Lončarić, I.; Etter, M.; Dinnebier, R. E.; Barišić, D. *J. Am. Chem. Soc.* **2019**, *141*, 19214–19220.

(42) Landaverde-Alvarado, C.; Morris, A. J.; Martin, S. M. *J. CO2 Util.* **2017**, *19*, 40–48.

(43) Frahm, D.; Hoffmann, F.; Fröba, M. *Cryst. Growth Des.* **2014**, *14*, 1719–1725.

(44) Haldar, R.; Sikdar, N.; Maji, T. K. *Mater. Today*. **2015**, *18*, 97–116.

(45) Jiang, H. L.; Makal, T. A.; Zhou, H. C. *Coord. Chem. Rev*. **2013**, *257*, 2232–2249.

(46) He, W. W.; Li, S. L.; Yang, G. S.; Lan, Y. Q.; Su, Z. M.; Fu, Q. *Chem. Commun.* **2012**, *48*, 10001–10003.

(47) Choi, S. B.; Furukawa, H.; Nam, H. J.; Jung, D.-Y.; Jhon, Y. H.; Walton, A.; Book, D.; O'Keeffe, M.; Yaghi, O. M.; Kim, J. *Angew. Chemie* **2012**, *124*, 8921–8925.

(48) He, X.; Lu, X. P.; Tian, Y. Y.; Li, M. X.; Zhu, S.; Xing, F.; Morris, R. E. *Cryst. Eng. Comm.* **2013**, *15*, 9437–9443.

(49) Furukawa, H.; Ko, N.; Go, Y. B.; Aratani, N.; Choi, S. B.; Choi, E.; Yazaydin, A. Ö.; Snurr, R. Q.; O'Keeffe, M.; Kim, J.; *Science* **2010**, *329*, 424–428.

(50) Guo, M.; Sun, Z. M. *J. Mater. Chem.* **2012**, *22*, 15939–15946.

(51) Batten, S. R. *Cryst*. *Eng. Comm.* **2001**, *3*, 67-72.

(52) Nguyen, T. T. M.; Le, H. M.; Kawazoe, Y.; Nguyen, H. L. *Mater. Chem. Front* **2018**, *2*, 2063.

(53) Blatov, V. A.; Carlucci, L.; Ciani, G.; Proserpio, D. M. *Cryst. Eng. Comm.* **2004**, *6*, 377-395.

(54) Yan, Y.; Juríček, M.; Coudert, F.-X.; Vermeulen, N. A.; Grunder, S.; Dailly, A.; Lewis, W.; Blake, A. J.; Stoddart, J. F.; Schröder, M. *J. Am. Chem. Soc.* **2016**, *138*, 3371–3381.

(55) El-Kaderi, H. M.; Hunt, J. R.; Mendoza-Cortes, J. L.; Cote, A. P.; Taylor, R. E.; O'Keeffe, M.; Yaghi, O. M.; Whalley, A. C.; Liu, Z.; Asahina, S. *Science* **2007**, *316*, 268–272.

(56) Klein, N.; Senkovska, I.; Baburin, I. A.; Grünker, R.; Stoeck, U.; Schlichtenmayer, M.; Streppel, B.; Mueller, U.; Leoni, S.; Hirscher, M. *Chem. - A Eur. J.* **2011**, *17*, 13007–13016.

(57) Gong, Y.-N.; Zhong, D.-C.; Lu, T.-B. *Cryst. Eng. Comm.* **2016**, *18*, 2596.

(58) Eddaoudi, M.; Kim, J.; Rosi, N.; Vodak, D.; Wachter, J.; O'Keeffe, M.; Yaghi, O. M. *Science* **2002**, *295*, 469 – 472.

Chapter 4 A Porous, Crystalline Ni(0) Organometallic Network Material with Redox and Structural Flexibility Properties

4.1 Introduction

Metal-organic frameworks (MOF) are a class of coordination networks that are prominent in the literature for superb high surface area, permanent porosity, and a well-defined crystalline lattice.[1–5] These properties and the array of options for assembly in metal nodes and organic linkers make these frameworks ideal for applications in gas separations, chemical storage, and heterogenous catalysis.[6–10] Furthermore, much progress has been reported for the fine tuning of these materials to improve on these properties by taking advantage of post-synthetic modifications (PSM) to build distinctive framework structures.[11–13] Namely, the incorporation of catalytic organometallic molecules by impregnation onto a framework to support a homogenous system onto a solid has seen much success.[14,15] However, because the molecules are incorporated into the structure post-synthetically, these materials tend to suffer from leaching of the molecules/metals and therefore are detrimental to the catalytic turn-over numbers.[16] Another approach to incorporate organometallic systems into MOFs was made by Yaghi et.al. by utilizing carboxylate linkers that were synthetically optimized to include a carbene group that would preferentially bind to a palladium (II) complex after the initial formation of the MOF.[17] Despite these impressive attempts, only a hand full of *in-situ* formation of organometallic frameworks are found in the literature due to hard-soft acid-base chemistry that dominates the foundation of self-assembly principles in MOF

synthesis.[18] Metal clusters commonly found in MOF literature are hard acids (e.g. Zf, Hf and Zn) that demand hard base ligands (e.g. carboxylates, imidazolates). Attempts to utilize heterogenous ligands with properties of both hard and soft ligand bases have been made by Humphrey et. al. with the synthesizes of a decorated MOF with phosphine ligands that preferentially coordinate softer, low-valent metal centers to embed the inner-lining of the MOF with Au(I) centers.[19] Targeting a direct metal-carbon link that functions as both linker and node would open avenues for softer metal node exploration where the metal would be immobilized without the threat of metal-leaching during catalytic conversions. For instance, Dong et. al. synthesized a Pd(II)-isocyanide OMF (organometallic framework) that was utilized as an effective Suzuki-coupling catalyst.[20] The palladium-isocyanide coordination bond in Pd-OMF is indisputable according to the spectroscopic evidence, however, rietveld refinement was performed in the absence of single crystals thereby leaving structural information such as interpenetration and packing details less definitive. Structural details are imperative for improvement of any catalytic system. Thus, *in-situ* formation of organometallic coordination networks still remains a challenge and an underdeveloped area of materials chemistry.

We have previously reported the first zero-valent nickel nodal coordination network by utilizing prior molecular knowledge and harnessing the true synthetic potential of *m*-terphenyl isocyanides.[21] Relying heavily on the molecular studies of $Ni(CNAr^{Mes2})_4$ (Ar^{Mes2} = 2,6-(2,4,6,-$Me_3C_6H_2$)C_6H_3) which forms a tetrahedral geometry about Ni(0) we were able to use this knowledge for the extension of the molecule into an extended framework.[22] Synthesizing a ditopic *m*-terphenyl isocyanide was necessary in order to preserve a similar coordination environment about the metal node. The addition of an acetonitrile (MeCN) solution of $[CNAr^{Mes2}]_2$ (Ar^{Mes2} = 2,6-(2,4,6,-$Me_3C_6H_2$)C_6H_3) to a solution of $Ni(COD)_2$ (COD = 1,5- cyclooctadiene) under an inert

atmosphere and solvothermal conditions generates single crystals of Ni-^{ISO}CN-2·([CNAr^{Mes2}]$_2$)$_{0.5}$ (^{ISO}CN = isocyanide coordination network). Ni-^{ISO}CN-2·([CNAr^{Mes2}]$_2$)$_{0.5}$ is a network of a 2-fold interpenetrated, diamondoid type with tetrakis-isocyanide Ni(0) nodes, providing a similar coordination environment to Ni(CNAr^{Mes2})$_4$. Importantly, this demonstrated that the use of π-acidic isocyanides enables stabilization of electron-rich Ni(0) metal centers,[23–26] a trait known in molecular systems but not yet confirmed in frameworks. However, assessment of the void space indicates partial occupation (50 %) by an uncoordinated isocyanide ligand. The presence of free ligand in the pore is postulated to be due to increasing structural stability to enable the material to crystallize. The removal of the ligand from the pores was unsuccessful after multiple washes in a variety of solvents and under vacuum rendering the ligand trapped inside the pores of this framework. Blocked pores in a framework can deeply impact a number of properties of a network especially frameworks containing zero-valent nodes that would otherwise be advantageous to chemically explore.[27,28] Recently, we published on Cu-^{ISO}CN-4, a tris-isocyanide Cu(I) node with an adduct THF molecule on each nodal site.[29] This framework was synthesized by modifying [CNAr^{Mes2}]$_2$ utilizing a *para*- positioned phenylene spacer (1,4-(CNAr^{Mes2})$_2$C$_6$H$_4$) to effectively elongate the linker and increase pore size by 4 times when compared to other Cu-^{ISO}CN frameworks (previously reported Cu-^{ISO}CN-3).[30] We sought to achieve this same increase in aperture for a Ni(0) nodal material that could then prevent the entrapment of a unit of ligand in the pores.

Accordingly, we report Ni-^{ISO}CN-3, a crystalline tetrakis-isocyanide Ni(0) nodal coordination network utilizing 1,4-(CNAr^{Mes2})$_2$C$_6$H$_4$ as linkers. While Ni-^{ISO}CN-3 features similar coordination geometries and electronic environments about the nickel nodal center compared to Ni-^{ISO}CN-2, it is important to note that there is no indication of a non-coordinated linker present

in the pores of Ni-^{ISO}CN-3 as determined by single-crystal diffraction and spectroscopic FTIR data. Furthermore, this coordination network can be chemically probed to undergo a one electron redox cycle as determined *via* FTIR data, suggesting a general trend for redox cycling in Ni(0) materials. Interestingly, Ni-^{ISO}CN-3 was also determined to be a flexible material that can structurally withstand a reversible dynamic change. The chemical and structural stability demonstrated by Ni-^{ISO}CN-3 signifies that coordination networks utilizing isocyanides as organic linkers not only behave similarly to anionic linkers in terms of strength and chemical resistance but can also permit the inclusion and study of low-valent metal centers to act as nodal centers.

4.2 Synthesis and Characterization

A MeCN solution of $Ni(COD)_2$ was stirred for 15 minutes at room temperature before being added to a warm pressure tube. A solution of 1,4-$(CNAr^{Mes2})_2C_6H_4$ in MeCN was quickly added to the same pressure tube and sealed with a Teflon cap. This dark-red polymeric mixture was quickly placed into a preheated programmable oven set to 120 °C for 24 hours with a slow cooling to 80 °C over the course of 48 hours to produce red single crystals of Ni-^{ISO}CN-3 suitable

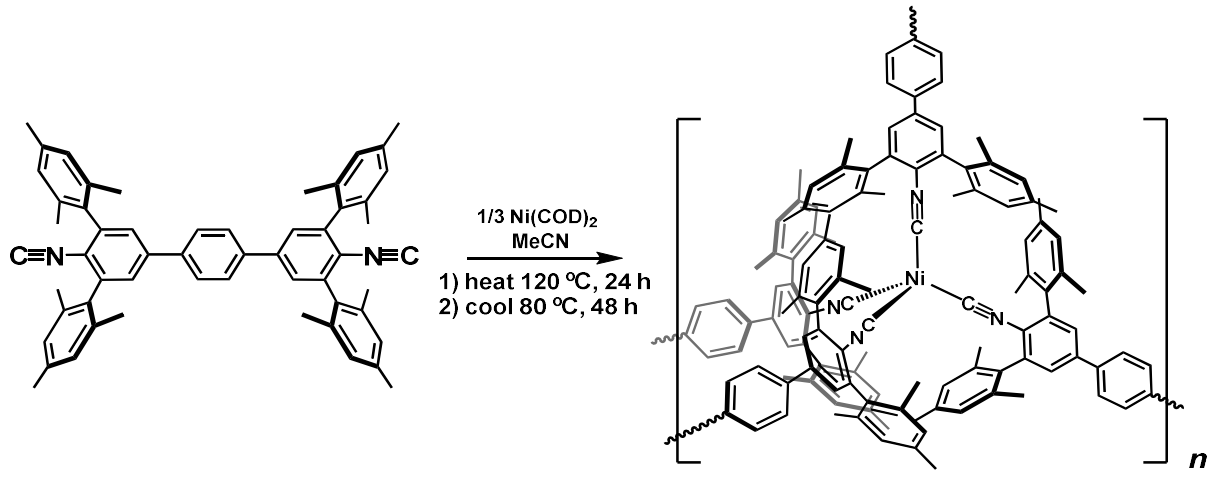

Scheme 4.1 Synthesis of Ni-^{ISO}CN-3

for X-ray diffraction (Scheme 4.1). Crystals of Ni-^{ISO}CN-3 were gently washed with acetonitrile five times for further analysis.

ATR-IR reveals a spectroscopic signal at ν_{CN} 1950 cm^{-1} and most importantly, the absence of a free isocyanide signal that would indicate the presence of free ligand (Figure 4.8). Ni-^{ISO}CN-3 is a diamondoid, three-dimensional structure featuring a Ni(0) node coordinated to four ditopic isocyanide ligands (1,4-(CNAr^{Mes2})$_2$C$_6$H$_4$) at each of these nodes as presented by crystallographic analysis (Figure 4.1). Importantly, examination of the void space in Ni-^{ISO}CN-3 reveals no indication of the presence of uncoordinated ditopic isocyanide ligand in accord with the FTIR spectroscopic data. Instead, this framework gains structural stability from being four-fold interpenetrated to promote the formation of single crystals. A significant amount of interpenetration is expected to occur as the length of the linker increases to avoid unfavored void space and mitigate collapse in the pores of the framework. Nevertheless, despite this heavy interpenetration, pores of approximately 12 x 7 Å are occupied by MeCN molecules that have been omitted for clarity. Solvent molecules with low temperature boiling points, such as acetonitrile,

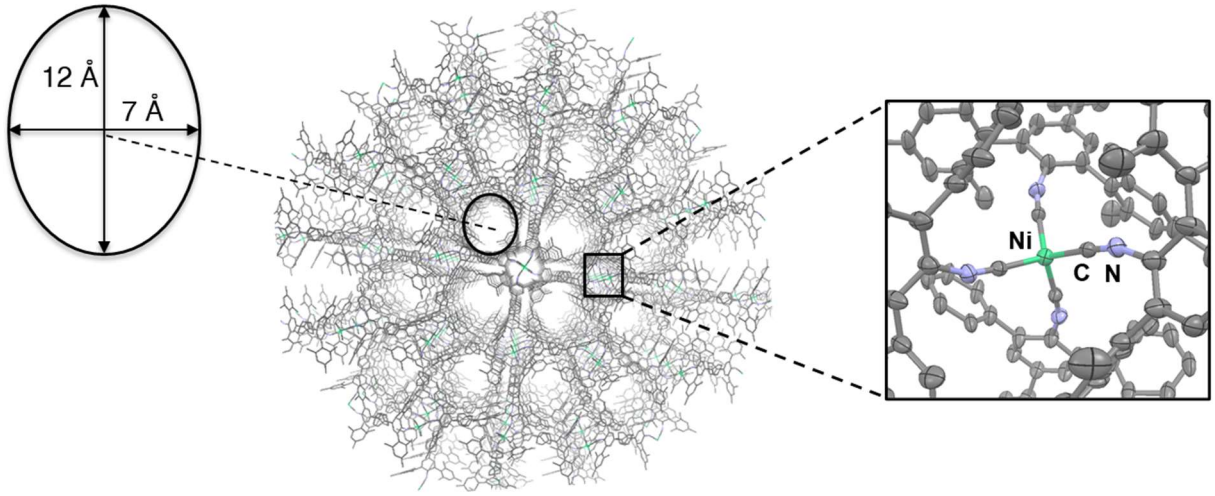

Figure 4.1 Crystal structure of Ni-^{ISO}CN-3. Inset (right) of Ni(0) node demonstrating coordinated isocyanide linkers. Inset (left) the void space available within the pore of the framework of ~ 12 x 7 Å.

can be evacuated during activation of the material and indicate that access throughout the framework is still feasible. Thermogravimetric analysis of Ni-^{ISO}CN-3 (Figure 4.14) reveals minimal loss of weight due to solvent and a single step attributed to the decomposition with an onset temperature of 320 °C.

Table 4.1 Structural and spectroscopic comparison across four-coordinate isocyanides about Ni(0) centers

	Ni-^{ISO}CN-3	**Ni-^{ISO}CN-2·([CNAr^{Mes2}])$_{2})_{0.5}$**	**Ni(CNAr^{Mes2})$_4$**
Interpenetration	four-fold	two-fold	n/a
τ_4	0.96	0.98	0.85
Avg. Ni-C Bond	1.84 Å	1.84 Å	1.91 Å
ν_{CN}	1950 cm^{-1}	1950 cm^{-1}	1984 cm^{-1}

Notably, the addition of Ni-^{ISO}CN-3 allows for the comparison of structural and electronic properties across the small library of tetrahedral geometries about a four-coordinate Ni(0) center (Table 4.1). A smaller degree of interpenetration is found in Ni-^{ISO}CN-2·([CNAr^{Mes2}]$_2$)$_{0.5}$ compared to Ni-^{ISO}CN-3 (two-fold and four-fold, respectively) as expected due to the length of the linker utilized for the synthesis of these materials. Furthermore, the presence of uncoordinated isocyanide ligand in the pores of Ni-^{ISO}CN-2·([CNAr^{Mes2}]$_2$)$_{0.5}$ precludes additional interpenetration. Simple calculation of the τ_4 value, a popular index for the classification of four-coordinate geometries,[31] reveals that both of the Ni(0) frameworks are much closer to a tetrahedral structure than the molecule. We reason that the lattice of the framework demands a more rigid structure due to the connectivity of the material. Ni(CNAr^{Mes2})$_4$ (τ_4 = 0.85) also features bent C≡N-R bonds indicating less orbital overlap that results in less backbonding from the electron rich nickel center when compared to the linear isocyanides in the structures of the materials. This observation of bent vs linear isocyanides is also supported by FTIR data. Less π^* donation would increase the energy required to perturb the C≡N-R bond, accordingly, ATR-IR analysis of both Ni(0)

frameworks reveals a single broad ν_{CN} absorbance band centered at 1950 cm^{-1} while $Ni(CNAr^{Mes2})_4$ features a higher in energy ν_{CN} stretch at 1984 cm^{-1}.

4.3 Ni-^{ISO}CN-3 Stability in Ambient Conditions

Obtaining air-stable Ni(0) catalyst is an ongoing interest for efficiency in organic chemical transformations.[32–34] Typically Ni(0) complexes, including $Ni(CNAr^{Mes2})_4$, rapidly decompose when exposed to air and are exclusively handled under air-free conditions such as a glovebox or Schlenk line. Ni-^{ISO}CN-2, the bulk ligand-free version of Ni-^{ISO}CN-2·$([CNAr^{Mes2}]_2)_{0.5}$, was reported to be sensitive to conditions in ambient atmosphere.[21] ATR-IR spectra revealed degradation to free $[CNAr^{Mes2}]_2$ (ν_{CN} = 2114 cm^{-1}) after 30 seconds of exposure. After 24 hours the absorbance peak at 2114 cm^{-1} was at a 1:1 ratio with the isocyanide absorption peak pertaining to Ni-^{ISO}CN-2 (ν_{CN} = 1950 cm^{-1}). While this spectroscopic data shows the vulnerability of Ni(0) materials to behave like Ni(0) complexes, it also indicates more stability towards air than the molecules by not fully decomposing at the 24-hour mark. ATR-IR stability studies on Ni-^{ISO}CN-

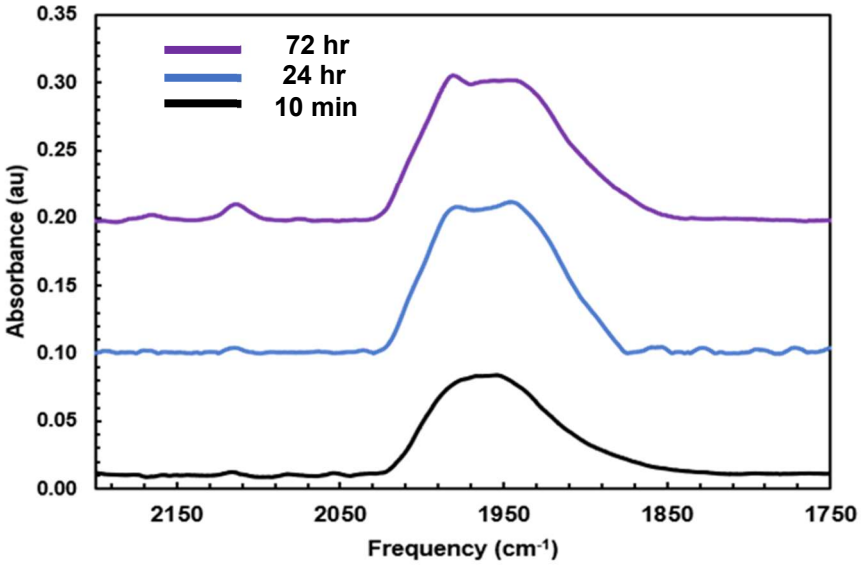

Figure 4.2 Stacked ATR-IRs of Ni-^{ISO}CN-3 exposed to ambient conditions on the bench at designated time points; 10 minutes (black line), 24 hr (blue line) and 72 hr (purple line).

3 demonstrates an even greater resistance to degradation in air (Figure 4.2). After being prepped in a glovebox and removed as a solid in a vial, Ni-^{ISO}CN-3 was opened to air. ATR-IR spectrum of Ni-^{ISO}CN-3 after 10 minutes of exposure indicates no sign of degradation by the presence of a free isocyanide ligand band. It is after 72 hours that a peak at 2114 cm^{-1} (uncoordinated ligand) begins to surface and a 1:1 peak ratio with the original ν_{CN} 1950 cm^{-1} and a new 1990 cm^{-1} are distinguishable. Under an inert atmosphere Ni-^{ISO}CN-3 is stable for months, indicating no degradation to FTIR signal of ν_{CN}. Therefore, to further probe the delayed decomposition observed when exposed to air, Ni-^{ISO}CN-3 was treated with 1 atm of O_2 gas in THF to facilitate the decomposition event. After 24 hours there is no observed change in the framework mirroring previous ambient atmospheric experiments, and it is only after 72 hours that a significant change to the FTIR is detected (Figure 4.7). Similar splitting of the ν_{CN} peak is observed as well as a 1:3 ratio of free isocyanide vs Ni-CNR signal. The presence of an isocyanate (OCNR) signal at 2255 cm^{-1}, which was absent from previous air exposure data, is likely due to the presence of solvent (THF) in the sample that can not only accelerate the loss of coordinated ligand but also enable the transformation of isocyanide to isocyanate in the presence of oxygen.[35,36]

Zero-valent, late transition metals are known to be extremely sensitive to the presence of H_2O and can hinder catalytic transformations specifically in Pd(0) and Ni(0) systems.[37–41] Previously, Cu-^{ISO}CN-4 was found to be extremely stable in water and air, this was partially attributed to the hydrophobic environment of the *m*-terphenyl groups.[29] Interested by the prospect to test if these *m*-terphenyl groups could inhibit H_2O from interacting with the highly susceptible Ni(0) metal nodes, we decided to degas Millipore H_2O under an atmosphere of Ar (g) for an hour that was then added to a sample of Ni-^{ISO}CN-3 under an inert atmosphere of N_2. After 24 hours there was no shift observed in the FTIR of ν_{CN} that would indicate oxidation of the metal nodal

centers and no signal attributed to free isocyanide that would indicate decomposition of the material (Figure 4.9). Again, mirroring previous stability results, after 72 hours we begin to see the small presence of isocyanide and isocyanate appear (Figure 4.10). Notably, Ni-^{ISO}CN-3 is also hydrophobic and will float on top of the water instead of sinking as can be seen in Figure 4.12, suggesting that the bulky *m*-terphenyl groups also play a role in the stability demonstrated in H_2O. We believe that the extra stability imparted by the extended crystalline lattice and interpenetration also plays a significant part to slow down reactivity with water or air in this framework. While these results do not suggest the prolonged stability under ambient conditions compared to Cu^{ISO}CN-4, they are significant in contrast to other Ni(0) complexes that display immediate oxidation and decomposition.[42]

4.4 Spectroscopic One Electron Chemical Redox-Cycling in the Solid State

Metal-organic framework materials are recognized for energy storage capabilities but their potential as charge transporters and electrical energy storage has only recently been explored.[43] Numerous reported attempts at improving the electrochemical properties of MOFs by incorporating anchored redox-cycling ligands into the pores or impregnating the frameworks with redox active nanoparticles have achieved impressive results that circumvent the inherent insulating properties of most frameworks.[44–48] A different approach to achieve electrochemical properties in MOFs is to take advantage of a well-known redox-active metal complex as Zhang et. al. did with a Ru^{II}/Ru^{III} bipyridine molecular system that was then cleverly incorporated into a Zn-carboxylate *in-situ*.[47] In a similar manner, known organometallic molecules with coordinated isocyanide ligands that impart considerable σ-donation are usually capable of multielectron cycling between oxidation states.[49–51] Since nickel is recognized to be able to access many oxidation states (0, 1, 2, 3, 4) as well,[52] we decided to inquire about the potential redox properties of Ni-^{ISO}CN-3.

The addition of a 100 mM solution of ferrocenium triflate in MeCN to Ni-^{ISO}CN-3 was left for 6 hours at room temperature under an inert atmosphere of N_2 where the framework slowly changed color from a bright red to dark orange. Spectroscopic analysis *via* FTIR demonstrates a blue shift of ~80 cm^{-1}(Figure 4.3) from the as-prepared sample to ν_{CN}: 2031 cm^{-1}, suggesting a one-electron oxidation to a Ni(I) metal center as similar energy shifts have been seen from previously reported monovalent nickel systems.[53] Unfortunately, several failed attempts were made at diffracting a crystal of this proposed oxidized framework. While spectroscopically this observation is possible, it is made clear from the loss of crystallinity during this reaction that structurally the full oxidation of the nickel nodes disrupts the crystalline lattice severely. Still chemically, a full one electron reduction of the oxidized material to obtain the return of the spectroscopic signal of ν_{CN}: 1950 cm^{-1} is possible with the addition of a 100 mM solution of

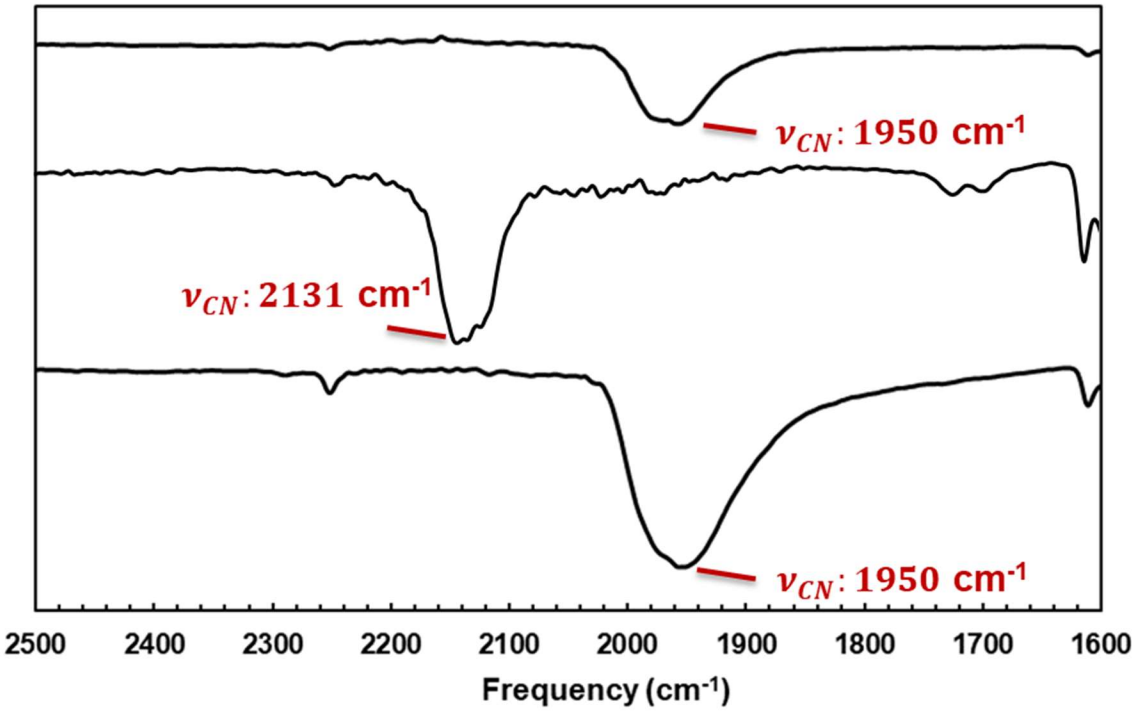

Figure 4.3 Stacked ATR-IRs of the one electron chemical redox cycle for Ni-^{ISO}CN-3. (bottom) As-prepared sample with one ν_{CN} stretch observable. (middle) One-electron oxidation of sample with 100 mM of ferrocenium triflate blue shifted ~ 80 cm^{-1}. (top) Subsequent one-electron reduction with 100 mM of cobaltocene shifted back to the original ν_{CN} frequency.

cobaltocene. This reduction to the as-prepared Ni(0) nodes occurs quickly (within minutes) as would be expected due to the preference of these nickel centers to favor an 18-electron instead of a 17-electron system. Ni-^{ISO}CN-3 withstanding a chemical one-electron full redox cycle is a tribute to the chemical stability of an isocyanide-based framework.

4.5 Structural Flexibility in Ni-^{ISO}CN-3

Structural flexibility is a unique property in frameworks that can arise due to the variety and tunability of assembly components that are utilized to form metal-organic materials. One of the earlier notable works demonstrated the effects of different pressure on the structure of ZIF-8.[54] In a diamond anvil cell, ZIF-8 was taken up to a pressure of 1.47 GPa where a new phase of the material was observed. Remarkably, they found that this structural change was reversible once the pressure was decreased. Further theoretical and experimental investigation in this area has led to different observations of breathability, pore gating and dynamic changes that help describe the role of the building blocks and functional groups to determine flexibility in MOFs with *in-situ* XRD studies.[55–58] The structural flexibility feature that certain materials possess helps explain behavior, such as, size inclusion of gas molecules that were predicted to not absorb based on the structural depictions of the static pore aperture.[59,60] However, understanding this physical property would have a fundamental impact on the performance of materials to be utilized as advanced molecular sieving membrane materials.

One individual framework of Ni-^{ISO}CN-3 can be classified as a mesoporous material (2-50 nm in width) with a width of approximately 33 Å because of the large diamondiod void that results due to the utilization of the phenylene spaced linker (Figure 4.13 and Figure 4.15). However, it is important to consider the four-fold interpenetration that impedes that available space from being occupied and shrinks the width of the aperture to approximately 12 Å (Figure 4.16), placing the

framework in the microporous region (less than 2 nm in width).[61,62] Furthermore, with the presence of smaller channels the orientation of heteroaryl rings, such as the ones present on the *m*-terphenyl groups of the isocyanide linker, with respect to one another can sufficiently block the pores from guest entry.[59] This blocked orientation imposed by the non-covalent interactions between different linkers in the interpenetrated structure could be unblocked and opened by the introduction of sorbents that also interact with the framework non-covalently and can result in gate-opening via ring rotation to obtain accessible porosity. Accordingly, the N_2 sorption data (type VI) (Figure 4.4) sees an increase in gas uptake along the lower pressure region (0 – 0.1 relative pressure), appropriate for a microporous uptake to take place. Importantly, the three steps present in the lower pressure region of the N_2 isotherm suggest a "pore-gating" mechanism that allows the uptake of more N_2 gas to occupy the framework. The stepped absorption profile is indicative of a structural change occurring and possibly the switching between the closed and open orientation for the pores, although no *in-situ* XRD studies were done to confirm. Moreover, the desorption curve does not align with the sorption curve resulting in hysteresis.[63] It is important to note that a hysteresis was also reported in the N_2 isotherm of Ni-^{ISO}CN-2 and it was attributed to pore-blocking of the *m*-

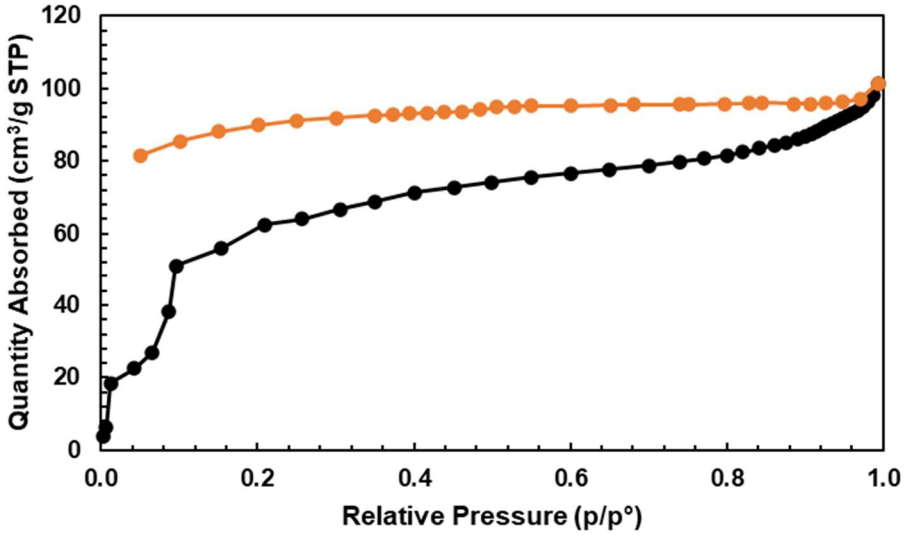

Figure 4.4 N_2 isotherm for Ni-^{ISO}CN-3, absorption curve is in black and the desorption curve in orange. Steps present in absorption and hysteresis suggest flexibility in the material.

terphenyl mesityl substituents that create microdomains for N_2 entrapment.[21] We contend that the same behavior is present in Ni-^{ISO}CN-3 due to the similar coordination environments at each nodal center.

To further probe this flexibility behavior, spectroscopic and powder-XRD analysis of the sample post-gasorption run were performed. ATR-IR of the sample revealed no change to the ν_{CN} stretching frequency and no evidence of the deterioration of the sample by free-ligand (Figure 4.11). This indicates the chemical stability of Ni-^{ISO}CN-3 to withstand the dynamic changes occurring within the framework. In Figure 4.5, a PXRD sample of crystalline Ni-^{ISO}CN-3 as prepared is compared to the post-gasorption analysis pattern that now appears similar to collapsed structures due to the lack of peaks as a result of the loss of crystallinity in the sample. Remarkably, after the post-gasorption sample is soaked in MeCN (same solvent from solvothermal conditions) for 24 hours another collected PXRD reveals the appearance of a crystalline sample very similar to the as prepared sample (differing amounts of solvent could affect shifts slightly). Ni-^{ISO}CN-3

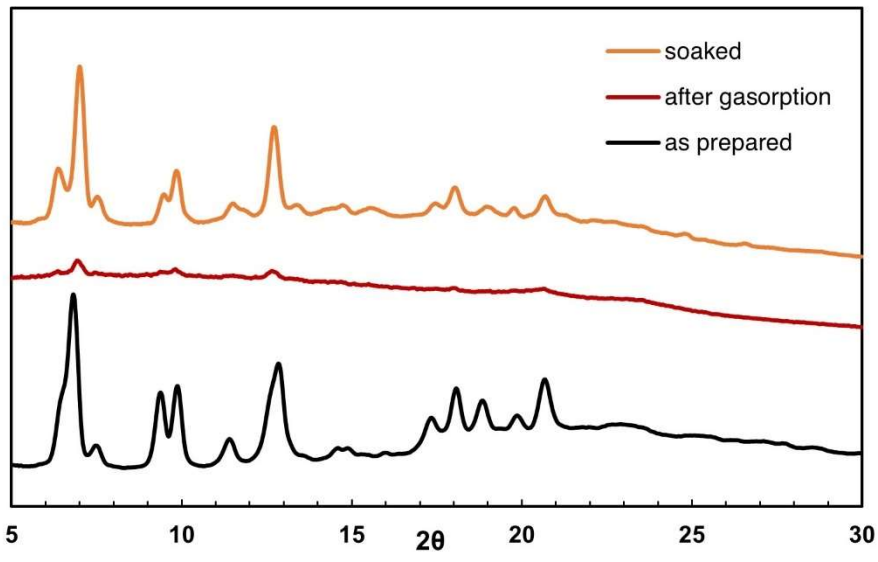

Figure 4.5 Stacked powder X-ray diffractions (PXRD) of Ni-^{ISO}CN-3. (black) As-prepared sample of Ni-^{ISO}CN-3, (red) sample after N_2 gasorption analysis and (orange) sample after soaking in MeCN for 24 hours.

regaining its crystallinity is evidence that the material has not collapsed and further adds to support the notion of its structural flexibility.

4.6 Conclusion

In conclusion, a novel 3D diamondoid coordination network Ni-^{ISO}CN-3 was reported, featuring Ni(0) nodal centers in a tetrahedral geometry by coordination to phenylene spaced *m*-terphenyl isocyanide linkers. This organometallic framework is an achievement of performing *in-situ* reactions with low-valent metal centers that have previously been proven difficult to synthesize but in this case aided through the prior knowledge of organometallic complexes. Furthermore, examination of the strength of the M-C bond was determined to be equally as stable and inert as most anionic bonds found in metal-organic frameworks. Ni-^{ISO}CN-3 is able to chemically endure a one-electron redox cycle, speaking to the chemical tolerance that can be found between a zero-valent metal center and a neutral isocyanide ligand. In addition, Ni-^{ISO}CN-3 was shown to possess flexibility properties and an ability to recuperate crystallinity, both addressing the structural stability features of this network. We believe that these studies support isocyanide-based frameworks as being chemically and structurally stable alternatives to anionic ligands for exploration into low-valent metal centers.

4.7 Supplemental Information

General Considerations. Unless otherwise stated, all manipulations were performed under an atmosphere of dry dinitrogen using standard Schlenk and glovebox techniques. Solvents were dried and degassed according to standard procedures.[64] Unless otherwise stated, reagent grade starting materials were purchased from commercial sources and purified where necessary according to standard procedures.[65] Solid-state IR spectra were collected at 2 cm^{-1} resolution as

either a KBr pellet or using a Bruker Platinum Alpha ATR-IR equipped with a diamond crystal. The following abbreviations are used to describe the intensity and characteristics of important IR absorption bands: vs = very strong, s = strong, m = medium, w = weak, vw = very weak, b = broad, vb = very broad, sh = shoulder.

General Crystallographic Information. Single X-ray structure determinations were performed at 100 K on Bruker Platform Diffractometers equipped with Mo-K_α or Cu-K_α radiation source and an APEX-II CCD area detector. All structures were solved via direct methods with SHELXS[66] and refined by full-matrix least-squares procedures using SHELXL within the Olex2 software package.[67] Crystallographic data collection and refinement information are listed in Table 4.2. MeCN solvent molecules of co-crystallization are present within the solvent-accessible channels. The Platon routine SQUEEZE[68] was used to account for the electron density of this disordered solvent as a diffuse contribution to the overall scattering without specific atom positions.

Powder X-ray diffraction studies on Cu-^{ISO}CN-4 were performed at 100 K on a Bruker D8 Advanced LynxEye CCD diffractometer, equipped with Cu-K_α radiation (λ = 1.54178 Å) and K_β filter. Diffraction measurements were set to 40V and 40 mA.

Synthesis of Ni-^{ISO}CN-3. To a warm pressure tube, a previously stirred $Ni(COD)_2$ (0.012 g, 0.045 mmol, 1 eq) solution in MeCN for 15 minutes was added. Followed by the quick addition of a MeCN solution of (1,4-$(CNAr^{Mes2})_2C_6H_4$) (0.061 g, 0.090 mmol, 2 eq). The dark red mixture was quickly sealed with a Teflon screw cap equipped with a Viton O-ring and placed in the oven for a temperature program that was set to heat at 120 °C for 24 hr with slow cooling to 80 °C over the course of 48 hr. Red single crystals of diffraction quality are produced. Gentle washing with MeCN 5 times produces material for further analysis. FTIR-ATR (diamond surface, 20 °C) 1950 cm^{-1}.

Thermal Analysis. Thermogravimetric analysis was performed on ~5–15 mg of material that had been dried under dynamic vacuum. Analysis was conducted under a stream of dry dinitrogen gas (80 mL/min) using a Mettler Toledo TGA/DSC 1 STARe System running from 30 ˚C to 800 ˚C with a ramping rate of 5 ˚C/min.

Surface Area Analysis. Samples were prepared on and measured using a Micrometrics ASAP 2020 Adsorption Analyzer. Approximately 62 mg of material was transferred to a pre-weighed sample tube and degassed at 110 ˚C for at least 24 hours or until the outgas rate was below 5 mmHg. The sample tube was reweighed to obtain a mass for the sample. Measurements were collected on three independent samples at 77 K employing N_2 of 99.999% purity using the volumetric technique.

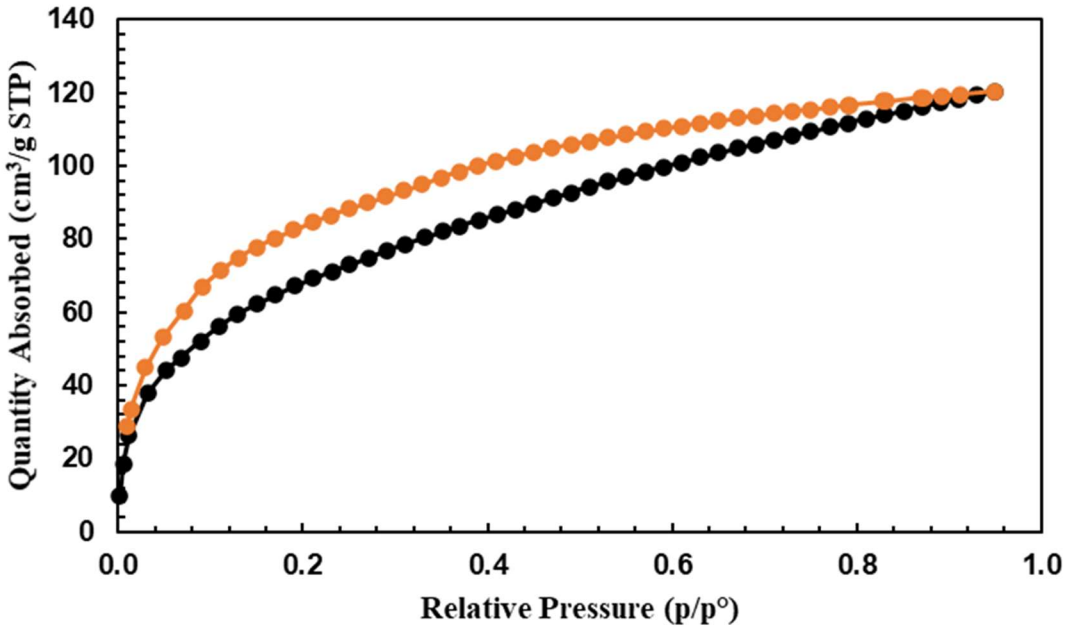

Figure 4.6 CO_2 isotherm collected at 195 K of Ni-^{ISO}CN-3. Black curve is absorption and orange curve desorption.

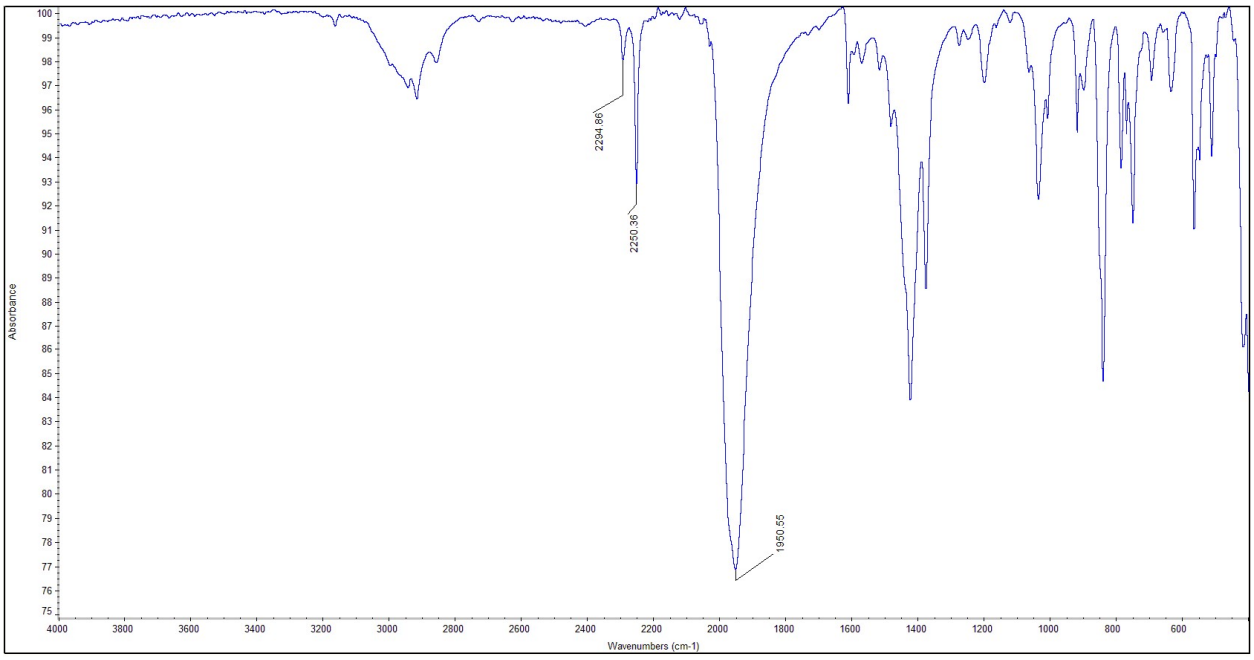

Figure 4.7 ATR-IR of as prepared sample of Ni-^{ISO}CN-3.

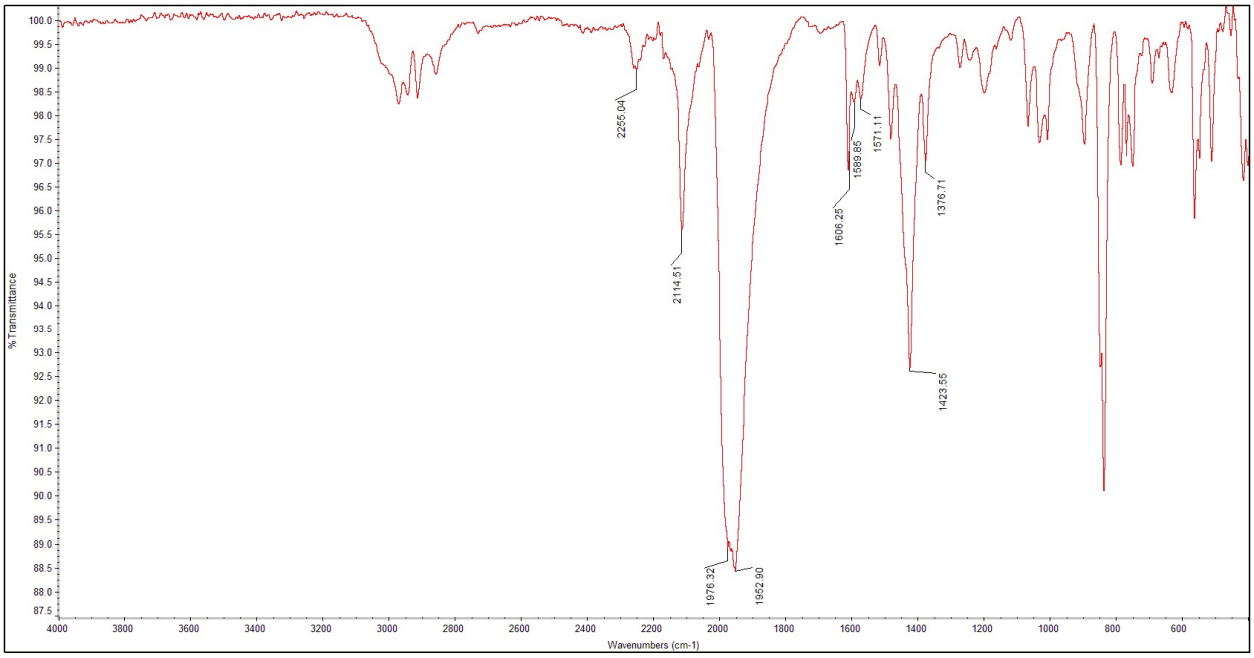

Figure 4.8 ATR-IR of Ni-^{ISO}CN-3 treated with 1 atm of O_2 (g) after 72 hr.

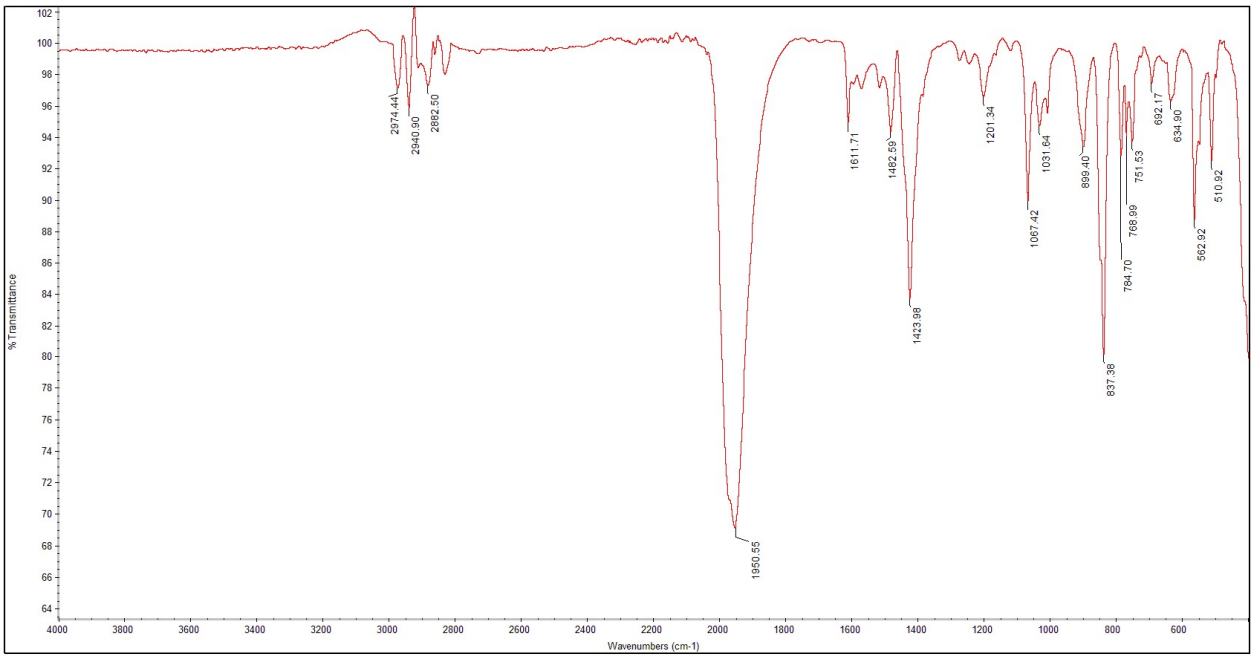

Figure 4.9 ATR-IR of Ni-^{ISO}CN-3 after being treated with 3 mL of Millipore water for 24 hours. No change is observed from as-prepared sample.

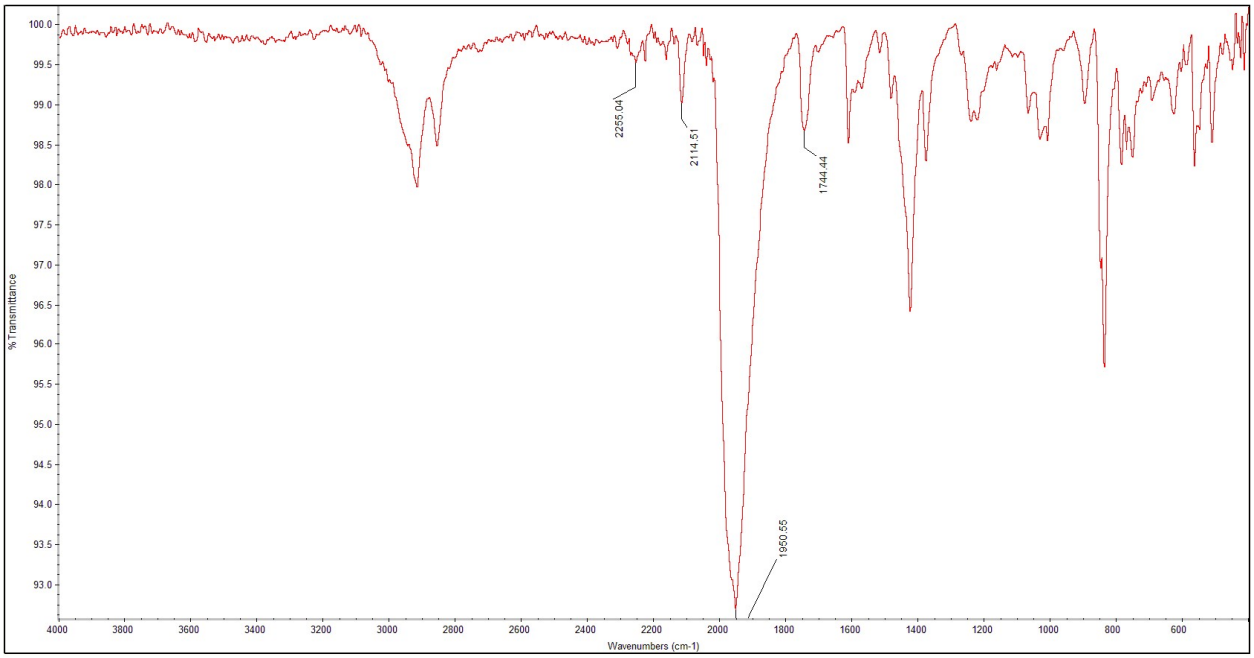

Figure 4.10 ATR-IR of Ni-^{ISO}CN-3 after being treated with 3 mL of Millipore water for 72 hours. The presence of both free isocyanide and isocyanate are now detected.

Figure 4.11 Ni-^{ISO}CN-3 in an ampoule with 3 mL of Millipore water. The red sample floats on top and sticks to the walls of ampoule and does not mix with the water.

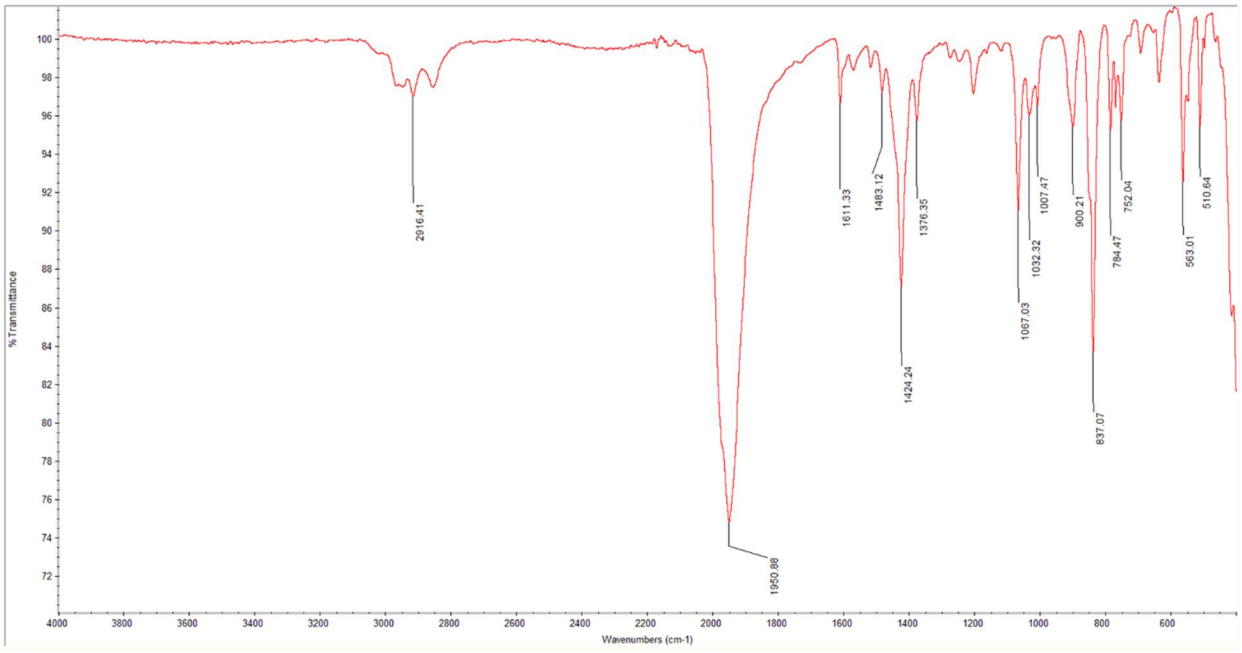

Figure 4.12 ATR-IR of a sample of Ni-^{ISO}CN-3 after a N_2 isotherm analysis run.

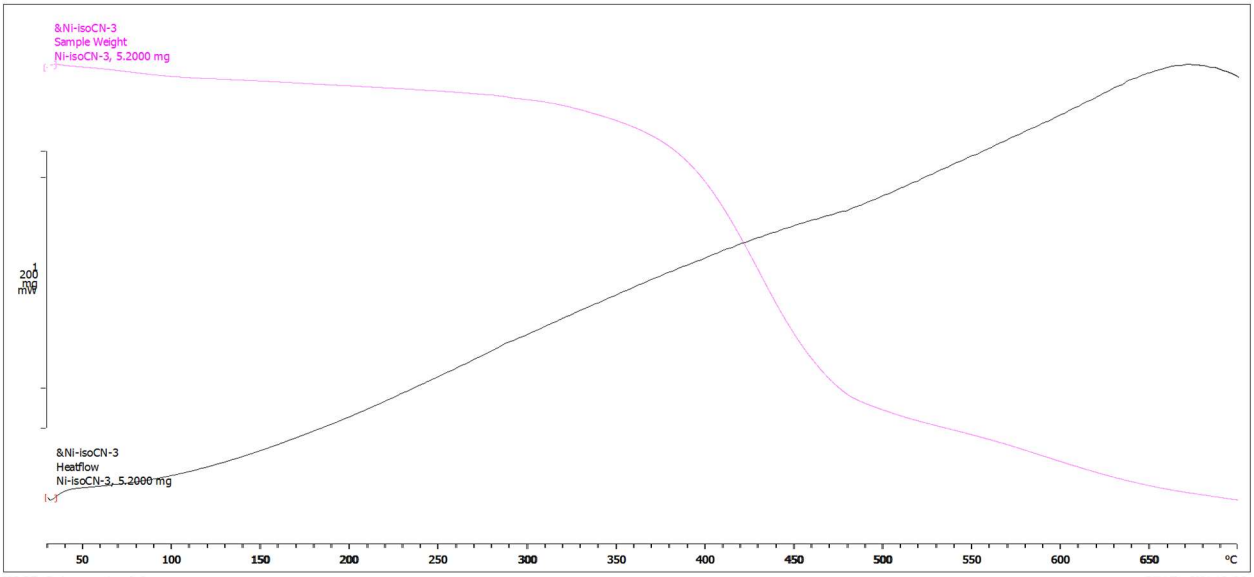

Figure 4.13 Thermogravimetric analysis (TGA) (pink trace) of Ni-^{ISO}CN-3.

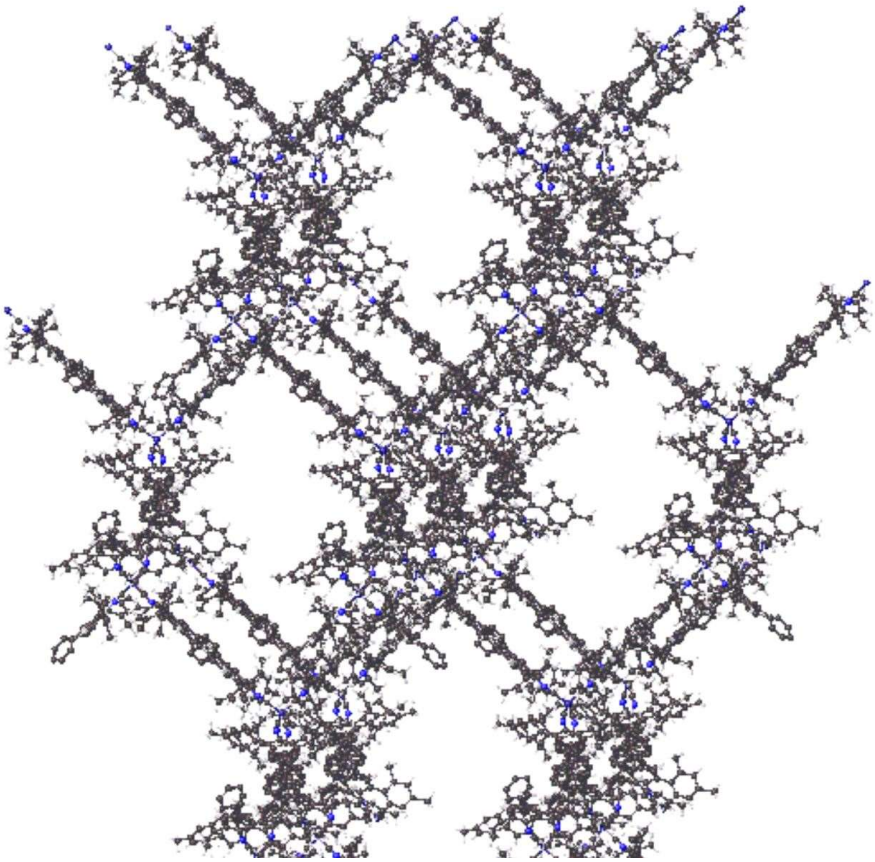

Figure 4.14 View of an individual network of the diamondoid Ni-^{ISO}CN-3.

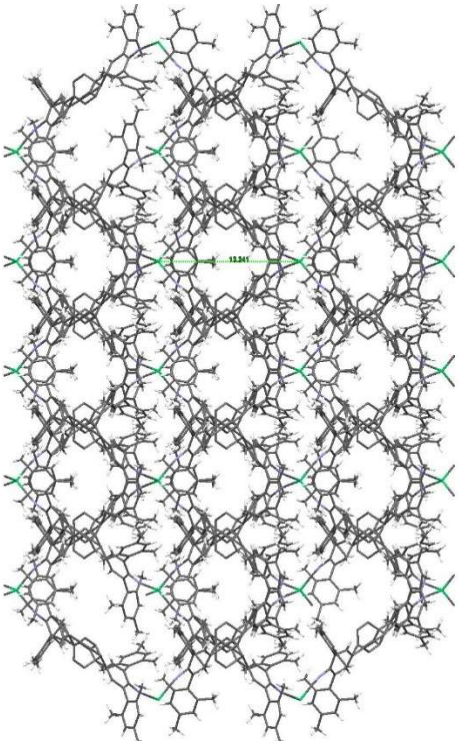

Figure 4.15 View along the b-axis of four-fold interpenetrated Ni-^{ISO}CN-3 revealing the smaller accessible pore space to classify as a microporous material.

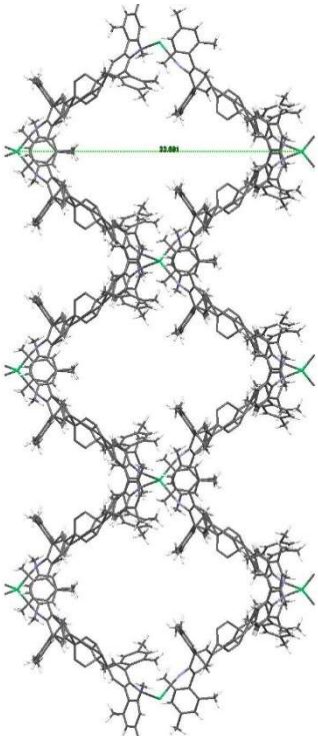

Figure 4.16 View along the b-axis of Ni-^{ISO}CN-3 of an individual framework of Ni-^{ISO}CN-3 suggesting if the material were not interpenetrated then it could be classified as a mesoporous material.

Table 4.2 Crystallographic Data Collection and Refinement Information

Name	Ni-^{ISO}CN-3
Formula	$C_{112}H_{104}N_4Ni$
Crystal System	Tetragonal
Space Group	p-4*b*2
a, Å	20.5707(8)
b, Å	20.5707(8)
c, Å	13.3409(8)
α, deg	90
β, deg	90
γ, deg	90
V, Å^3	5645.3(6)
Z	2
Radiation (λ, Å)	Cu-Kα, 1.54178
ρ (calcd.), g/cm^3	0.984
μ (Mo Ka), mm^{-1}	0.552
Temp, K	100
θ max, deg	134.352
data/parameters	2419/288

R_1	0.0906
wR_2	0.2245
GOF	1.072

4.8 Acknowledgements

Chapter 4 is adapted from a manuscript currently in preparation for publication by A. Arroyave, M. Gembicky, A. L. Rheingold, and J. S. Figueroa. Permission to include published material in this dissertation has been obtained from all coauthors. The dissertation author is the first author of this paper.

4.9 References

(1) Furukawa, H.; Ko, N.; Go, Y. B.; Aratani, N.; Choi, S. B.; Choi, E.; Yazaydin, A. Ö.; Snurr, R. Q.; O'Keeffe, M.; Kim, J. *Science* **2010**, *329*, 424–428.

(2) Farha, O. K.; Eryazici, I.; Jeong, N. C.; Hauser, B. G.; Wilmer, C. E.; Sarjeant, A. A.; Snurr, R. Q.; Nguyen, S. T.; Yazaydin, A. Ö.; Hupp, J. T. *J. Am. Chem. Soc.* **2012**, *134*, 15016–15021.

(3) Farha, O. K.; Özgür Yazaydın, A.; Eryazici, I.; Malliakas, C. D.; Hauser, B. G.; Kanatzidis, M. G.; Nguyen, S. T.; Snurr, R. Q.; Hupp, J. T. *Nat. Chem.* **2010**, *2*, 944–948.

(4) Hönicke, I. M.; Senkovska, I.; Bon, V.; Baburin, I. A.; Bönisch, N.; Raschke, S.; Evans, J. D.; Kaskel, S. *Angew. Chemie - Int. Ed.* **2018**, *57*, 13780–13783.

(5) Grünker, R.; Bon, V.; Müller, P.; Stoeck, U.; Krause, S.; Mueller, U.; Senkovska, I.; Kaskel, S. *Chem. Commun.* **2014**, *50*, 3450–3452.

(6) Eddaoudi, M.; Kim, J.; Rosi, N.; Vodak, D.; Wachter, J.; O'Keeffe, M.; Yaghi, O. M. *Science* **2002**, *295*, 469–472.

(7) Bux, H.; Chmelik, C.; Krishna, R.; Caro, J. Ethene/Ethane Separation by the MOF

Membrane ZIF-8: Molecular Correlation of Permeation, Adsorption, Diffusion. *J. Memb. Sci.* **2011**, *369*, 284–289.

(8) Zhao, Z.; Ma, X.; Kasik, A.; Li, Z.; Lin, Y. S. *Ind. Eng. Chem. Res.* **2013**, *52*, 1102-1108.

(9) Li, H.; Wang, K.; Sun, Y.; Lollar, C. T.; Li, J.; Zhou, H. C. Recent Advances in Gas Storage and Separation Using Metal–Organic Frameworks. *Mater. Today* **2018**, *21*, 108–121.

(10) Desai, S. P.; Ye, J.; Islamoglu, T.; Farha, O. K.; Lu, C. C. *Organometallics* **2019**, *38*, 3466–3473.

(11) Wang, Z.; Tanabe, K. K.; Cohen, S. M. *Chem. Soc. Rev.* **2009**, *38*, 1315-1329.

(12) Ren, J.; Lan, P. C.; Chen, M.; Zhang, W.; Ma, S. *Organometallics* **2019**, *38*, 3460–3465.

(13) Huxley, M. T.; Young, R. J.; Bloch, W. M.; Champness, N. R.; Sumby, C. J.; Doonan, C. J. *Organometallics* **2019**, *38*, 3412–3418.

(14) Meilikhov, M.; Yusenko, K.; Esken, D.; Turner, S.; Van Tendeloo, G.; Fischer, R. A. *Eur. J. Inorg. Chem.* **2010**, *2010*, 3701–3714.

(15) Thornton, A. W.; Nairn, K. M.; Hill, J. M.; Hill, A. J.; Hill, M. R. *J. Am. Chem. Soc.* **2009**, *131*, 10662–10669.

(16) Hermannsdörfer, J.; Friedrich, M.; Kempe, R. *Chem. - A Eur. J.* **2013**, *19* , 13652–13657.

(17) Oisaki, K.; Li, Q.; Furukawa, H.; Czaja, A. U.; Yaghi, O. M. *J. Am. Chem. Soc.* **2010**, *132*, 9262–9264.

(18) Dincă, M.; Gabbaï, F. P.; Long, J. R. *Organometallics*. **2019**, *38*, 3389–3391.

(19) Dunning, S. G.; Reynolds, J. E.; Walsh, K. M.; Kristek, D. J.; Lynch, V. M.; Kunal, P.; Humphrey, S. M. *Organometallics* **2019**, *38*, 3406–3411.

(20) Dong, Y.; Jv, J. J.; Wu, X. W.; Kan, J. L.; Lin, T.; Dong, Y. Bin. *Chem. Commun.* **2019**, *55*, 14414–14417.

(21) Agnew, D. W.; DiMucci, I. M.; Arroyave, A.; Gembicky, M.; Moore, C. E.; MacMillan, S. N.; Rheingold, A. L.; Lancaster, K. M.; Figueroa, J. S. *J. Am. Chem. Soc.* **2017**, *139*, 17257–17260.

(22) Brian J., F.; Matthew D., M.; Antonio G., D.; Arnold L., R.; Joshua S., F. *Angew. Chemie Int. Ed.* **2009**, *48*, 3473–3477.

(23) Carpenter, A. E.; Mokhtarzadeh, C. C.; Ripatti, D. S.; Havrylyuk, I.; Kamezawa, R.; Moore, C. E.; Rheingold, A. L.; Figueroa, J. S. *Inorg. Chem.* **2015**, *54*, 2936–2944.

(24) Labios, L. A.; Millard, M. D.; Rheingold, A. L.; Figueroa, J. S. *J. Am. Chem. Soc.* **2009**, *131*, 11318–11319.

(25) Margulieux, G. W.; Weidemann, N.; Lacy, D. C.; Moore, C. E.; Rheingold, A. L.; Figueroa, J. S. *J. Am. Chem. Soc.* **2010**, *132*, 5033–5035.

(26) Agnew, D. W.; Moore, C. E.; Rheingold, A. L.; Figueroa, J. S. *Angew. Chemie Int. Ed.* **2015**, *54*, 12673–12677.

(27) Haldoupis, E.; Nair, S.; Sholl, D. S. *J. Am. Chem. Soc.* **2010**, *132*, 7528–7539.

(28) Gao, W.; Cardenal, A. D.; Wang, C.; Powers, D. C. *Chem. – A Eur. J.* **2019**, *25*, 3465–3476.

(29) Arroyave, A.; Gembicky, M.; Rheingold, A. L.; Figueroa, J. S. *Inorg. Chem.* **2020**, *59*, 11868–11878.

(30) Agnew, D. W.; Gembicky, M.; Moore, C. E.; Rheingold, A. L.; Figueroa, J. S. *J. Am. Chem. Soc.* **2016**, *138*, 15138–15141.

(31) Yang, L.; Powell, D. R.; Houser, R. P. *J. Chem. Soc. Dalt. Trans.* **2007**, *9*, 955–964.

(32) Nattmann, L.; Saeb, R.; Nöthling, N.; Cornella, J. *Nat. Catal.* **2020**, *3*, 6-13.

(33) Nett, A. J.; Canellas, S.; Higuchi, Y.; Robo, M. T.; Kochkodan, J. M.; Haynes, M. T.; Kampf, J. W.; Montgomery, J. *ACS Catal.* **2018**, *8*, 6606–6611.

(34) Standley, E. A.; Jamison, T. F. *J. Am. Chem. Soc.* **2013**, *135*, 1585–1592.

(35) Johnson, H. W.; Daughhetee, P. H. *J. Org. Chem*. **1964**, *29*, 246–247.

(36) Baldwin, J. E.; Bottaro, J. C.; Riordan, P. D.; Derome, A. E. *J. Chem. Soc., Chem. Commun.***1982**, *16*, 942-943.

(37) Bihani, M.; Bora, P. P.; Nachtegaal, M.; Jasinski, J. B.; Plummer, S.; Gallou, F.; Handa, S. *ACS Catal.* **2019**, *9*, 7520–7526.

(38) Clement, N. D.; Cavell, K. J.; Jones, C.; Elsevier, C. J. *Angew. Chemie Int. Ed.* **2004**, *43*, 1277–1279.

(39) Handa, S.; Slack, E. D.; Lipshutz, B. H. *Angew. Chemie Int. Ed.* **2015**, *54*, 11994–11998.

(40) Metin, Ö.; Özkar, S. *Int. J. Hydrogen Energy* **2011**, *36*, 1424–1432.

(41) Oh, K.; Mériadec, C.; Lassalle-Kaiser, B.; Dorcet, V.; Fabre, B.; Ababou-Girard, S.; Joanny, L.; Gouttefangeas, F.; Loget, G. *Energy Environ. Sci.* **2018**, *11*, 2590–2599.

(42) Ittel, S. D.; Berke, H.; Dietrich, H.; Lambrecht, J.; Härter, P.; Opitz, J.; Springer, W. *Complexes of Nickel(0)* John Wiley & Sons, Ltd, 2007.

(43) Zhang, Z.; Awaga, K. *MRS Bull.* **2016**, *41*, 883–889.

(44) Chen, Q.; Sun, J.; Li, P.; Hod, I.; Moghadam, P. Z.; Kean, Z. S.; Snurr, R. Q.; Hupp, J. T.; Farha, O. K.; Stoddart, J. F. *J. Am. Chem. Soc.* **2016**, *138*, 14242–14245.

(45) Mohammad-Pour, G. S.; Hatfield, K. O.; Fairchild, D. C.; Hernandez-Burgos, K.; Rodríguez-López, J.; Uribe-Romo, F. J. *J. Am. Chem. Soc.* **2019**, *141*, 19978–19982.

(46) Cheon, Y. E.; Suh, M. P. *Angew. Chemie - Int. Ed.* **2009**, *48*, 2899–2903.

(47) Xu, Y.; Yin, X. B.; He, X. W.; Zhang, Y. K. *Biosens. Bioelectron.* **2015**, *68*, 197–203.

(48) Moon, H. R.; Kim, J. H.; Suh, M. P. *Angew. Chemie - Int. Ed.* **2005**, *44*, 1261–1265.

(49) Barybin, M. V.; Meyers, J. J.; Neal, B. M. *Renaissance of Isocyanoarenes as Ligands in Low-Valent Organometallics.* In *Isocyanide Chemistry*; Wiley-VCH Verlag GmbH & Co. KGaA, 2012.

(50) Sarapu, A. C.; Fenske, R. F. *Inorg. Chem.* **1975**, *14*, 247–253.

(51) Drance, M. J.; Mokhtarzadeh, C. C.; Melaimi, M.; Agnew, D. W.; Moore, C. E.; Rheingold, A. L.; Figueroa, J. S. *Angew. Chemie Int. Ed.* **2018**, *57*, 13057–13061.

(52) Tamaru, Y. *Modern Organonickel Chemistry*; Wiley, 2005.

(53) Fox, B. J.; Millard, M. D.; DiPasquale, A. G.; Rheingold, A. L.; Figueroa, J. S. *Angew. Chem. Int. Ed. Engl.* **2009**, *48* , 3473–3477.

(54) Moggach, S. A.; Bennett, T. D.; Cheetham, A. K. *Angew. Chemie Int. Ed.* **2009**, *48*, 7087–7089.

(55) Li, H.; Wang, K.; Sun, Y.; Lollar, C. T.; Li, J.; Zhou, H. C. *Mater. Today*. **2018**, *21*, 108–121.

(56) Bourrelly, S.; Llewellyn, P. L.; Serre, C.; Millange, F.; Loiseau, T.; rard Fé rey, G. *J. Am. Chem. Soc.* **2005**, *127*, 13519-13521.

(57) Zhao, Z.; Ma, X.; Kasik, A.; Li, Z.; Lin, Y. S. *Ind. Eng. Chem. Res.* **2013**, *52*, 1102–1108.

(58) Kondo, A.; Yashiro, T.; Okada, N.; Hiraide, S.; Ohkubo, T.; Tanaka, H.; Maeda, K. *J. Mater. Chem. A* **2018**, *6*, 5910–5918.

(59) Lin, R. B.; Li, L.; Wu, H.; Arman, H.; Li, B.; Lin, R. G.; Zhou, W.; Chen, B. *J. Am. Chem. Soc.* **2017**, *139*, 8022–8028.

(60) Fairen-Jimenez, D.; Moggach, S. A.; Wharmby, M. T.; Wright, P. A.; Parsons, S.; Düren, T. *J. Am. Chem. Soc.* **2011**, *133*, 8900–8902.

(61) Haldar, R.; Sikdar, N.; Maji, T. K. *Mater. Today*. **2015**, *18*, 97–116.

(62) Sing, K. S. W.; Everett, D. H.; Haul, R. A. W.; Moscou, L.; Pierotti, R. A.; Rouquerol, J.; Siemieniewska, T. *Pure Appl. Chem.* **1985**, *57*, 603–619.

(63) Zhao, X.; Xiao, B.; Fletcher, A. J.; Thomas, K. M.; Bradshaw, D.; Rosseinsky, M. J. *Science* **2004**, *306*, 1012–1015.

(64) Pangborn, A. B.; Giardello, M. A.; Grubbs, R. H.; Rosen, R. K.; Timmers, F. J. *Organometallics* **1996**, *15*, 1518–1520.

(65) Armarego, W. L. F.; Li, C.; Chai, L.; York, N.; *Purification of Laboratory Chemicals Seventh Edition*; Elsevier 2013.

(66) Sheldrick, G. M. *Acta Crystallogr., Sect. A: Found. Crystallogr*. **2008**, *64*, 112–122.

(67) Dolomanov, O. V.; Bourhis, L. J.; Gildea, R. J.; Howard, J. A. K.; Puschmann, H. *J. Appl. Crystallogr.* **2009**, *42*, 339–341.

(68) Van Der Sluis, P.; Spek, A. L. *Acta Crystallogr. Sect. A* **1990**, *46*, 194–201.